

NON-ORTHOGONAL MULTIPLE ACCESS FOR NEXT-GENERATION WIRELESS COMMUNICATIONS

A THESIS SUBMITTED TO AUCKLAND UNIVERSITY OF TECHNOLOGY
IN FULFILMENT OF THE REQUIREMENTS FOR THE DEGREE OF
DOCTOR OF PHILOSOPHY

By

Asim Anwar

School of Engineering, Computer and Mathematical Sciences

May 2018

Copyright

Copyright in text of this thesis rests with the Author. Copies (by any process) either in full, or of extracts, may be made **only** in accordance with instructions given by the Author and lodged in the library, Auckland University of Technology. Details may be obtained from the Librarian. This page must form part of any such copies made. Further copies (by any process) of copies made in accordance with such instructions may not be made without the permission (in writing) of the Author.

The ownership of any intellectual property rights which may be described in this thesis is vested in the Auckland University of Technology, subject to any prior agreement to the contrary, and may not be made available for use by third parties without the written permission of the University, which will prescribe the terms and conditions of any such agreement.

Further information on the conditions under which disclosures and exploitation may take place is available from the Librarian.

© Copyright 2018. Asim Anwar

Attestation of Authorship

I hereby declare that this submission is my own work and that, to the best of my knowledge and belief, it contains no material previously published or written by another person nor material which to a substantial extent has been accepted for the qualification of any other degree or diploma of a university or other institution of higher learning.

Asim Anwar

May, 2018

Acknowledgements

At the very outset, I would like to wish my deepest gratitude to my primary supervisor Associate Professor Boon-Chong Seet for his dedicated interest, understanding, patience and consistent encouragement during my PhD studies at AUT. His epidemic passion and brainstorming discussions have been major driving factors during my candidature. He always showed faith in my abilities and has always been a strong advocate for me. My deepest thanks to my secondary supervisor Dr. Xue Jun Li for his open-handed support and interactive behaviour. His valuable suggestions have greatly contributed to improve the quality of my research and this thesis. I would also like to express my appreciation to AUT for granting me a Doctoral fee scholarship and living stipend to support my studies. My special thanks to the SECMS staff members, especially to Postgraduate Coordinator Ms. Josephine Prasad for her great assistance with many administrative matters.

I also offer profound thanks to my friends and colleagues (former/present) in WD307. Further, I thank all my friends outside of AUT: Faisal Bhatti, Abdul Raees, Syed Fakhar, Rizwan Butt, Arif Rizvi, Muhammad Asif and many others in making my time enjoyable in New Zealand.

Last but not least, I would like to extend my thanks to my family members especially my parents, wife, brothers, sister and their families for their role in making me what I am today. My achievement could not have come to existence without their unflinching care and support.

Abstract

Non-orthogonal multiple access (NOMA) is considered as a strong candidate for enhancing the spectrum efficiency of future fifth generation (5G) wireless systems. A key feature of NOMA is the superposition of multiple users' messages in a single resource by allocating different power levels to each user and applies successive interference cancellation (SIC) at receiver to suppress intra-user interference.

The current literature is sparse in exploring the application of NOMA to multi-tier cellular network, group device-to-device (D2D) communication and wireless sensor networks (WSN). Previous studies have also shown that NOMA has no significant gain over OMA in low signal-to-noise ratio (SNR) regime, and there are some potential drawbacks of SIC that can limit NOMA performance. In order to address these gaps in knowledge, extensive research is conducted in this thesis.

The first three chapters provide introduction and research motivations, background concepts relevant to this thesis, and literature review to identify the research gaps. In particular, research work conducted in this thesis can be divided into two parts. The first part considers the application and performance analysis of NOMA for multi-tier cellular networks, group device-to-device (D2D) communications and ubiquitous wireless sensor networks (UWSNs). Based on the work done in first part, three problems are identified to be addressed: a) to enhance the performance of NOMA in low SNR regime; b) to enhance the performance of NOMA under similar channel conditions; c) to resolve the issues related to the use of SIC with NOMA. As a result, the second part

of the thesis proposes solutions to solve the aforementioned problems.

The specific novel contributions of this thesis can be summarised as follows: 1) developed a novel analytical framework to investigate multi-tier NOMA networks with underlay D2D communications; 2) proposed a quality of service (QoS) based NOMA group D2D communication scheme where unlike existing works, the D2D users (DRs) are ordered in NOMA according to their QoS requirements; 3) investigated and analysed NOMA for ubiquitous wireless sensor networks (UWSNs) in the presence of cross-technology (CT) nodes; 4) proposed a hybrid multiple access (HMA) scheme where users are scheduled either for NOMA and OMA in order to enhance the performance in low SNR regime; and 5) designed an alternate receiver structure based on parallel interference cancellation (PIC) to alleviate the SIC issues as well as an equivalent transmission model for downlink NOMA. Moreover, in order to analyse the performance of all the considered NOMA systems, closed-form expressions for outage probability are also derived.

Contents

Copyright	ii
Attestation of Authorship	iii
Acknowledgements	iv
Abstract	v
List of Tables	xi
List of Figures	xii
List of Symbols	xiv
Glossary	xv
1 Introduction	1
1.1 Motivation and Scope	1
1.2 Contributions	4
1.2.1 Publications	7
1.3 Thesis Organisation	8
2 Background	9
2.1 Multiple Access Techniques for Wireless Communication	9
2.2 Non-Orthogonal Multiple Access (NOMA)	12
2.3 Device-to-Device Communications	15
2.4 Point Processes	16
2.4.1 Poisson Point Process (PPP)	18
2.4.2 Determinantal Point Process (DPP)	19
2.4.3 Poisson Cluster Process (PCP)	21
2.4.4 Poisson Hole Process (PHP)	22
2.4.5 Marked Point Process (MPP)	23
2.4.6 Interference over a Point Process	24
2.5 Chapter Summary	25

3	Literature Review	27
3.1	NOMA for Cellular Networks	27
3.1.1	Single-Cell Single-Tier Scenario	27
3.1.2	Single-Cell Multi-Tier Scenario	34
3.1.3	Multi-Cell Single-Tier Scenario	35
3.1.4	Multi-Cell Multi-Tier Scenario	36
3.2	NOMA for D2D Communications	38
3.2.1	Paired D2D Communications	38
3.2.2	Group D2D Communications	40
3.3	NOMA based Hybrid Multiple Access	41
3.4	NOMA Receiver Structure	43
3.5	Chapter Summary	44
4	An Analytical Framework for Multi-Tier NOMA Networks with Underlay D2D Communications	46
4.1	Introduction	46
4.2	System Model	48
4.2.1	Spatial Setup and Key Assumptions	49
4.2.2	Propagation Model	52
4.2.3	NOMA and D2D Systems	52
4.3	Association Probabilities and Interference Distributions	55
4.3.1	Association Probability	55
4.3.2	Interference Distributions	57
4.4	Performance Analysis	63
4.4.1	Proposed SIE Receiver Design for Cellular Users	64
4.4.2	Outage Analysis	65
4.4.3	Link Throughput Analysis	69
4.5	Results and Discussion	70
4.6	Chapter Summary	78
5	Quality of Service based NOMA Group D2D Communications	79
5.1	Introduction	79
5.2	System Model	81
5.2.1	Spatial Distribution of D2D Users	82
5.3	Proposed QoS NOMA Group D2D Communications	83
5.3.1	Power Allocation Coefficients Policies	84
5.3.2	Interference Distribution	85
5.4	Outage Analysis	86
5.5	Numerical Results and Discussion	89
5.6	Chapter Summary	93

6	NOMA for Ubiquitous Wireless Sensor Networks	95
6.1	Introduction	95
6.2	Network Model	98
6.3	Outage and Diversity Analysis	102
6.3.1	Diversity Analysis	104
6.4	Throughput and Energy Consumption Efficiency Analysis	106
6.4.1	Link Throughput Efficiency	106
6.4.2	Energy Consumption Efficiency	106
6.5	Results and Discussion	108
6.6	Chapter Summary	113
7	Hybrid Multiple Access with Channel Gain Stretching	114
7.1	Introduction	114
7.2	System Model	115
7.3	Proposed Scheme	117
7.3.1	Optimal Throughput and Group Size	119
7.3.2	Channel Gain Stretching Method for G_2 Users in HMA	120
7.4	Outage Analysis	122
7.5	Results and Discussion	125
7.6	Chapter Summary	129
8	PIC-based Receiver Structure for NOMA	130
8.1	Introduction	130
8.2	Proposed PIC-based Receiver Design for NOMA	132
8.2.1	Filter Bank Design for Decoder of Users	134
8.2.2	Design Challenges for Proposed Receiver	135
8.3	Modeling and Estimation of Intra-User Interference in NOMA Signal	137
8.3.1	Equivalent Transmission Model for NOMA	137
8.3.2	Intra-User Interference Modeling and Estimation	138
8.3.3	Outage Analysis	140
8.4	Results and Discussion	143
8.5	Chapter Summary	149
9	Conclusion and Future Work	151
9.1	Summary of Contributions	152
9.2	Future Work	154
	Appendix A Proof of Lemma 4.1	157
	Appendix B Proof of Lemma 4.2	158
	Appendix C Proof of Lemma 4.3	160
	Appendix D Proof of Lemma 4.4	166

Appendix E	Proof of Lemma 4.5	168
Appendix F	Proof of Lemma 4.6	171
Appendix G	Proof of Lemma 4.7	172
Appendix H	Proof of Theorem 4.1	174
Appendix I	Proof of Lemma 5.1	177
Appendix J	Proof of Theorem 6.1	180
Appendix K	Proof of Theorem 8.1	183
References		185

List of Tables

4.1	Commonly used variables.	48
4.2	Simulation parameters	71
5.1	Commonly used variables.	81
5.2	Simulation parameters.	89
5.3	Average outage comparison between two implementations of quality of service based non-orthogonal multiple access (Q-NOMA) group device-to-device (D2D) communications.	93
5.4	Average outage comparison between paired device-to-device (D2D) and quality of service based non-orthogonal multiple access (Q-NOMA) group D2D communications ($M > 3$).	93
6.1	Commonly used variables in Chapter 6.	98
6.2	Simulation parameters.	109
6.3	Computational time per bit decision by SIC unit	113
7.1	Commonly used variables.	117
7.2	Simulation parameters.	125
7.3	Average outage probability (for $M > 3$)	129
8.1	Commonly used variables.	134
8.2	Simulation parameters.	146
8.3	Computational time of PIC for each mobile SoC.	147

List of Figures

2.1	Downlink NOMA transmission.	13
2.2	NOMA transmitter architecture.	14
2.3	NOMA receiver architecture.	15
4.1	Proposed two-tier network model. The squares, triangles, circles and diamonds show the positions of MBSs, SBSs, clustered users, and non-clustered users, respectively.	49
4.2	Classifications of users under proposed network model.	50
4.3	Representative macrocell with underlaid small cells.	53
4.4	Illustration of interference at non-clustered MBS user from clustered DT. The solid dot, triangle and square represent non-clustered MBS user, SBS user, and clustered DT, respectively.	58
4.5	Proposed SIE receiver.	63
4.6	Outage comparison among MBS user, SBS user and DR, with $p = q = p_m = 0.5$ and $\bar{c} = 5$	73
4.7	Outage comparison among non-clustered and clustered MBS user and DR, with $p = q = p_m = 0.5$ and $\bar{c} = 5$	74
4.8	Probability of clustered cellular user to connect MBS or SBS.	76
4.9	Link Throughput comparison among MBS user, SBS user, DR and OMA user.	76
4.10	Impact of varying SBS density on link throughput of cellular user.	77
4.11	Outage of DR under NOMA and OMA networks.	77
5.1	Example of inband non-orthogonal multiple access (NOMA) group device-to-device (D2D) communications with overlay cellular network.	83
5.2	Impact of R_D on outage probability.	90
5.3	Impact of d on outage probability.	91
5.4	Outage comparison between paired and group D2D.	91
6.1	A realisation of Φ_{SE} , Φ_{SK} , and Φ_{CT} transmitter processes.	99
6.2	An illustration of sink-to-sensors communication using NOMA under interference of other sink, sensor and CT nodes.	100
6.3	Impact of different R on outage probability.	110
6.4	Impact of κ on average outage probability.	110
6.5	Impact of α on outage probability.	111

6.6	Link throughput efficiency comparison between NOMA and OMA.	111
6.7	Energy consumption efficiency comparison between NOMA and OMA.	112
6.8	Computational complexity of NOMA receivers.	112
7.1	Outage comparison among HMA, NOMA and OMA.	127
7.2	Outage comparison of G_2 HMA users with and without CGS under CGS method 1.	127
7.3	Outage performance comparison of G_2 HMA users with and without CGS and OMA under CGS method 2.	128
7.4	Throughput comparison among HMA, NOMA and OMA.	128
8.1	Proposed receiver structure for UE m	132
8.2	Equivalent Transmission Model for DL NOMA.	138
8.3	Probability of bit error and number of UEs	144
8.4	Downlink NOMA BER performance for 3 UEs	145
8.5	Computational complexity and number of UEs	145
8.6	Estimation of interference.	148
8.7	Impact of different $\mathcal{R}_{\mathcal{D}}$ on outage probability of m -th user.	148
8.8	Impact of different α on outage probability of m -th user.	149
8.9	Performance comparison between NOMA under proposed approach and NOMA with SIC.	150

List of Symbols

α	Pathloss exponent
\mathbb{E}_X	Expected value of random variable X
$\mathcal{G}[\cdot]$	Probability generating functional of point process
\mathcal{I}	Interference at typical interference
$\mathcal{L}_{\mathcal{I}}$	Laplace transform of interference \mathcal{I}
λ	Intensity of a point process
Φ	Point process
$\mathbf{1}$	Indicator function
a_m	Power allocation coefficient of user m
F_X	Cumulative distribution function of random variable X
f_X	Probability density function of random variable X
h_m	Channel gain between user m and base station
K	Kernel of determinantal point process
P	Transmit power of the source

Glossary

2D Two-dimensional.

4G Fourth generation.

5G Fifth generation.

AMC Adaptive modulation and coding.

AWGN Additive white Gaussian noise.

BER Bit error rate.

BPCU Bits per channel use.

BPSK Binary phase shift keying.

BS Base station.

CDF Cumulative distribution function.

CDMA Code division multiple access.

CGS Channel gain stretching.

CR-NOMA Cognitive radio inspired NOMA.

CSI Channel state information.

CT Cross technology.

D2D Device-to-device.

DPP Determinantal point process.

DR D2D receiver.

DT D2D transmitter.

DVS Dynamic voltage scaling.

F-NOMA Fixed power allocation NOMA.

FD Full duplex.

FDMA Frequency division multiple access.

FEC Forward error correction.

FSPA Full search power allocation.

FTPA Fractional transmit power allocation.

GPP Gauss Poisson process.

GT Group transmitter.

HARQ Hybrid automatic repeat request.

HMA Hybrid multiple access.

i.i.d Independent and identically distributed.

LTE Long term evolution.

MA Multiple access.

MBMS Multimedia broadcast/multicast service.

MBS Macro-cell base station.

MCP Matern cluster process.

MIMO Multiple input multiple output.

MPP Marked point process.

MRC Maximum ratio combining.

MSE Mean-squared-error.

NOMA Non-orthogonal multiple access.

OFDM Orthogonal frequency division multiplexing.

OFDMA Orthogonal frequency division multiple access.

OLLA Outer loop link adaption.

OMA Orthogonal multiple access.

PCP Poisson cluster process.

PDF Probability density function.

PF Proportional fairness.

PGFL probability generating functional.

PHP Poisson hole process.

PIC Parallel interference cancellation.

PP Point process.

PPP Poisson point process.

Q-NOMA QoS based NOMA.

QoS Quality of service.

RV Random variable.

SBS Small-cell base station.

SCMA Sparse code multiple access.

SIC Successive interference cancellation.

SIE SIC with intra-user interference estimation.

SINR Signal-to-interference-plus-noise ratio.

SNR Signal-to-noise ratio.

SoC System-on-chip.

SOS Second order statistic.

TCP Thomas cluster process.

TDMA Time division multiple access.

TPA Transmit power allocation.

UE User equipment.

UG User group.

Glossary

UWSN Ubiquitous WSN.

WSN Wireless sensor network.

Chapter 1

Introduction

1.1 Motivation and Scope

The last decade has witnessed a rapid growth in the number of mobile subscribers with portable devices such as smart phones and tablets to enjoy a wide range of services from simple voice to interactive multimedia. A major challenge facing current fourth generation (4G) mobile network operators is the ever-increasing number of mobile subscribers and their demands for high data-rate real-time multimedia services due to the scarce spectrum, along with a vigorous requirement of seamless connectivity, anywhere and anytime. Consequently, the wireless communications industry and academia researchers have been compelled to define a new paradigm of technological solutions to support the requirements of future fifth generation (5G) mobile communication systems [1, 2].

Some of the colossal expectations of 5G systems include $1000\times$ increase in cell throughput capacities over current 4G systems; wide expansion in traffic and number of simultaneous connections; personalized user experience; service access from anywhere, anytime, and any device; exceptionally low end-to-end latency; and a $10\times$ increase in battery life for battery-operated services [3–5].

In order to meet the aforementioned demands, many potential solutions have been proposed, such as ultra-densification, massive multiple input multiple output (MIMO) and millimetre wave [5]. Nevertheless, the role of multiple access scheme always remains a vital factor in cellular networks for enhancing the system capacity in a cost-effective manner, while utilising the bandwidth in such a way that overall spectral efficiency will be increased [3,6].

Non-orthogonal multiple access (NOMA) is considered as a promising candidate due to its potential of enhancing system capacity by efficient utilisation of the available spectrum resources. Unlike conventional orthogonal multiple access (OMA), NOMA superimposes message signals of different users in power domain and transmits this conglomerate signal using the same time, frequency or code resource. Successive interference cancellation (SIC) technique is employed at each receiver to cancel the intra-user interference [7].

The concept of NOMA is originally proposed for cellular networks in order to obtain significant performance gains over existing OMA techniques. In this context, NOMA and its integration with other techniques to enhance system capacity is well-investigated in the literature under single-cell single-tier scenario. These studies demonstrate the performance gains over OMA in terms of lower outage probability, better achievable rates, improved cell-edge user throughput and enhanced cell capacity. However, a practical cellular network is comprised of multi-cell architecture with potentially a multi-tier deployment to meet the capacity and massive-connectivity requirements of the future 5G cellular systems. In this perspective, current literature is still scarce on analysing NOMA systems under multi-cell and multi-tier scenario. The performance gains achieved by NOMA in single-cell single-tier situations can not be extended to multi-cell multi-tier cases in a straightforward manner. This is because the presence of inter-cell and inter-tier interferences require accurate system modeling and analysis under these scenarios, particularly with a frequency reuse factor of one.

In addition to NOMA, device-to-device (D2D) communication is another emerging technique, which has the ability to improve the spectral efficiency of conventional cellular network by sharing the same spectrum resources among cellular and D2D users [8–11]. In order to obtain further capacity improvements, NOMA can be applied to group D2D communications, but very few studies have been made in the literature on NOMA based group D2D networks. Moreover, NOMA exhibits strengths that can be considered as highly relevant for addressing the deployment challenges of ubiquitous wireless sensor networks (UWSNs) for ubiquitous monitoring of physical environments. Specifically, for a given spectrum bandwidth, NOMA can enable more simultaneous connections than existing approaches without the overheads of coding and spreading to facilitate the separation of users' signals at the receiver [12]. This is particularly attractive to support massive connectivity without requiring more spectrum resources in UWSNs.

Despite that NOMA can improve system capacity by efficient spectrum utilisation, NOMA based systems are inherently more interference limited than OMA due to superposition coding. Hence, NOMA requires a higher signal-to-interference-plus-noise ratio (SINR) for successful decoding. Further, previous studies showed that NOMA has no significant gain over OMA in low signal-to-noise ratio (SNR) regime [13], which makes it less attractive for those users with low SNR. Hence, there is a need to enhance the system performance in low SNR regime. Moreover, existing NOMA systems typically employ SIC receiver. However, SIC technique has potential issues that include high dependency on the correct decoding of the first user, error propagation, power sensitivity and increased decoding delay with large number of users. These SIC associated issues can limit NOMA performance, and hence there is a need to design an alternate receiver for NOMA that can alleviate these problems.

The aforementioned issues motivated the investigation on the application of NOMA for multi-cell multi-tier cellular networks, group D2D communications and UWSNs

in this thesis, utilising stochastic geometry tools to model and analyse interference in these networks. Closed-form expressions for outage probability at the probe receiver are derived to evaluate the performance of these networks. In addition, a notion of hybrid multiple access (HMA) is presented to improve the system performance in low SNR regime. Further, an alternate receiver based on parallel interference cancellation (PIC) is investigated for NOMA to alleviate the SIC-related issues.

1.2 Contributions

- In Chapter 4, NOMA for multi-cell multi-tier cellular network, comprising of macro-cell base stations (MBSs) and small-cell base stations (SBSs) with underlaid D2D communications, is investigated. Both MBSs and SBSs are equipped with NOMA functionality. The deployment of SBSs is user-centric and hence locations of SBSs and users in small-cells are correlated. Based on stochastic geometry tools, an analytical framework to model and analyse the considered network is developed. An important characteristic of the developed modeling approach is that it captures the correlation between locations of SBSs and small-cell users. Based on the network modeling, the association probabilities for each user to connect with MBS or SBS are calculated. Further, interference distributions are derived for a typical user with three possible instances, i.e. MBS user, SBS user and D2D receiver (DR). In addition, a SIC with intra-user interference estimation (SIE) receiver to improve the decoding performance at MBS/SBS user by locally estimating the intra-user interference, is proposed. Both perfect and imperfect cancellation for SIE are considered. The outage, throughput and energy efficiency performances of a typical user for both conventional SIC and proposed SIE operations, are evaluated.

- In Chapter 5, NOMA is applied to group D2D communications. A quality of service (QoS) based NOMA (Q-NOMA) group D2D communications in which D2D users are randomly distributed over a two-dimensional plane, is proposed. Unlike existing proposals, the D2D receivers (DRs) are ordered according to their QoS requirements, which is more appropriate for the D2D communications scenario. The spatial topology of D2D transmitters (DTs) is modeled by Gauss Poisson process (GPP) and DRs are considered to be randomly clustered around DTs. In addition, based on the QoS ordering, two policies to compute power allocation coefficients that can lead to two implementations of the proposed Q-NOMA group D2D communications, are proposed. Based on stochastic geometry results, the interference at the probe DR is characterised and insightful results are obtained by applying Gaussian–Chebyshev and Gauss–Laguerre quadratures. In order to evaluate the performance, the closed-form expression for outage probability of DRs in the proposed Q-NOMA group D2D communications, is further derived.
- In Chapter 6, NOMA is proposed as a spectrum efficient means of supporting massive connectivity in UWSNs, and its performance in a downlink scenario where sink transmits to a group of sensors using NOMA in the presence of cross-technology (CT) nodes and other interferences is investigated using stochastic geometry. The sensors, sinks and CT nodes can reside randomly and independently of each other in a two-dimensional (2D) plane. Hence, their spatial topologies are modeled with three different homogeneous Poisson point processes (PPPs). The closed-form expression for outage probability at the probe receiver’s location is further derived and its diversity order analysed. The average link throughput and energy consumption efficiency performances are compared between NOMA and OMA based UWSNs. Moreover, in order to assess the

practicality of utilising NOMA for UWSNs, a computational complexity analysis is performed to evaluate the complexity required by SIC units of sensor receivers to decode NOMA message signals.

- In order to enhance the system performance in low SNR regime, a HMA scheme that dynamically schedules users for either OMA or NOMA while satisfying a necessary condition derived based on the transmit SNR and user targeted rate, is proposed. The scheme is flexible enough to be applied to any NOMA group size and aims to achieve a better overall system performance than pure NOMA and OMA. Further, a channel gain stretching (CGS) scheme for applying NOMA effectively in HMA under similar channel conditions is designed. An optimisation problem is formulated, which is solved numerically to obtain the K for G_2 that results in the optimal throughput for the proposed HMA system. In addition, the exact closed-form expression for the outage probability is derived to evaluate the decoding performance of proposed HMA.
- To address the SIC issues that can limit the NOMA performance, an alternative receiver design based on PIC technique is investigated. The possible implementations of PIC-based receiver structure for downlink NOMA are presented and the associated design challenges are discussed. The estimation of intra-user interference from downlink NOMA signal is an important design consideration for the proposed receiver as it has a major impact on the decoding performance of the NOMA user. Hence, in the second half of this chapter, an equivalent model for downlink NOMA transmission is presented and stochastic geometry is applied to model the intra-user interference in downlink NOMA signal. Based on the modeling results, a simple algorithm is proposed to estimate and cancel the intra-user interference from the received downlink NOMA signal. Unlike NOMA-SIC which requires proper rate and power allocation to keep NOMA

operational, the proposed algorithm eliminates this requirement by estimating and canceling the intra-user interference in a single step. The closed-form expression for outage probability is derived and a performance comparison between NOMA under the proposed algorithm and NOMA-SIC is made.

1.2.1 Publications

J1: A. Anwar, B.-C. Seet, S. F. Hasan, X. J. Li, P. H. J. Chong, and M. Y. Chung, "An Analytical Framework for Multi-Tier NOMA Networks with Underlay D2D Communications," accepted for publication in *IEEE Access*.

J2: A. Anwar, B.-C. Seet, and Z. Ding, "Non-orthogonal multiple access for Ubiquitous Wireless Sensor Networks," *Sensors*, 8(2): 516, 2018.

J3: A. Anwar, B.-C. Seet, and X. J. Li, "Quality of Service based NOMA Group D2D Communications ," *Future Internet*, 9(4):73, 2017.

J4: A. Anwar, B.-C. Seet, and X. J. Li, "Hybrid Multiple Access with Channel Gain Stretching for 5G Downlink Systems ," under submission to a journal.

C1: A. Anwar, B.-C. Seet, and X. J. Li, "NOMA for Similar Channel Conditions," *3rd EAI International Conference on Smart Grid and Innovative Frontiers in Telecommunications (SMARTGIFT)* , Auckland, New Zealand, April 2018.

C2: A. Anwar, B.-C. Seet, and X. J. Li, "Interference Modeling and Outage Analysis for 5G Downlink NOMA," *IEEE VTC Workshop on Emerging NOMA Techniques for 5G*, Sydney, Australia, June 2017.

C3: A. Anwar, B.-C. Seet, and X. J. Li, "PIC-based receiver structure for 5G Downlink NOMA," *IEEE 10th International Conference on Information, Communications and Signal Processing (ICICS)* , Singapore, December 2015. /hl(nominated for best paper)

BC1: A. Anwar, B.-C. Seet, and X. J. Li, "Non-Orthogonal Multiple Access: Recent Advancements and Future Trends", In *Recent Advances in Information, Communications*

and Signal Processing (Eds. Khong et al.), River Publishers, Denmark, 2018.

1.3 Thesis Organisation

The rest of this thesis is organised as follows:

Chapter 2 provides the background concepts underlying this thesis. Specifically, it gives an overview of the two paradigm technologies of NOMA and D2D which are considered as promising candidates to enhance the spectral efficiency of 5G systems. Moreover, an introduction to point processes is also given, which are employed for system modeling and analysis in this thesis.

Chapter 3 reviews the relevant research literature, which is organised as follows: First, representative works on NOMA for cellular networks are discussed. Then, considering D2D communications as a promising technology to enhance the spectrum efficiency, the works exploring the application of NOMA to D2D communications are reviewed. Next, the works investigating the potential of applying NOMA to WSNs are analysed. Consequently, sections 3.1-3.3 review the existing works that consider the application of NOMA to three different networks (cellular, D2D, and WSN). Observing the negligible gain of NOMA over OMA at low SNRs and the SIC related issues that impact NOMA performance, sections 3.5 and 3.6 are dedicated to reviewing works related to HMA, and receiver structure for NOMA, respectively.

Chapter 4 investigates the multi-tier NOMA networks with underlay D2D communications. Chapters 5 and 6 explore the potential of applying NOMA to group D2D communications and UWSNs, respectively, under interference limited environment. Chapter 7 presents the HMA scheme with channel gain stretching for improving the system performance in low SNR regime. In Chapter 8, PIC-based receiver structure is proposed for NOMA to alleviate the SIC related issues.

Finally, Chapter 9 concludes the thesis with some suggestions for future work.

Chapter 2

Background

This chapter briefly visits and describes the background theory and concepts which are extensively utilised in the rest of this thesis.

2.1 Multiple Access Techniques for Wireless Communication

Every wireless system must implement a defined procedure to support multiuser communication by sharing a common access medium among different users. Depending on the type of wireless system, it may explicitly share or divide the common access medium into smaller parts termed *resources* such as frequency channels and time slots. These resources are then utilised to grant multiple users access to communicate over this common medium access. In particular, a single resource is utilised by one transmit/receive pair for communication. However, the pool of resources available to a wireless system is typically far less than the number of transmit/receive pairs present in the system. As a consequence, in order to realise multiuser communication, every wireless system must have some set of protocols which are used to share available resources to facilitate communication between active transmit/receive pairs. This protocol/procedure to share

available channel(s) among different transmit/receive pair is known as *multiple access* (MA) or *medium access* [14, 15].

The MA schemes can be broadly classified as contention-free and contention-based techniques. The *contention-free* techniques implement some mechanisms under which the available transmission resources are assigned to active transmit/receive pairs to realise communication. As a result, each user is assigned with a dedicated resource for the entire duration of its communication. As such, the contention-free MA schemes particularly suit scenarios where users require continuous access to a resource. Consequently, this type of MA scheme is attractive to cellular networks, where users require regular transmission/reception of voice or data [16]. In what follows, an overview of contention-free and contention-based MA schemes is provided.

The major types of contention-free MA schemes include frequency division multiple access (FDMA), time division multiple access (TDMA), code division multiple access (CDMA), and orthogonal frequency division multiple access (OFDMA). In *FDMA* systems, the resources are defined in terms of frequency channels. That being said, every transmitter is allocated with a fraction of an available spectrum which enables all the transmitters to remain active simultaneously. In contrast to FDMA, multiple users in a *TDMA* system can access the entire available spectrum but each user is granted access for a predetermined time, termed *time slot*. The transmission in TDMA system occurs in terms of frames, where each frame has a fixed number of time slots. As a result, the users served per frame in TDMA are equal to the number of time slots per frame. In addition, due to imperfect synchronisation among users, guard times are inserted within each frame in order to avoid inter time slot collisions. In terms of efficiency, both TDMA and FDMA schemes are equivalent and are considered as orthogonal multiple access (OMA) schemes due to the absence of co-channel interference [17, 18].

It is evident from the aforementioned discussion that TDMA and FDMA systems maintain orthogonality between user transmissions in time and frequency domains,

respectively. CDMA is another class of contention-free MA scheme where resources are in terms of user codewords. Each user in CDMA system is allocated with a unique codeword which is orthogonal to those of all other users. The codewords in CDMA system are pseudo-random waveforms that are used to spread the users' messages over the entire spectrum bandwidth. In this way, every user has an access to complete available spectrum for communication [19].

Another important class of contention-free MA schemes is OFDMA, which is based on an orthogonal frequency division multiplexing (OFDM) transmission technique. The OFDM system divides the entire available spectrum into orthogonal subchannels of relatively small bandwidth. Each subchannel is assigned with a separate subcarrier which results in a flat fading response for small subcarrier spacing. The information bits of an incoming message are spread among subcarriers. Separate modulation is performed at each subcarrier and the resulting signal, termed OFDM symbol, is then transmitted by superimposing all of those modulated signals. As a result, all the subcarriers in OFDM system are used to transmit the message signal of a single user [20]. In order to facilitate multiuser communication, OFDM can be combined with FDMA to result in a MA scheme known as OFDMA. In an OFDMA system, the total subcarriers in a single OFDM symbol are shared among multiple users in an orthogonal manner, where a fraction of available subcarriers in an OFDM symbol is allocated to each user [21].

In situations when traffic is bursty, the users require access to resources only for a short period of time and hence contention-free MA schemes are not very efficient. A promising solution to serve users under bursty traffic situations is to utilise *contention-based* MA schemes, which consider the entire available spectrum as one frequency channel. Such MA schemes are suitable for communication in wireless sensor networks (WSNs) where users contend or compete for the channel whenever they want to transmit [14]. Having this succinct overview of contention-free and contention-based MA

schemes, a new member of MA schemes known as NOMA, is discussed in the next subsection.

2.2 Non-Orthogonal Multiple Access (NOMA)

NOMA is considered as a promising MA scheme to increase the system capacity for future 5G communication systems. The basic idea of NOMA with power domain multiplexing is to allocate different power levels to multiple users and send the superimposed signal using same time, frequency or code resources. Multiuser detection is performed at the user receiver by using SIC technique. NOMA with power domain multiplexing can be implemented in both downlink and uplink to increase the system capacity [22–24]. It should be noted that there are various forms of NOMA which are proposed and investigated in literature. However, this thesis focuses on the power domain NOMA, which is simply referred to as NOMA in the rest of this thesis. The basic operational principle of downlink NOMA can be described as follows.

Let us consider a scenario of downlink cellular transmissions in which a base station (BS) is simultaneously transmitting signal to all the UEs in a cell, as shown in Figure 2.1. Assume that there are a maximum of N UEs in a cell. Let h_n be a channel gain (power) between UE n and the BS. Consider that users are ordered as $h_1 \leq \dots \leq h_n$, then according to NOMA principle, the power allocation coefficients are given as $a_1 \geq \dots \geq a_N$, where a_n is the power allocation coefficient for UE n . In addition, assume that the total transmission power at the BS is constrained to P , such that $\sum_{n=1}^N a_n P = 1$. As a result, the superimposed signal of all the UEs transmitted by the BS is then given by [25, 26]:

$$s = \sum_{i=1}^N \sqrt{h_i a_i P} s_i, \quad (2.1)$$

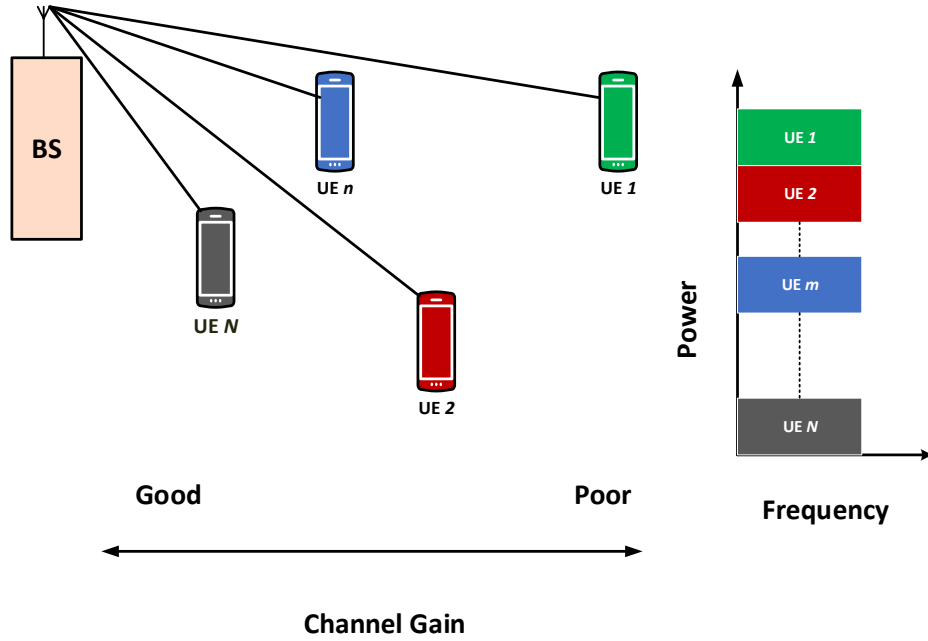


Figure 2.1. Downlink NOMA transmission.

where s_i is the message signal for UE i . The received signal at the UE n can be represented as:

$$r_n = \sum_{i=1}^N \sqrt{h_i a_i P} s_i + v_n, \quad (2.2)$$

where v_n is the additive white Gaussian noise (AWGN) at UE n receiver.

The optimal decoding order for the users is in the order of increasing channel gains. Hence, in this case of channel gains order, the UE having the least channel gain will decode its signal in a straightforward manner, as it will treat all the signals from other UEs as noise. At the receiver of UE n , all the message signals for higher order UEs $1, \dots, n-1$ will be considered as interference and they will be removed in a successive fashion using SIC. After the removal of the interference from higher order UEs, it will decode its own message signal by treating messages for lower order UEs $n+1, \dots, N$

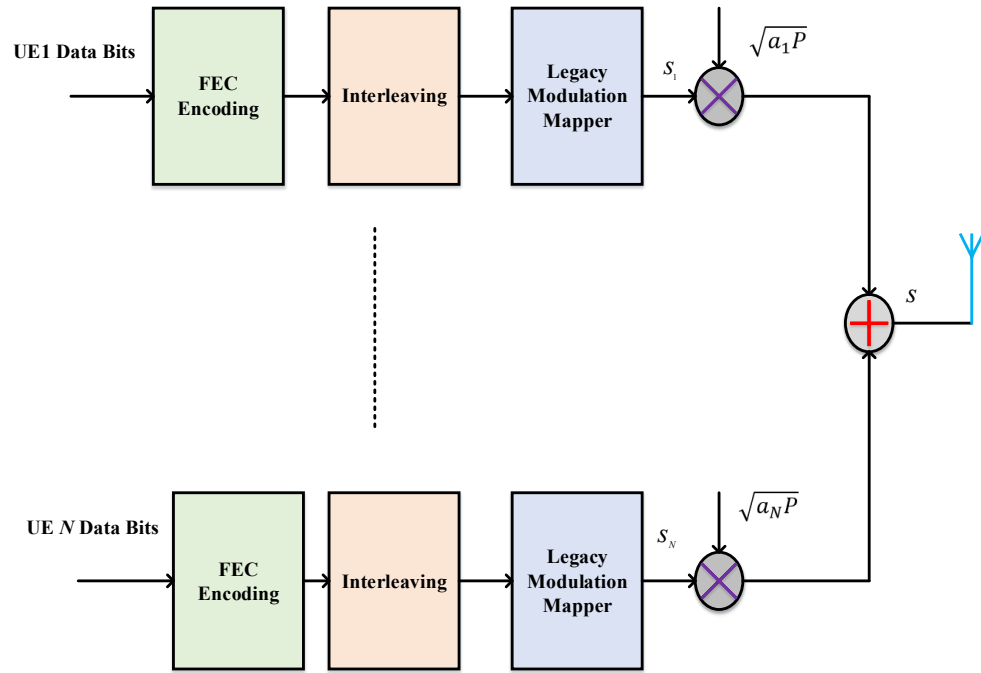


Figure 2.2. NOMA transmitter architecture.

as noise [25].

NOMA Transmitter and Receiver Architectures

A transmitter and receiver architectures for downlink NOMA system are shown in Figures 2.2 and 2.3, respectively. At the transmitter side, the input data bits are converted into the codewords by forward error correction (FEC) encoding block. The output of the FEC block is interleaved by the interleaving block, which is then fed into modulation block to obtain the transmitted signal s_n for UE n , where $1 \leq n \leq N$. In order to realize a power domain multiplexing, the message signal of every UE is multiplied by the allocated power, i.e., s_n is multiplied with $\sqrt{a_n P}$. The transmitted NOMA signal s is then constructed by adding the message signals of all the UEs. At the receiver side, SIC is performed to remove the intra-user interference followed by demodulation. The output of the demodulation is then fed into the deinterleaving block. Finally, the FEC decoding is performed to obtain an estimate of the message signal of

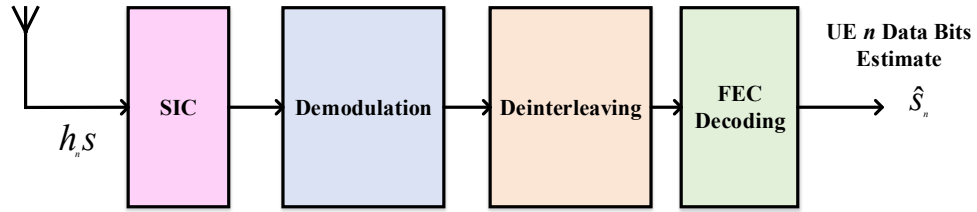


Figure 2.3. NOMA receiver architecture.

UE.

2.3 Device-to-Device Communications

Apart from NOMA, another capacity enhancement approach that has recently gained popularity for 5G networks is to invoke direct communication between devices or D2D communications. This approach can boost the overall spectral efficiency of the system due to its ability of offloading traffic from the cellular network. The D2D communication can be broadly classified into two categories, namely *inband* and *outband* D2D communications.

In *inband* D2D, the D2D links still operate in licensed band and available cellular spectrum resources are utilised for both D2D and cellular users. In particular, the *inband* D2D communication can be further divided into *underlay* and *overlay* modes. In the *underlay* mode, the entire licensed spectrum is shared by both cellular and D2D users for communication i.e., no resources are specifically reserved for D2D or cellular users. As a result, the *underlay* D2D operation enhances the overall spectrum efficiency at the cost of increased interference. In the *overlay* mode, the D2D users are allocated with dedicated spectrum resources, which helps to avoid interference but results in poorer spectral efficiency than the *underlay* mode [27, 28].

On the other hand, *outband* D2D operates in the unlicensed spectrum, and thus the D2D users do not cause interference to the cellular users. In order to realise

outband D2D, an extra air interface (such as WiFi Direct) in addition to that for cellular network, is also required at the users' receiver [27]. As a result, outband D2D can be further classified into controlled and autonomous modes. In *controlled* mode, the cellular network controls the D2D interface of user's device [29, 30], whereas in an *autonomous* type, the D2D users themselves control the interface [31]. It should be noted that the outband D2D causes no interference to the cellular users, but due to the uncontrolled nature of transmissions in the unlicensed spectrum, the D2D users can experience interferences from other devices that are transmitting in the same unlicensed spectrum [27].

2.4 Point Processes

A general wireless communication system can be regraded as a collection of nodes randomly distributed in a two dimensional (2D) space (higher dimensions are possible, but the research in this thesis only considers 2D networks). In other words, the wireless nodes in a network can be viewed as a random pattern of points in 2D space, where the physical location of each node typify a point in the 2D space. Stochastic geometry offers elegant methods and tools to model and analyse wireless networks by averaging over all possible configurations of the randomly distributed wireless nodes. In particular, the network snapshot at some time instant is considered as a realisation of a spatial point process (PP). The PPs offer flexibility of modeling a wide range of wireless networks and ease of analysing such networks in a probabilistic manner using a minimum number of physical parameters [32, 33].

Based on the different wireless networks considered in the chapters that follow, this thesis utilises and applies different types of PPs (to be discussed in subsequent sections) in order to model the spatial topology of the considered network. More specifically, the random spatial locations of different network entities such as BSs, cellular users, and

sensors are modeled by applying the appropriate PP model. In what follows, a brief discussion of different types of PPs that are utilised in this thesis is presented.

A PP can be formally defined as follows:

Definition 2.1. (*Point Process [34]*): A PP, denoted by Φ , is a collection of countable randomly distributed points in some measure space, such as Euclidean space, \mathbb{R}^2 .

Random measure formalism is a general way of describing a PP in which a number of points belonging to sets $B \subset \mathbb{R}^2$ are used to characterise PP. Consider a non-negative random variable (RV) $N(B)$ to represent the number of points in set B , then, given Φ , N can be obtained as:

$$N(B) = \sum_{\Phi} \mathbf{1}_{\Phi \cap B}, \quad (2.3)$$

where $\mathbf{1}$ is an indicator function and the RV N in (2.3) is known as *random counting measure*.

A very useful quantity to describe a PP is an *intensity*, denoted as λ , which is defined as the average number of points of Φ per unit area or volume. The PP process Φ is called *uniform* or *homogeneous* if its intensity measure does not depend on the location. However, if the intensity measure is a function of location, then the resulting PP is termed as *inhomogeneous* or *non-uniform* PP. Based on intensity λ , the expected number of points in a set B can be obtained as: $\Delta(B) = \mathbb{E}[N(B)] = \int_B \lambda(x) dx$, where Δ is known as *intensity measure* of Φ .

Depending on the type of wireless network and communication scenario, different PPs are utilised for modeling the networks under consideration. Particularly, PPs provide analytical tools to characterise interference at a typical user (randomly chosen receiver) under interference-limited environments where multiple nodes are transmitting simultaneously using the same spectrum resources. This in turn allows the performance

evaluation of a given network in terms of metrics such as outage probability and throughput.

The interference (formally defined later in subsection 2.4.6) at a typical user is viewed as the sum of transmissions from all active transmitters in the network. In order to evaluate the performance of a typical user, the distributional characterisation of interference is necessary. As such, the probability generating functional (PGFL) of a PP is defined, and then utilised to characterise the distribution of interference in terms of the Laplace transform. The PGFL of a PP Φ can be formally defined as follows:

Definition 2.2. (*Probability generating functional of a point process [35]*): Let v be a function such that $v : \mathbb{R}^2 \mapsto [0, 1]$, then, PGFL of PP Φ , denoted as $\mathcal{G}[v]$ is defined as:

$$\begin{aligned} \mathcal{G}[v] &\triangleq \mathbb{E} \left[\prod_{x \in \Phi} v(x) \right] \\ &= \mathbb{E} \left[\exp \left(\int_{\mathbb{R}^2} \log v(x) \Phi(dx) \right) \right]. \end{aligned} \quad (2.4)$$

The two sufficient conditions for the existence of PGFL for PP are 1) Φ has a finite number of points, and 2) $v : \mathbb{R}^2 \mapsto [0, 1]$, and intensity measure Δ satisfies $\int_{\mathbb{R}^2} |\log v(x)| \Delta(dx) < \infty$. Readers may refer to [[35]] for more detailed discussion of the topic. Now having the definition and description of Φ , $\Delta(\cdot)$, λ and $\mathcal{G}(\cdot)$ in hand, some important PPs used for modeling and analysis in this thesis are discussed in the next section.

2.4.1 Poisson Point Process (PPP)

A PP Φ with intensity measure Δ is a PPP on \mathbb{R}^2 if it possesses the following properties [36]:

- The RV $N(B)$ is Poisson distributed with mean $\Delta(B)$, where $B \subset \mathbb{R}^2$. If Δ has

an intensity λ , then,

$$P(N(B) = k) = \exp\left(-\int_B \lambda(x) dx\right) \frac{\left(\int_B \lambda(x) dx\right)^k}{k!};$$

- Whenever B_1, \dots, B_n are disjoint, then $N(B_1), \dots, N(B_n)$ are independent.

Note that homogeneous PPP is a special case where $\Delta(B) = \lambda|B|$. The PGFL for a PPP is given as [34],

$$\begin{aligned} \mathcal{G}[v] &\triangleq \mathbb{E}\left[\prod_{x \in \Phi} v(x)\right] \\ &= \exp\left(-\int_{\mathbb{R}^2} [1 - v(x)] \Delta(dx)\right) \end{aligned} \quad (2.5)$$

Due to the independence property of PPPs, they are considered to be completely random spatial models. That being said, there is no interaction between the points of PPP. This eventually leads to a very useful result for PPP under which the conditioning on a point x of PPP does not change the distribution of the rest of the process. This result for PPP is known as Slivnyak's theorem [35]. These characteristics made PPPs very popular for modeling wireless networks due to their simplicity and analytical tractability. As a result, PPPs are accurate for modeling networks where nodes reside independently of each other. Examples of such situations include those users in the cellular networks who are located independent of the BS locations or sensors in WSNs.

2.4.2 Determinantal Point Process (DPP)

PPP offers a reasonable approach for modeling completely random spatial networks. However, there are situations where points of PP exhibit interaction (repulsion/attraction). For example, the PP generated by macro-cell BSs (MBSs) is not completely random

due to the existence of interaction (repulsion) between the nodes of the PP. This means that in reality, no two MBSs can lie in proximity of each other if the distance between them is less than the minimum separation distance. Hence, modelling locations of MBSs with PPP is not realistic, as the PPs generated by MBSs are more regular and less random as compared to PPP [37].

Determinantal point process (DPP) is a class of PPs that is used to model the regular PP. The analytical tractability of DPP makes it a reasonable choice to model the PPs that exhibit interaction [37, 38]. DPP can be formally defined as follows.

Let Φ be a PP defined on the Euclidean plane \mathbb{R}^2 , then Φ is known as a determinantal point process if its n -th joint intensity obeys the following relationship:

$$\varphi^{(n)}(n) = \det (K(x_i, x_j))_{1 \leq i, j \leq n}, (x_1, \dots, x_n) \in (\mathbb{R}^2)^n,$$

where $K : \mathbb{R}^2 \times \mathbb{R}^2 \rightarrow \mathbb{C}$ is a square matrix known as DPP kernel and \mathbb{C} denotes the complex plane. Readers are referred to [39, 40] and references therein for details of the conditions required for the existence of DPP.

If K is a kernel such that it guarantees the existence of DPP Φ , then the PGFL of a DPP is given as [41]:

$$\begin{aligned} \mathcal{G}[v] &\triangleq \mathbb{E} \left[\prod_{x \in \Phi} v(x) \right] \\ &= \sum_{n=0}^{\infty} \frac{(-1)^n}{n!} \int_{(\mathbb{R}^2)^n} \det (K(x_i, x_j))_{1 \leq i, j \leq n} \prod_{i=1}^n [1 - v(x_i)] dx_1 \dots dx_n. \end{aligned} \quad (2.6)$$

A DPP is said to be *stationary* if its kernel K has the following form:

$$K(x, y) = K_0(x - y), \quad x, y \in \mathbb{R}^2,$$

where K_0 is termed covariance function of the stationary DPP. It should be noted that

the intensity measure of stationary DPP is constant over \mathbb{R}^2 .

Among different types of DPP models, Gauss DPP maintains a balanced tradeoff between modeling accuracy and analytical tractability [37]. A stationary PP Φ is called a Gauss DPP if its covariance function K_0 assumes the following form [40]:

$$K_0(x) = \lambda \exp\left(-\frac{\|x\|^2}{\kappa^2}\right), \quad x \in \mathbb{R}^2. \quad (2.7)$$

where λ and κ represent the intensity and measure of repulsiveness for Gauss DPP, respectively.

2.4.3 Poisson Cluster Process (PCP)

Apart from completely random spatial wireless networks that have interaction among nodes, there are situations when users exhibit correlation with some geographical locations and are distributed in a clustered manner around these locations. For example, the areas of high user density in cellular networks represent such spatial locations where users show clustered behaviour. The geographical centres of these areas may represent user hotspots or positions of user-centric deployed small cell SBSs in order to meet capacity requirements in these congested areas. As such, PCP is a class of PP that offers flexibility to model networks in which users show clustered behaviour. In particular, PCP is defined in terms of parent PP and daughter PPs. The parent points themselves are not included in PCP. The PCP can be formally defined as follows.

Consider the parent process is a homogeneous PPP denoted as $\Phi_p = \{x_1, x_2, \dots\}$ with intensity λ_p . Then PCP can be generated by considering independent daughter PPs, one per parent point location, and translating them to the position of their parent. Let n represents the total number of parent points, and Φ_i denotes the family of untranslated daughter process. The PCP Φ is then given by the union of all the translated clusters

as [34]:

$$\Phi = \bigcup_{i \in [n]} \Phi_i + x_i.$$

The two important types of PCP are Thomas cluster process (TCP) and Matern cluster process (MCP) in which the number of points in the daughter processes are Poisson distributed with mean \bar{c} . The intensity of PCP Φ is given as $\lambda = \lambda_p \bar{c}$. The daughter point in MCP and TCP is distributed according to uniform and normal distributions (with variance σ^2), respectively, around the parent point. Hence, probability density function (PDF) of daughter point $y \in \mathbb{R}^2$ relative to parent point (cluster centre) is given by [42]:

$$f_{\text{MCP}}(y) = \begin{cases} \frac{1}{\pi r^2}, & \|y\| \leq r \\ 0, & \text{otherwise.} \end{cases} \quad (2.8)$$

$$f_{\text{TCP}}(y) = \frac{1}{2\pi\sigma^2} \exp\left(-\frac{\|y\|^2}{2\sigma^2}\right). \quad (2.9)$$

The PGFL for MCP and TCP is given as [34, 35]:

$$\begin{aligned} \mathcal{G}[v] &\triangleq \mathbb{E} \left[\prod_{x \in \Phi} v(x) \right] \\ &= \exp \left(-\lambda_p \int_{\mathbb{R}^2} \left[1 - \exp \left(\bar{c} \left[\int_{\mathbb{R}^2} v(x+y) f(y) dy - 1 \right] \right) \right] dx \right), \end{aligned} \quad (2.10)$$

where f in (2.10) is given for MCP and TCP in (2.8) and (2.9), respectively.

2.4.4 Poisson Hole Process (PHP)

The PHP is useful in modeling wireless networks where exclusion zones (holes) are considered around nodes such that no transmitter inside holes is allowed to transmit. This

naturally captures the notion of interference management by restricting the transmitters away from receiver at distances greater or equal to hole radius. An example scenario consists of inband (underlay) D2D communication where exclusion regions are created around cellular users by BS to avoid excessive interference from D2D transmitters by restricting them to outside the holes.

The PHP can be defined formally as follows.

Consider two independent homogeneous PPPs $\Phi_1(\lambda_1)$ and $\Phi_2(\lambda_2)$, with $\lambda_1 > \lambda_2$, then PHP Φ can be defined as [43]:

$$\Phi = \{x \in \Phi_1 : x \notin E_D\} = \Phi_1 \setminus E_D, \quad (2.11)$$

where $E_D = \bigcup_{y \in \Phi_2} b(y, D)$ is the region covered by the holes and $b(y, D) \equiv \{z \in \mathbb{R}^2 : \|z - y\| < D\}$ is a ball of radius D centred at location y .

It should be noted that conditioned on Φ_2 (holes locations), the PHP is simply a PPP of intensity λ_1 over $\mathbb{R}^2 \setminus E_D$. As a result, Slivnyak's theorem for PPP is also applicable to PHP.

2.4.5 Marked Point Process (MPP)

It is often desirable in wireless networks to differentiate between different types of nodes on the basis of some information associated with the nodes. For example, in heterogeneous networks, it is useful to signify the type of node (e.g. mobile user, BS, WiFi access point etc). Another situation is to determine the state of a node as either transmitter or receiver. This information about the points of PP can be attached to each point by assigning them a RV known as mark [34]. This leads to the definition of MPP as follows.

Consider a PP Φ , known as *ground process*, which is defined over a 2D plane \mathbb{R}^2 . Consider another space \mathbb{M} known as a marked space. A MPP $\tilde{\Phi} = \{(x, m_x)\}$ is defined

over space $\mathbb{R}^2 \times \mathbb{M}$ such that $\tilde{\Phi}(B \times \mathbb{M}) < \infty$, is considered as a collection of random points $\{x\} \equiv \Phi$ with marks $\{m_x\}$ from \mathbb{M} attached to each point [44].

The MPP $\tilde{\Phi}$ is said to be an independent MPP if the mark m_x for point x depends only on x and not on any other point or mark with distribution $F(\cdot)$ on \mathbb{M} . In addition, when marks are identically distributed, i.e. they do not depend on ground points locations, the resulting process is termed independent and identically distributed (i.i.d) MPP. An independent MPP has two implications. 1) The ground process Φ is a PPP on \mathbb{R}^2 with intensity measure Δ and conditioned on Φ , the marks are independent with distribution $F(\cdot)$ on \mathbb{M} , and 2) $\tilde{\Phi}$ is a PPP on $\mathbb{R}^2 \times \mathbb{M}$ [34].

In case of independent MPP, the PGFL is given as [44].

$$\mathcal{G}[v] = \exp \left[- \int_{\mathbb{R}^2} \left(1 - \int_{\mathbb{M}} v(x, m) F_x(dm) \right) \Delta(dx) \right], \quad (2.12)$$

where v is a family of all functions such that $v : \mathbb{R}^2 \times \mathbb{M} \rightarrow \mathbb{R}^+$.

2.4.6 Interference over a Point Process

Sharing the same spectrum resources by users in a wireless network gives rise to an interference limited network. Under such scenarios, the interference at a typical user is defined as the sum of all signals (power) from each unwanted transmitter in the network. If locations of users are modeled by some spatial PP Φ , then the interference is considered as the sum of functions over the points of PP. As a result, the interference, denoted as \mathcal{I} , at typical user located at x_0 is given as:

$$\mathcal{I} = \sum_{x \in \Phi} P_x h_x \|x - x_0\|^{-\alpha}. \quad (2.13)$$

where P_x are the transmit power of transmitter at x , h_x is the channel between typical user at x_0 and transmitter at x , and $\alpha > 2$ is the pathloss exponent. Note that interference

\mathcal{I} in (2.13) is a random function defined over the points of Φ . As such, the distribution of \mathcal{I} can be characterised by determining the Laplace transform of \mathcal{I} as follows:

$$\begin{aligned}
 \mathcal{L}_{\mathcal{I}}(s) &= \mathbb{E} \left[e^{-s\mathcal{I}} \right] = \mathbb{E} \left[e^{-s \sum_{x \in \Phi} P_x h_x \|x - x_0\|^{-\alpha}} \right] \\
 &= \mathbb{E} \left[\prod_{x \in \Phi} e^{-s P_x h_x \|x - x_0\|^{-\alpha}} \right] \\
 &= \mathbb{E}_{\Phi} \left[\prod_{x \in \Phi} \mathbb{E}_{h_x} \left(e^{-s P_x h_x \|x - x_0\|^{-\alpha}} \right) \right] \\
 &= \mathcal{G} [v(x)], \tag{2.14}
 \end{aligned}$$

where $v(x) = \mathbb{E}_{h_x} \left(e^{-s P_x h_x \|x - x_0\|^{-\alpha}} \right)$.

The Laplace transform characterises the complete distribution of the random process/RV. Therefore, based on (2.14) and using the corresponding PGFL for the PP Φ , the interference \mathcal{I} defined over points of Φ can be completely characterised.

2.5 Chapter Summary

This chapter has provided a brief overview of the background concepts and theories underlying this thesis. In particular, two broad classifications of MA schemes extensively used in wireless networks are discussed. Moreover, being the latest member of the MA family, the fundamental principles of downlink NOMA with SIC operation, are introduced. Further, owing to the random spatial topology of wireless networks, various PP models that offer a reasonably accurate approach and rich tools for modeling and analysing the networks considered in this thesis, are briefly discussed. Finally, based on the discussed PP theory, the distribution of interference at a typical user can be completely characterised with the aid of its Laplace transform, providing the basis for deriving other performance metrics such as outage probability and link throughput in

CHAPTER 2. BACKGROUND

the subsequent chapters.

Chapter 3

Literature Review

In order to design the study conducted in this thesis, it is necessary to identify the research gaps in existing literature on NOMA. Hence, this chapter presents an in-depth literature review, which leads to the identification of several problems that inform this research.

3.1 NOMA for Cellular Networks

3.1.1 Single-Cell Single-Tier Scenario

In current literature, the downlink NOMA is investigated with SIC receiver at the user equipment (UE) side. In [6, 25, 45], the performance of NOMA technique is evaluated with SIC receiver by performing system level simulations. In [25], the authors suggested NOMA a promising multiple access scheme for future cellular systems. The utilisation of additional power domain by NOMA for user multiplexing, the expected increase in the device processing capabilities for future systems and robust performance gain are the key motivations behind this proposal. The authors performed system level simulations and compared the performance between NOMA and OFDMA. They presented the

comparison in terms of the number of users and the overall cell throughput under frequency-selective/wideband scheduling and power allocation. The authors reported a performance gain of 30 – 35% in the overall cell throughput for NOMA over OFDMA.

In order to achieve a further performance gain using NOMA, the authors proposed combination of NOMA with MIMO and multi-site extensions as possible future extensions. The authors adopted SIC receiver for NOMA as a standard decoding scheme at the UE side. This choice implies that the performance of NOMA is directly dependent upon the decoding performed by SIC receiver. Hence, a decoding failure by SIC results in performance limitation of NOMA. However, in the comparisons presented in [6], they assumed a perfect decoding for SIC and hence, neglected the impact of decoding failure and error propagation of SIC on the performance of NOMA.

In [13], the authors considered a single cell case for downlink NOMA and modelled the cell using a circular disc geometry of radius R_D . They assumed that the users are distributed randomly with uniform distribution in the circular disc. In order to evaluate the performance of downlink NOMA, they presented two scenarios for user's rate and calculated the corresponding performance metric. In the first scenario, the QoS requirements of the user are utilized to determine the data rate. They considered two events: the idealistic suppression of the interference caused by all the higher order users and the ability of the NOMA in order to satisfy the QoS requirements of the user. In the second scenario, they calculated the user's rate opportunistically based on his channel conditions. The outage probability is considered as a performance metric in first scenario, while for the second scenario, the achievable ergodic sum rate by NOMA transmission protocol is adopted. The analytical and numerical results show that the NOMA is able to achieve better outage and ergodic sum rate performance than OMA. However, there are two critical factors that can adversely affect the outage performance of the system, namely the selection of user's targeted rate and the choice of power allocation coefficient. The reason is that a wrong or inappropriate choice of a power

allocation coefficient will result in a decoding failure for SIC and consequently this will lead to high outage probability.

In [6] and [45], to incorporate the practical prospects of the cellular systems into their system level simulation evaluations of downlink NOMA with SIC receiver, the authors combined LTE radio interface functionalities such as time/frequency domain scheduling, adaptive modulation and coding (AMC), hybrid automatic repeat request (HARQ) and outer loop link adaptation (OLLA) with NOMA specific operations such as dynamic power allocation. A proportional fairness (PF) scheduler was used to achieve the multi-user scheduling. Furthermore, dynamic transmit power allocation scheme (TPA) was used to distinguish the users in power domain. The HARQ mechanism was used in case if decoding error occurs.

In [6], the authors also presented an algorithm to implement the complete NOMA signal generation in the downlink. The authors in [45] used full search power allocation (FSPA) and fractional transmit power allocation (FTPA) to distribute the power among NOMA users. The signalling cost related to SIC decoding order and power assignment ratios will be enhanced with the use of dynamic TPA. FSPA scheme for NOMA achieved the best performance but it is computationally complex, as all combinations of power allocation are considered. However, FTPA provides a low complexity method for power allocation among NOMA users. The power decay factor (whose value ranges from 0 to 1) in FTPA is responsible for power allocation relative to the channel gain and is a parameter which requires optimisation in order to meet the required performance targets. In [45], the authors choose the value of power decay factor as 0.4. The impact of varying the power decay factor during FTPA is not considered by the authors, and the chosen power decay factor may not be a suitable choice for NOMA under some other communication scenarios such as users having comparable channel quality, equal power allocation or having fairness constraints.

The consequence of user grouping for NOMA with the power allocation is also

studied in [45]. The purpose of user grouping is to group those users who have a significant difference in their channel gains, so that the amounts of power allocated to them using TPA or FTPA will differ substantially. The authors reported a performance gain of 35 – 40% in [6,45] over OFDMA in terms of cell throughput and user rate under power allocations schemes of TPA and FTPA with multiuser scheduling. However, in both these works, the authors assumed a significant difference in channel conditions of the scheduled users, which may not always be true in practice. There exists a finite probability that at some of the transmission times, the scheduled users may not differ significantly in terms of channel gains, which implies negligible differences among their power allocations. This will lead to difficulty in grouping/pairing the users. Further, the SIC receiver is power sensitive [46], thus the performance of SIC will degrade intensely if two or more users have similar or comparable power. Consequently, by making an assumption of holding a significant difference in channel gains of the scheduled users, the authors of [6] and [45] ensure different power allocation to multiple users in order for SIC to work properly and hence neglected the impact of SIC decoding failure that may happen when there is not a significant difference in channel conditions of the scheduled users.

The impact of user pairing on the performance of NOMA was also investigated in [47]. The authors considered two downlink systems namely fixed power allocation NOMA (F-NOMA) and cognitive radio inspired NOMA (CR-NOMA), and then demonstrated the effect of user grouping on their performance. In F-NOMA system, the authors considered a case of two users and studied the impact of user grouping on the system performance. The authors analysed the system from the perspective of achievable sum rate (probability that F-NOMA achieves lower sum rate than conventional OMA) and user's individual rate (probability that F-NOMA achieves higher rate than OMA) and presented their closed form analytical expressions. Their results depicted a superior performance of F-NOMA over OMA.

However, they reported that the careful user grouping is required to obtain this performance, and in order to attain this performance benefit, the users with significant difference in channel qualities should be paired together. This implies that the performance gap achieved in F-NOMA over OMA is directly dependent upon the fact that how large is the difference in channel qualities for the grouped users. If the grouped users have similar channel conditions, then the benefit of using NOMA will be rather limited. This performance limitation is due to the inherent constraint attached to the use of SIC receiver with NOMA i.e. how efficiently the SIC receiver performs decoding and detection of multi-users is hugely relied on the spread of user powers [46, 48]. This was the reason why authors emphasised to maintain a significant difference between the channel conditions of the grouped users in order to achieve the performance gap over OMA by using F-NOMA scheme.

In CR-NOMA scheme proposed by the authors in [47], the user having lower channel gain is considered as primary user, while the user with strong channel is regarded as a secondary user. The secondary user has been allocated power opportunistically and is permitted to transmit on the channel of primary user only on the condition that it will not cause the performance of the primary user to degrade adversely. This condition is fair enough to maintain power difference between primary and secondary users and is sufficient for SIC technique employed at primary user's receiver to decode his data from downlink signal received in CR-NOMA scheme.

Therefore, the core purpose of CR-NOMA scheme is to serve primary user (user having poor channel gain) by allowing the secondary user to transmit on the condition that its transmission will not harm the primary user's signal. Consequently, this arrangement will achieve higher sum rate as compared to OMA. Apart from the requirement of having significant difference in channel gains to group the users and allowing secondary user to transmit on the primary user channel under the condition mentioned above so that the SIC will work properly, in both of the proposed schemes, the authors investigated

the user grouping impact by considering the case of two users. This makes grouping simple as only two users are picked from a large set of users. However, it is not a trivial problem to group more than two users (e.g., five) by maintaining the significant difference in channel conditions.

The issue of fairness achieved by downlink NOMA protocol is addressed by the authors in [5]. They considered a problem of distributing a total available power at the BS among the NOMA users and investigated its impact on the fairness under two situations: 1) determination of the user's data rate under perfect knowledge of channel state information (CSI) and 2) the user's data rate is determined on the average CSI i.e. a fixed targeted data rate. In first case, they adopted max-min fairness that aimed to maximise the minimum achievable rate by the user as a performance comparison metric, while in the second case, the outage probability was considered as a performance metric. In both cases, the authors considered the user's rate and outage probability as a function of power allocation coefficient and formulated them as a non-convex optimization problems. The authors proposed low complexity iterative power allocation coefficients as optimal solutions in both cases.

This work can be regarded as an extension of [13] by finding an optimal power allocation coefficients under two assumptions of perfect and average CSI for the users, with a focus on investigating its impact on the fairness achieved by downlink NOMA with SIC. The numerical results showed that with the use of proposed optimal power allocation schemes, NOMA maintains high fairness and can achieve superior performance in terms of rate and outage probability as compared to TDMA and fixed power allocation in [13]. However, this fairness will only be maintained when the power is allocated appropriately and deviation from this condition will result in high outage probability due to the decoding failure by SIC receiver.

The authors in [49] considered both uplink and downlink NOMA systems and investigated the problem of dynamic user clustering and power allocation. In order to

obtain optimal cluster size and power allocation for NOMA, they formulated a sum-rate maximisation problem subject to constraints of transmission power, SIC, and users QoS requirements. The optimal solution is obtained by dividing the given optimisation problem into two sub-problems, 1) user clustering, and 2) determination of their optimal power allocation. In order to obtain solution of sub-problem 1, they presented a low-complexity sub-optimal user clustering scheme by utilising distinctiveness among users channel gains. Based on user clustering algorithm, the optimal power allocation method is proposed to maximise the overall system sum-rate. The numerical results demonstrate that maintaining significant channel gain difference among users in each cluster can outperform conventional OMA scheme in terms of achievable throughputs. In addition, it is reported that there exists an optimal cluster size for NOMA users beyond which the performance of downlink NOMA deteriorates. However, their system model is restricted to single cell, thereby neglecting the impact of intra-cell interference from other BSs transmission in the performance of their proposed user clustering and power allocation methods.

The performance of downlink NOMA system with randomly distributed users is investigated in [50] for cases of imperfect and second order statistic (SOS) CSI. In order to evaluate the performance of the considered system, they derived closed-form expressions for outage probability and average sum rate for both cases. Numerical results are also presented to validate the accuracy of the derived results. The results demonstrate that under both cases of partial CSI, NOMA still outperforms its counterpart OMA in terms of both outage and sum rate. Although the derived analytical framework provides very useful system and performance insights, it is desirable to extend these results for the case of more realistic multi-cell and interference limited networks.

Considering a more realistic Nakagami-m fading channel model, the performance of NOMA system is studied in [51]. The considered network is comprised of a single

BS which communicates with NOMA users with the aid of amplify-and-forward relay. Closed-form expressions for outage probability are provided to investigate the performance of considered system. In addition, outage results are extended to obtain the diversity gain of the network in high SNR regime. Further, they also derived the ergodic sum-rate for the considered network and provide its upper and lower bounds. The accuracy of the derived analytical expressions is validated by numerical simulations. The results demonstrated that under Nakagami-m fading channels, the considered NOMA network is able to achieve superior performance and also provide better user fairness compared to the conventional OMA. However, the considered network model is more realistic to benefit those users who are much far from the BS to improve their SINR. But in realistic deployments and situations, BS may directly communicate with near users who have good SINR. As a result, in order to serve these users, there is no need to use relay node. Consequently, the considered network introduces additional complexity and delay to serve users with good SINR by restricting direct communication between users and BS and is not general to cover situations where direct communication between users and BS is not possible.

3.1.2 Single-Cell Multi-Tier Scenario

The problem of resource allocation for NOMA based single cell heterogeneous (multi-tier) networks is investigated in [52]. In the considered model, NOMA protocol is applied by only SBSs to communicate with their users. In order to maximise the sum rate of the SBS users, the authors presented a resource allocation problem in terms of many-to-one matching game. The authors then proposed a novel distributed algorithm to obtain the solution of the formulated game. The results demonstrated the fast convergence of their proposed algorithm to global optimal solution and SBS users achieve superior sum rate over OMA under the proposed resource allocation

strategy. However, the SBSs are typically deployed in areas of higher user density, i.e. they usually follow user-centric deployments in which the locations of users and SBS are correlated. Without considering this aspect, their modeling approach may not be accurate for modeling users' locations in heterogeneous networks with SBSs.

3.1.3 Multi-Cell Single-Tier Scenario

The authors in [53] analyse the uplink NOMA for large-scale cellular networks. The spatial locations of the BSs are modeled by a homogeneous PPP. Considering the locations of BSs as a parent PP, the spatial topology of users is modeled by PCP, in which users are clustered around the locations of BSs. This captures the correlation between the location of users and BS. In particular, they considered three scenarios of SIC, namely perfect SIC, imperfect SIC, and imperfect worst case SIC. In order to evaluate the performance of the considered network, the authors first derived a closed-form expression for intra-cluster interference. Then, based on the interference results, an expression for rate coverage is provided under all three scenarios of SIC. Numerical simulations are conducted to validate the accuracy of the derived analytical results and compare the proposed network with PPP- and OMA-based networks. The results show that the PCP-based network outperforms OMA-based network and offers more accurate analysis than the PPP-based approach, which provides optimistic results for NOMA. However, the considered system model is limited to a single tier case.

The problem of power allocation for OFDM based NOMA systems is studied in [54]. The considered cellular network is composed of 19 hexagonal grid sites having 3 cells per site. The authors formulated an optimisation problem to maximise the weighted sum rate of the entire system. Due to the intractability of the presented optimisation problem, it was solved in two steps. In the first step, the user selection across each subchannel and power assignment are performed by using greedy, and sub-optimal

iterative power allocation algorithms, respectively. In the second step, using the iterative power allocation algorithm of the first part, the power assignment across the sub-channel is achieved. The simulation results demonstrate the superiority of their proposed scheme over existing ones in terms of achievable system throughput. However, a fundamental limitation of their system model is the assumption of hexagonal grids with a regular shape and size, which may not always hold true in real cell site deployments.

A NOMA based multi-cell network is analysed in [55]. The locations of BSs are modeled by a homogeneous PPP, and a more realistic Voronoi cell structure is considered. The authors provided close-form expressions for the coverage probability and achievable rate. Numerical simulations are conducted to validate the accuracy of derived analytical results, and compare the achieved performance with that of OMA-based network. The results show that NOMA achieves higher coverage and achievable rate than OMA under the considered network setting. However, there are two potential shortcomings: 1) The performed analysis is limited to a case of only two users for single-tier networks; and 2) Modeling locations of MBSs by PPP is not accurate because real deployments of MBSs exhibit interaction between MBSs locations, whereas PPP does not capture this property due to its completely spatial random property.

3.1.4 Multi-Cell Multi-Tier Scenario

In [56], the authors consider the application of NOMA to K-tier multi-cell network. A comprehensive hybrid transmission framework is proposed under which MBSs and SBSs utilise massive MIMO and NOMA technologies to enhance the overall spectral efficiency. Under the considered K-tier network, the authors proposed a BS association policy for MBS and SBS users based on the biased average received power metric. The performance of the network is evaluated in terms of spectrum efficiency achieved by each tier, where the closed-form expressions are derived by using stochastic geometry

tools. Numerical results demonstrate that the proposed hybrid massive MIMO for NOMA based multi-tier network can achieve better spectrum efficiency than its OMA counterpart. Its potential shortcoming is the use of less realistic user distributions that do not capture the coupling between users' and SBS locations. In addition, MBS locations are modeled by homogeneous PPP, which does not reflect the deployment trend of real MBSs.

The application of NOMA to multimedia broadcast/multicast service (MBMS) is investigated for multi-cell K-tier network in [57]. Such a network aims to meet the high data rate demands of emerging applications by enjoying the efficient spectrum utilisation of both NOMA and MBMS techniques. The BS spatial topology of each tier is modeled by independent homogeneous PPP. Based on NOMA and MBMS, the authors proposed two transmission schemes and evaluated the performance of these schemes using stochastic geometry. An analytical framework is developed which is general enough to cover the cases of synchronous and asynchronous non-orthogonal MBMS transmission. Based on this framework, the authors derived closed-form expressions for coverage probability, sum rate and the number of users served. Simulations are conducted to verify the analysis. It was shown that non-orthogonal MBMS outperforms orthogonal MBMS. In addition, synchronous transmission mode can achieve better performance than the asynchronous one. However, the users in each tier are modeled by independent homogeneous PPPs. While this distribution is accurate for users who are located independent of BS locations, it does not capture the location coupling between users and SBS of multi-tier networks, where the latter is often deployed to enhance the service in areas of high congestion.

In [58], the authors considered a large-scale NOMA based multi-tier cellular network in which SBSs communicate with their users with the aid of NOMA protocol, whereas MBSs are equipped with massive MIMO capability. A tractable analytical framework is developed to analyse the performance of considered network. Closed-form expressions

for coverage probability are obtained for NOMA SBSs users. In addition, a lower bound for achievable ergodic rate is derived for a user served by massive MIMO enabled MBSs. Based on the coverage results, the energy efficiency of hybrid multi-tier networks is also investigated. Numerical results reveal that the performance of SBSs NOMA users is highly dependent on the choice of user targeted rates and power allocation coefficients. Moreover, equipping MBSs with massive MIMO capability significantly enhances the network's spectrum efficiency. While the developed model is analytically tractable, it suffers from two shortcomings: (i) NOMA is not utilised for MBSs, and (ii) it uses homogeneous PPPs to model MBSs and SBSs.

3.2 NOMA for D2D Communications

3.2.1 Paired D2D Communications

Recently, the authors in [59] proposed a full-duplex (FD) D2D aided cooperative NOMA. The BS sends a NOMA signal to one strong and one weak NOMA user, where the strong user is equipped with FD ability. By invoking D2D communication between strong and weak NOMA user pair, the authors proposed to improve the outage performance of the weak user using D2D-aided direct and cooperative transmissions. However, they only considered a single-cell scenario where NOMA is conducted at BS while strong and weak users communicate via conventional paired D2D communication.

The authors in [60] developed an analytical framework using stochastic geometry to analyse cellular networks with underlay D2D communications. The D2D users are also equipped with FD transceivers and can operate in FD mode. The authors proposed a criteria to select between FD and D2D modes of operation. They derived closed-form expression for outage probability to evaluate the performance of cellular and D2D users. However, they modeled spatial topology of D2D users by a PPP that may not be a

realistic distribution choice for D2D users. The reason is that PPP cannot capture the features of device clustering and spatial separation of D2D communications due to its completely random nature [61]. Furthermore, NOMA protocol is not applied for both cellular and D2D communications.

The authors in [62] considered a downlink multiuser MIMO NOMA cellular network with underlay D2D communications. They proposed two beamforming schemes in order to eliminate the inter-beam interference and the interference caused to D2D users by BS transmission. In addition, they formulated an optimisation problem to jointly optimise the performance of both cellular and D2D users. A potential limitation to their approach is that the considered system model is limited to single cell and no specific random distribution is utilised to model the spatial topologies of cellular and D2D users. Hence, it is not straightforward to generalise the results for the case of multi-cell network. Further, they considered a paired D2D communication where D2D users do not apply NOMA protocol to communicate with each other.

The authors in [63] considered a paired D2D communication underlying a NOMA based cellular network in which a single hybrid access point is used to receive from both D2D and cellular users. In particular, they investigate the problem of resource allocation and propose a low complexity energy efficient algorithm for D2D pair while meeting the QoS requirements of cellular users. The results demonstrated fast convergence of their proposed algorithm to an optimal solution while achieving superior energy efficiency over the existing schemes. A major limitation of their network model is that they considered only a single D2D active pair, whereas in real situations, there can be more than one active D2D pairs in the network, which requires joint optimisation of energy efficiency of all active D2D pairs.

Similarly, the problem of resource allocation in terms of power control and channel assignment for D2D communication underlying a NOMA based cellular network is investigated in [64]. The authors derived the optimal conditions for cellular users under

which power control on each subchannel is conducted. Based on the derived conditions, they proposed an algorithm to maximise the sum rate of D2D pairs while simultaneously satisfy the QoS requirements of cellular users. However, the considered cellular network is restricted to the case of a single cell, thereby neglecting the impact of interference from multiple BSs. In addition, NOMA is not utilised for D2D communications, which may result in less efficient resource utilisation.

The concept of NOMA assisted D2D relaying is proposed in [65], where the transmission is composed of two phases. In the first phase, the BS transmits NOMA signal to near and far users. By exploiting the overhearing of this NOMA transmission at intermediate D2D relay node, in the second phase, this relay node transmits superimposed overheard NOMA signal from first phase and its own signal for D2D receiver using NOMA. This helps to boost the performance of far user. Although NOMA is used by D2D relay node, it is still communicating with a single D2D receiver to form a paired D2D communication.

3.2.2 Group D2D Communications

In [66], the authors considered a NOMA-based D2D communications and introduced the concept of D2D group, where a D2D transmitter (DT) is communicating with multiple D2D receivers (DRs) using NOMA protocol. The authors proposed an optimal resource allocation strategy for interference management to realize NOMA-based D2D group communications. This work is extended in [66], where the problem of joint subchannel and power allocation for NOMA based group D2D communication is studied. In order to maximise the sum rate achieved by D2D communication, an algorithm that jointly assigns subchannel and power to each D2D user in a group is proposed. The results showed that the proposed joint subchannel and power allocation algorithm offers near optimal performance at the expense of reasonable complexity. Although the concept

of NOMA group D2D was introduced in [66, 67], their system model was comprised of single-cell and lack of interference characterisation at DR. Furthermore, it requires interference modeling and performance evaluation at the DR in order to extend the concept of NOMA group D2D to a general scenario, where DTs and DRs are distributed in the entire network.

The authors in [68] further proposed cooperative HARQ assisted NOMA in large-scale D2D networks. They studied the outage and throughput performances of D2D users under the considered network and demonstrated that cooperative HARQ assisted NOMA achieves lower outage probability than non-cooperative case and OMA scheme. However, their NOMA based D2D network model is limited to two-user case only, i.e., they only considered two-user NOMA transmission from D2D source. Furthermore, they considered a significant difference between channels of two D2D users by assuming that one user is always closer to D2D source compared to the other user. This assumption may not always hold, particularly in the scenario of NOMA based D2D communications because DRs typically clustered around DTs, and are located near each other and consequently have very similar channel conditions.

3.3 NOMA based Hybrid Multiple Access

In [69], the authors proposed a dynamic power allocation scheme based on hybrid NOMA. They derived a condition that is used to switch a transmission between NOMA and OMA modes. Under this condition, OMA is utilised to serve the users whenever the strong user's channel quality falls below a threshold value determined by the weak user's fixed target data rate. The closed-form expression for the outage probability is derived, and the proposed scheme is compared with two existing schemes: fixed power allocation NOMA (F-NOMA) and cognitive radio inspired NOMA (CR-NOMA). The results show that it achieves a more balanced performance tradeoff than F-NOMA and

CR-NOMA. In particular, it successfully avoids the situations of complete outage that occur in F-NOMA due to improper rate and power allocation. On the other hand, it obtains higher diversity gain than CR-NOMA. A potential shortcoming of this scheme is that it is designed for the case of only two users, and its extension to cover situations of having more than two users is not very straightforward because the derivation of the condition under which NOMA or OMA is selected will become analytically challenging.

A low complexity downlink multi-user transmission method is proposed in [70]. Under this scheme, using the SNRs of users, BS divides all users in its coverage into multiple user groups (UGs). Based on UGs, the BS applies NOMA to communicate with users within each UG, whereas each UG is scheduled for transmission in a TDMA fashion. The authors analysed the performance of the proposed scheme in terms of achievable sum-rate. Expectedly, the results show that the throughput achieved by this schemes resides between that of conventional NOMA and OMA techniques. However, due to fewer number of users scheduled per group, this technique reduces the number of SIC-levels at each user for decoding compared to conventional NOMA. Moreover, their analysis lacks the consideration of SINR for successful decoding, which is an important metric to analyse multiuser systems.

A hybrid MA scheme based on sparse code MA (SCMA) and NOMA is proposed in [71]. This scheme divides the users into near and far user categories. At the BS, SCMA and binary phase shift keying (BPSK) are applied to encode near and far users' messages, respectively. These encoded signals for near and far users are then transmitted by applying NOMA principles, i.e. SCMA and BPSK are superimposed by allocating them different power levels. The authors analysed the performance of the considered system in terms of bit-error rate. The proposed scheme has two shortcomings: 1) receiver complexity is significantly higher because after removing far user's message, it requires an additional message passing algorithm block to decode near user's message; and 2) this scheme is designed to only accommodate the two-user case.

Inspired by user grouping, a hybrid MA is constructed in [47] by combining NOMA and OMA. The key motivation behind this proposal is to not schedule all users for NOMA because it may result in high intra-user interference. Thus, the authors considered a user pair for conducting NOMA and evaluated the impact of user pairing on system performance. Closed-form expressions for outage probability are derived for F-NOMA and CR-NOMA cases. The results show that by pairing users with distinctive channel conditions, F-NOMA always outperforms conventional OMA and achieves a larger sum-rate. It is also shown that the performance of CR-NOMA is sensitive to the channel conditions of poor user because the transmit power allocated to the other user in a pair is constrained by it.

3.4 NOMA Receiver Structure

Based on the labelling method, an alternate scheme to SIC for decoding downlink NOMA signal was investigated in [72]. The authors considered a two-user OFDM based downlink NOMA system. A special case was studied where strong user avoids SIC operation in order to decode its message. Analytical expressions were provided to evaluate the performance in terms of symbol error rate, block error rate and ϵ -feasible rate metrics. The performance was compared for three types of labelling methods, namely Gray, non-Gray and natural labelling. The results showed that Gray labelling outperforms the other two labelling methods, while allowing strong user to achieve comparable performance with and without SIC. One potential drawback of this labelling method for decoding is that it is designed for the case of only two NOMA users. This poses a challenge in terms of assigning labels to data bits from different users in cases with more than two users. Furthermore, the complexity of the proposed scheme will increase with the number of users due to the label design and assignment for multiple users.

The authors in [73] proposed a decoding strategy for a cooperative relaying system with NOMA. A network with a single source, relay, and destination is considered. Since the destination is farther than the relay from the source, the message for destination is allocated with more power. The proposed scheme has two transmission phases: 1) direct transmission where source uses NOMA to send the superposition of two messages s_1 and s_2 to the relay and destination, with message s_1 allocated more power than s_2 . The relay uses SIC to retrieve message signal s_2 ; 2) cooperation where relay sends message s_2 with full transmit power to destination. Using maximum ratio combining (MRC), the destination combines the buffered signal from first phase and relayed signal from second phase to decode its signal. In addition, a suboptimal power allocation policy is proposed. The results show improved outage probability and ergodic sum rate. The receiver structure proposed in [73] is applicable for cooperative relaying NOMA systems only. Moreover, it is designed for a very specific scenario having a single source, relay and destination. Increasing the number of relays or destinations will result in increased complexity and latency due to the cooperation phase. Further, the proposed design still relies on conventional SIC operation. As a result, this design inherits all shortcomings of the SIC receiver and its performance is again dependent on the successful SIC operation.

3.5 Chapter Summary

This chapter reviews the state-of-the-art prior works on NOMA. The review is organised into three major categories: 1) Application of NOMA to cellular and D2D networks; 2) Hybrid MA schemes based on NOMA; and 3) Receiver design for NOMA. The review identified the following research gaps in existing works, which have led to the main contributions of this thesis that are to be presented in Chapters 4-8.

- In the context of cellular networks, single cell scenarios have been well investigated. However, very few works have considered NOMA based multi-tier cellular network, and they did not consider NOMA to be employed by each tier BS. In addition, MBSs and users are usually modeled by homogeneous PPPs, which are shown to be inaccurate models for real MBSs deployments and user distributions in multi-tier networks. This led to the work presented in Chapter 4.
- It is observed that very little attention has been paid in the literature to create NOMA based group D2D communications. Further, the literature is scarce in investigating the application of NOMA to WSNs. These gaps led to the studies undertaken in Chapters 5 and 6.
- Utilising both conventional OMA and NOMA to create a hybrid MA is another area which has been relatively unexplored. As such, a new hybrid MA scheme is presented in Chapter 7 to achieve a more balanced tradeoff between decoding reliability and system throughput.
- Finally, nearly all works in the literature on downlink NOMA have utilised SIC receiver for decoding. However, there are potential drawbacks of SIC that can impact NOMA operation and performance. This motivated the research performed in Chapter 8, which aims to alleviate the SIC related issues for NOMA.

Chapter 4

An Analytical Framework for Multi-Tier NOMA Networks with Underlay D2D Communications

From the literature review conducted in previous chapter, it is found that existing works are still scarce in applying NOMA for multi-tier cellular networks. Consequently, this chapter investigates and analyses NOMA based multi-tier cellular networks by proposing a novel mathematical framework utilising the tools of point processes and stochastic geometry.

4.1 Introduction

NOMA and its applications are well-researched in literature for mostly single-tier single-cell networks. Much less attention has been paid to exploring the potentials of NOMA in multi-tier cellular networks, where the BS at each tier is equipped with NOMA functionality. Nevertheless, the reported performance conclusions for NOMA in single-tier single-cell scenarios cannot be claimed in a straightforward manner for

multi-tier multi-cell networks. Further, in the current literature, NOMA is proposed with SIC receiver. However, the presence of intra-user interference impacts the performance of NOMA with SIC [49], and hence there is a need to improve the SIC design for better decoding performance at the end users.

Moreover, due to irregularity exhibited by the BS locations under real deployments in multi-tier cellular networks, stochastic spatial models are seen as elegant tools for accurate modeling and tractable analysis of these networks. The most prevalent method is to model the locations of BSs in each tier by independent PPPs and evaluate the performance of typical user chosen randomly and independently of the BS locations [32, 33, 74]. However, there are two major shortcomings of this approach. First, although simple and tractable, PPP models are shown to be inaccurate for modeling real deployments of macro-cell BSs (MBSs). Second, the correlation between user (cellular and D2D) and small-cell BS (SBS) locations under user-centric deployments is not captured by assuming independence between their locations. To the best of our knowledge, none of the prior works has focused on developing tools to model and analyse multi-tier NOMA networks with underlay D2D communications and exhibiting realistic distribution of BSs and user locations. Comprehensive modeling and development of new tools for performance analysis of such networks with a two-tier structure is the main goal of this chapter.

The rest of the chapter is organised as follows. Section 4.2 describes the system model while Section 4.3 derives the association probabilities and interference distributions. Performance analysis is provided in Section 4.4 followed by results and discussion in Section 4.5. Finally, Section 4.6 summarises the chapter.

Table 4.1: Commonly used variables.

Notation	Description
$\Phi_m (\Phi_s)$	Spatial PPs for MBSs (SBSs) locations
$\Phi_{\text{PHP}}, \Phi_{\text{PCP}}$	Baseline PHP and PCP for users locations
$\lambda_m (\lambda_s)$	Intensity of $\Phi_m (\Phi_s)$
$\mathcal{R}_1, \mathcal{R}_2, \mathcal{R}_3$	Coverage radius of MBS, SBS, and DT, respectively
P_m, P_s, P_d	Transmit power of MBS, SBS, and DT, respectively
M	Total MBS users in representative cell
S	Total SBS users in representative cell
a_j^k	Power allocation coefficient of j -th MBS user from tier k
$\Upsilon_m, \Upsilon_s, \Upsilon_d$	Transmit SNR of MBS, SBS, and DT, respectively
\bar{N}, \bar{L}	Gaussian-Chebyshev parameters
\bar{S}	Laguerre polynomial degree
U	Term for Laplace transform inversion

4.2 System Model

A two-tier cellular network comprising of NOMA enabled MBSs and SBSs, with inband D2D communications in the underlay mode is considered. For this network, the users are broadly classified as clustered or non-clustered users, as shown in Figure 4.1. It can be observed that the clustered users are distributed around the locations of SBSs, whereas non-clustered users are distributed randomly in the network. A comprehensive breakdown of different types of users is provided in Figure 4.2. It is evident from Figure 4.2 that clustered users can be of type MBS, SBS and D2D, whereas non-clustered users can be of MBS and D2D type. This implies that a clustered cellular user is permitted to connect to any MBS or SBS in the network. However, since non-clustered cellular users do not fall inside any small cells, they are by default connected to MBS. This setup is inspired by three facts. First, NOMA utilises available resources more efficiently by applying superposition coding to multiplex different users in a single resource. Second, SBSs are typically deployed in areas of higher user density in order to effectively meet the cellular traffic demands in these areas. Third, invoking D2D communications can further boost the spectrum efficiency of the cellular network.

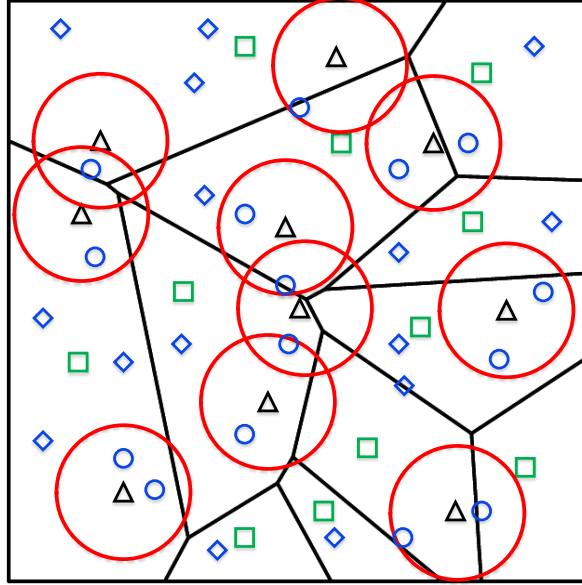


Figure 4.1. Proposed two-tier network model. The squares, triangles, circles and diamonds show the positions of MBSs, SBSs, clustered users, and non-clustered users, respectively.

The analysis is performed for a typical user, which is a randomly chosen cellular (MBS/SBS) user or DR in a downlink scenario. Only the dominant interferers that practically contribute to interference at the typical user are considered, i.e. out-of-range transmitters to the typical user are excluded. The presented system model is, in principle, extensible for cellular networks with any arbitrary number of tiers. However, for notational simplicity and ease of exposition, discussions herein are restricted to a two-tier setup. For quick reference, a list of commonly used variables in this chapter is provided in Table 4.1.

4.2.1 Spatial Setup and Key Assumptions

The spatial locations of MBSs in a two-tier cellular network are firstly modeled by an independent Gauss DPP $\{x_m\} \equiv \Phi_m(K)$ with density λ_m . This model captures the repulsive nature of MBSs locations, and is considered to be a statistically accurate

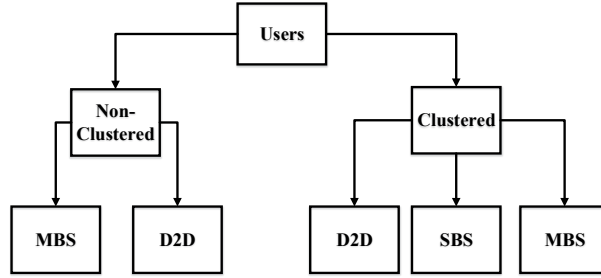


Figure 4.2. Classifications of users under proposed network model.

model for real MBSs deployments [37]. Here, K is known as the DPP kernel that ensures the existence of Φ_m . Next, the locations of SBSs are modeled by homogeneous PPP $\{x_s\} \equiv \Phi_s$, with density λ_s . The assumption of PPP for modeling SBS locations is justified because multiple SBSs can be deployed independently in areas of high user density in order to enhance service quality.

Now, there is a more challenging task of modeling users in this two-tier setup. It is observed from Figure 4.1 that the SBS locations can have two implications. First, they are acting as cluster centres. Second, each SBS also acts a hole centre with hole radius equal to SBS coverage. This interpretation has led to classifying network users as clustered or non-clustered users. Specifically, users inside the coverage of SBSs (holes) are classified as clustered users, whereas those outside of the coverage of SBSs (holes) are termed non-clustered users. This classification permits us to model clustered and non-clustered users by PCP and PHP. Hence, two independent PCP $\Phi_{PCP}(\lambda_{PCP})$ and $\Phi_{PHP}(\lambda_{PHP})$ are considered to model clustered and non-clustered users, respectively, λ_{PCP} and λ_{PHP} are the densities of Φ_{PCP} and Φ_{PHP} , respectively. Note that SBS locations Φ_s are considered as the parent process of Φ_{PCP} and hole centres for Φ_{PHP} . In this way, the proposed modeling approach not only captures the correlation between clustered user and SBS locations, but also successfully models the network users who are located independently of BS locations. The complete user distribution is the superposition of Φ_{PCP} and Φ_{PHP} .

Next, considering Φ_{PCP} and Φ_{PHP} as the baseline user processes, the clustered and non-clustered user types, i.e. cellular and D2D users, in the network are modeled. Note that a cellular (MBS/SBS) user is always referred to as a downlink user. Now, at a certain time instant, a user can be of cellular or D2D type. Consider that a user can be a cellular user with probability $1 - p$, or D2D user with probability p . Further consider that a D2D user can be a DT or DR with probability q and $1 - q$, respectively. As a result, based on Φ_{PCP} and Φ_{PHP} , the different types of clustered and non-clustered user processes, which are subsets of Φ_{PCP} and Φ_{PHP} , respectively, are defined as follows:

1. Clustered and non-clustered cellular user processes are defined as, $\{w_{cc}\} \equiv \Phi_{CC} ((1 - p) \lambda_{PCP})$, and $\{w_{nc}\} \equiv \Phi_{NC} ((1 - p) \lambda_{PHP})$, respectively.
2. Clustered and non-clustered DR processes are defined as $\{w_{\bar{c}}\} \equiv \Phi_{CDR} (p(1 - q)\lambda_{PCP})$, and $\{w_{\bar{n}}\} \equiv \Phi_{NDR} (p(1 - q)\lambda_{PHP})$, respectively.
3. Clustered and non-clustered DT processes are defined as $\{y_c\} \equiv \Phi_{CDT} (pq\lambda_{PCP})$, and $\{y_n\} \equiv \Phi_{NDT} (pq\lambda_{PHP})$, respectively.

It should be noted that there are now four types of independent transmitter processes Φ_m , Φ_s , Φ_{CDT} , and Φ_{NDT} that can contribute towards interference at the typical user. In addition, the typical user belongs to one of the receiver processes Φ_{CC} , Φ_{NC} , Φ_{CDR} or Φ_{NDR} . Due to the stationarity of these processes, a typical user can be assumed to be always located at the origin [75].

Finally, in this chapter, a TCP as discussed in Section 2.4.3 is considered. In TCP, the number of points in the representative cluster are Poisson distributed with mean \bar{c} . As a result, the PCP Φ_{PCP} has a density $\bar{c}\lambda_s$ [42]. Note that the clustered DTs process Φ_{CDT} is a subset of Φ_{PCP} with density $pq\bar{c}\lambda_s$ ($pq\bar{c}$ DTs per cluster). Further note that the locations of SBSs act as hole centres, as shown in Figure 4.1. Therefore, based on (2.11), $\Phi_2 = \Phi_s$ is assumed in the rest of this chapter, and the transmitter process Φ_{NDT} is a subset of Φ_1 .

4.2.2 Propagation Model

Consider that a typical user is located at the origin, then, the received power at the typical user from a transmitter at location z is given as,

$$P_r = P_z h_z \|z\|^{-\alpha}, \quad (4.1)$$

where P_z is the transmit power of the transmitter at location z , h_z and $\|z\| = d_z$ are the fading (power) gain and distance between typical user and transmitter at z , respectively, and $\alpha > 2$ is the path-loss exponent. Note that in the considered network, $z \in \{x_m, x_s, y_c, y_n\}$. For notational simplicity, denote $P_{x_m} = P_m$, $P_{x_s} = P_s$, $P_{y_c} = P_{y_n} = P_d$ to represent MBS, SBS and DT transmit powers, respectively.

Next, based on the received power model defined in (5.2), an association policy under which a cellular user connects to the BS that maximizes its received power is assumed. The location of such candidate serving BS from Φ_k is given by,

$$z_k^* = \arg \max_{z_k \in \Phi_k} \|z_k\|^{-\alpha}, \quad (4.2)$$

where the index $k \in \{m, s\}$, m and s refer to macro cell and small cell tier, respectively, z_k represents the distance between typical user and k -th tier BS, and z_k^* represents the location of the nearest BS of the k -th tier that acts as a serving BS to the typical user.

4.2.3 NOMA and D2D Systems

NOMA System:

Consider that each MBS and SBS in the network is located at the centre of a disc \mathcal{D}_1 and \mathcal{D}_2 , with radius \mathcal{R}_1 and \mathcal{R}_2 , modeling the coverage of each MBS, and SBS, respectively. For analysis purpose, further consider a representative macro cell, in which multiple small cells are underlaid. Let there be a total of M and S NOMA users

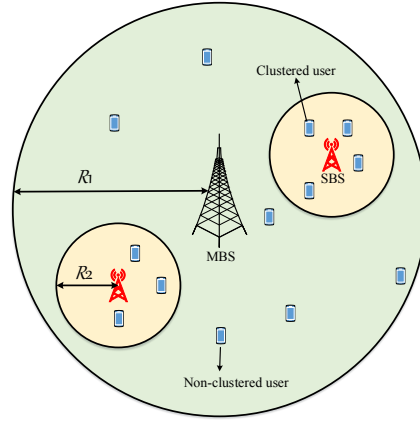


Figure 4.3. Representative macrocell with underlaid small cells.

distributed randomly inside coverage of the macro cell and small cells, respectively, as shown in Figure 4.3. According to NOMA principles, the MBS and SBS users in respective cells are ordered according to channel gains as, $\bar{h}_1^k \leq \dots \leq \bar{h}_j^k$, where $\bar{h}_j^k = h_j^k (d_j^k)^{-\alpha}$, h_j^k and d_j^k are the fading (power) and distance between user j and associated tier k BS, respectively, $j \in \{m, s\}$, $J \in \{M, S\}$, $1 \leq m \leq M$, and $1 \leq s \leq S$. As a result, the power allocation coefficients are sorted as $a_1^k \geq \dots \geq a_j^k$, with $\sum_{j=1}^J a_j^k = 1$. The power allocation coefficient for user j of tier k can be expressed as [6]:

$$a_j^k = \frac{b_j^k}{\sum_{i=1}^J b_i^k}, \quad (4.3)$$

where $b_j^k = \frac{1}{\bar{h}_j^k}$. Based on (4.1), the overall received power after receiving the NOMA signal at user j associated to tier k BS, denoted by $P_{r_j^k}$ can be expressed as:

$$P_{r_j^k} = \underbrace{\bar{h}_j^k P_k a_j^k}_{\text{useful signal power}} + \overbrace{\bar{h}_j^k P_k \sum_{\substack{i=1 \\ i \neq j}}^J a_i^k}^{\text{intra-user interference}} + \mathcal{I}_j^k + \sigma^2, \quad (4.4)$$

where \mathcal{I}_j^k is the total received interference (power) at k -tier j -th NOMA user and σ^2 is the power of additive noise.

Note: Since NOMA is considered as a baseline transmission scheme for communication between cellular users and BSs, the terms NOMA user and cellular user are used interchangeably in subsequent discussions, unless otherwise stated.

D2D System:

Paired D2D communication which refers to each DT having only one intended DR is considered. Furthermore, it is assumed that each clustered (non-clustered) D2D device has certain contents of interest that can be requested by other clustered (non-clustered) D2D devices. On the other hand, clustered and non-clustered devices have little tendency to communicate with each other. This assumption can be justified in many practical scenarios. For example, sports-related contents are of more interest for clustered devices found in a sports bar as opposed to non-clustered devices whose contents of interest are likely to lie in other areas [75]. Note that while the tools developed in this chapter can be extended to cover the situation where communications between clustered and non-clustered devices are permitted, it is beyond the scope of this chapter and is left as potential direction for future work.

Consider that each DT is located at the centre of a disc \mathcal{D}_3 , with a radius \mathcal{R}_3 representing the coverage of DT. The intended DR is assumed to be located randomly inside disc D_3 . A typical D2D pair is considered for analysis. Based on (5.2), the cumulative received power at DR, denoted by $P_{r_{\bar{w}}}$ can be expressed as,

$$P_{r_{\bar{w}}} = P_d \bar{h}_{\bar{z}} + \mathcal{I}_{\bar{w}} + \sigma^2, \quad (4.5)$$

where $\bar{w} \in \{w_{\bar{c}}, w_{\bar{n}}\}$, $\bar{h}_{\bar{z}} = h_{\bar{z}} d_{\bar{z}}^{-\alpha}$, $h_{\bar{z}}$ and $d_{\bar{z}}$ are the fading (power) gain and distance between typical D2D device pair, $\bar{z} \in \{y_c, y_n\}$, and $\mathcal{I}_{\bar{w}}$ represents the total interference at the typical DR.

By inspecting (4.4) and (4.5), it is evident that interference characterisation is necessary in order to evaluate the system performance. Hence, in the Section 4.3, the

relevant interference distributions are derived.

4.3 Association Probabilities and Interference Distributions

This section firstly derives the association probability for a cellular user to connect to the k -th tier BS. Recall that non-clustered cellular user always connects to MBS because it does not fall inside the coverage of any SBS. Therefore, the goal is to derive the association probability for a clustered cellular user to connect to SBS or MBS. Then the interference for two types of typical user i.e. cellular and DR user, will be derived. Without loss of generality, consider a typical user is located at the origin.

4.3.1 Association Probability

The association probability can be formally defined as the probability that a typical cellular user is served by the k -th tier BS. Based on the association policy in (4.2), the candidate serving BS is one which maximises the received power averaged over fading. In order to derive the association probability, the association events for a typical user to connect to MBS and SBS are firstly defined as follows:

- $\varepsilon_1 = \{ \mathbf{1} (\arg \max_{k \in \{m,s\}} P_k R_k^{-\alpha} = m) \}$ denotes the association event to MBS.
- $\varepsilon_2 = \{ \mathbf{1} (\arg \max_{k \in \{m,s\}} P_k R_k^{-\alpha} = s) \}$ denotes the association event to SBS.

Here $\mathbf{1}(\cdot)$ represents the indicator function and the random variable $R_k = \|z_k^*\|$ denotes the distance of typical user to nearest point of Φ_k , i.e. distance between a typical user and the serving BS. In order to obtain the association probability, the distribution of random variable R_k is required. Since Φ_k are the independent homogeneous Gauss DPP and PPP, their cumulative distribution function (CDF) and probability density function

(PDF) of R_k are given as [37, 76]:

$$\text{PDF: } f_{R_m}(r_m) = 2\pi r_m \sum_{n=0}^{\infty} \frac{(-1)^n}{n!} \times \int_{(B(0,r_m))^n} \det \left(K \left(\mathbf{x}_{m_{\bar{i}}}, \mathbf{x}_{m_{\bar{j}}} \right) \right)_{0 \leq \bar{i}, \bar{j} \leq n} \Big|_{\mathbf{x}_{m_0}=(r_m,0)} \times d\mathbf{x}_{m_1} \dots d\mathbf{x}_{m_n} \quad (4.6)$$

$$\text{CDF: } F_{R_m}(r_m) = \sum_{n=1}^{\infty} \frac{(-1)^n}{n!} \int_{(B(0,r_m))^n} \det \left(K \left(\mathbf{x}_{m_{\bar{i}}}, \mathbf{x}_{m_{\bar{j}}} \right) \right)_{1 \leq \bar{i}, \bar{j} \leq n} d\mathbf{x}_{m_1} \dots d\mathbf{x}_{m_n} \quad (4.7)$$

$$\text{PDF: } f_{R_s}(r_s) = 2\pi \lambda_s r_s \exp(-\pi \lambda_s r_s^2) \quad (4.8)$$

$$\text{CDF: } F_{R_s}(r_s) = 1 - \exp(-\pi \lambda_s r_s^2) \quad (4.9)$$

where $K \left(\mathbf{x}_{m_{\bar{i}}}, \mathbf{x}_{m_{\bar{j}}} \right) = \lambda_m e^{\left(-\frac{\|\mathbf{x}_{m_{\bar{i}}} - \mathbf{x}_{m_{\bar{j}}}\|^2}{\kappa^2} \right)}$ is Gauss DPP kernel to ensure the existence of Φ_m and κ is a parameter to measure the repulsiveness of Φ_m [37].

Now with distribution of R_k in hand, the probabilities of the events ε_1 and ε_2 can be found. Denote $\mathcal{A}_m = P(\varepsilon_1)$ and $\mathcal{A}_s = P(\varepsilon_2)$ to represent the probabilities of typical user to associate with MBS and SBS, respectively. Then, the following lemma states probabilities of the events ε_1 and ε_2 .

Lemma 4.1. *The association probabilities of the typical user \mathcal{A}_m and \mathcal{A}_s to connect to MBS and SBS, respectively, are expressed as:*

$$\mathcal{A}_s = \int_0^{\infty} [1 - F_{R_m}(\Omega^\alpha r_s)] f_{R_s}(r_s) dr_s \quad (4.10)$$

$$\mathcal{A}_m = 1 - \mathcal{A}_s. \quad (4.11)$$

where $\Omega = \frac{P_m}{P_s}$.

Proof. See Appendix A. □

The integral in (4.10) is computationally expensive. As such, the association

probabilities are approximated in the following lemma.

Lemma 4.2. *The computationally efficient approximations of association probabilities \mathcal{A}_m and \mathcal{A}_s for typical user are given as follows:*

$$\mathcal{A}_s \approx (1 + 2\beta\Omega^\delta)^{-1} \quad (4.12)$$

$$\mathcal{A}_m \approx 1 - (1 + 2\beta\Omega^\delta)^{-1}, \quad (4.13)$$

where $\delta = \frac{2}{\alpha}$ and $\beta = \frac{\lambda_m}{\lambda_s}$ is a parameter representing number of SBSs deployed per MBS in the network.

Proof. See Appendix B. □

It should be noted that \mathcal{A}_m and \mathcal{A}_s depend on the received power ratio Ω at the typical clustered cellular user under approximations obtained in Lemma 4.2. This is intuitively plausible because the parameter Ω reflects from which BS a typical user is receiving a larger power. This completes the discussion of association probabilities, and the interference distributions at typical user are derived in the next subsection.

4.3.2 Interference Distributions

There are three types of users in the network, namely MBS user, SBS user, and DR, which may receive interference from Φ_m , Φ_s , Φ_{CDT} and Φ_{NDT} . Hence, the interference distribution for each type of users is derived, considering only the dominant interferers as mentioned in the system model.

1. *When typical user is of MBS type:*

Recall that MBS user can be classified as a clustered or non-clustered user. Hence, the interference at typical user (non-clustered or clustered) under this classification can be defined as follows:

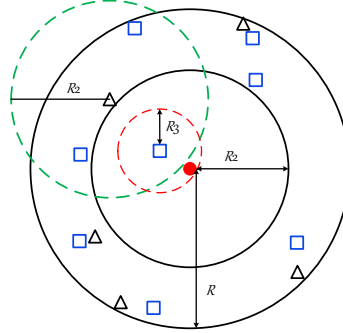


Figure 4.4. Illustration of interference at non-clustered MBS user from clustered DT. The solid dot, triangle and square represent non-clustered MBS user, SBS user, and clustered DT, respectively.

- Denote $\mathcal{I}_{nm} = \mathcal{I}_{nm}^m + \mathcal{I}_{nm}^{\text{NDT}} + \mathcal{I}_{nm}^{\text{CDT}}$ as the interference at the non-clustered MBS user, where $\mathcal{I}_{nm}^m = \sum_{x_m \in (\Phi_m \cap \bar{B}(R_m, \mathcal{R}_1)) \setminus z_m^*} P_m h_{x_m} \|x_m\|^{-\alpha}$, $\mathcal{I}_{nm}^{\text{NDT}} = \sum_{y_n \in \Phi_{\text{NDT}} \cap b(0, \mathcal{R}_3)} P_d h_{y_n} \|y_n\|^{-\alpha}$, and $\mathcal{I}_{nm}^{\text{CDT}}$ represent the interference at non-clustered MBS (typical) user from all MBSs except the serving MBS, non-clustered DTs and clustered DTs, respectively. Note that $\mathcal{I}_{nm}^{\text{CDT}}$ is the interference at non-clustered MBS user from clustered DTs. As such, all possible interfering clusters need to be found by locating the cluster centres. Considering only dominant interferers, the interfering clusters centres would be located in $\bar{B}(\mathcal{R}_2, \mathcal{R})$, as shown in Figure 4.4, where $\mathcal{R} = \mathcal{R}_2 + \mathcal{R}_3$. Let \mathcal{B}^{x_s} represents the set of DTs in the cluster centred at x_s . With this description, the interference at typical user is considered from all DTs which fall inside $\mathcal{B}^{x_s} \cap b(0, \mathcal{R}_3)$, as shown in Figure 4.4. Now $\mathcal{I}_{nm}^{\text{CDT}}$ can be expressed as,

$$\mathcal{I}_{nm}^{\text{CDT}} = \sum_{x_s \in \Phi_s \cap \bar{B}(\mathcal{R}_2, \mathcal{R})} \sum_{y_c \in \mathcal{B}^{x_s} \cap b(0, \mathcal{R}_3)} P_d h_{y_c} \|x_s + y_c\|^{-\alpha}.$$
- Denote $\mathcal{I}_{cm} = \mathcal{I}_{cm}^m + \mathcal{I}_{cm}^s + \mathcal{I}_{cm}^{\text{NDT}} + \mathcal{I}_{cm}^{\text{CDT}}$ as the interference at clustered MBS user, where $\mathcal{I}_{cm}^m = \mathcal{I}_{nm}^m$, $\mathcal{I}_{cm}^s = \sum_{x_s \in \Phi_s \cap b(0, \mathcal{R}_2)} P_s h_{x_s} \|x_s\|^{-\alpha}$, $\mathcal{I}_{cm}^{\text{NDT}} = \mathcal{I}_{nm}^{\text{NDT}}$, and $\mathcal{I}_{cm}^{\text{CDT}}$ represent the interference at clustered MBS (typical) user from all other MBSs excluding the serving MBS, SBSs, non-clustered DTs and clustered

DTs, respectively. Similar to representing $\mathcal{I}_{nm}^{\text{CDT}}$, in order to specify $\mathcal{I}_{cm}^{\text{CDT}}$, the possible interfering clusters are first determined by locating the positions of their cluster centres. In this case, the locations of such interfering cluster centres would be located inside $b(0, \mathcal{R})$. Now the interference from all DTs is considered to fall inside $\mathcal{B}^{xs} \cap b(0, \mathcal{R}_3)$. As a result, the interference at (typical) clustered cellular user from clustered DTs is expressed as, $\mathcal{I}_{cm}^{\text{CDT}} = \sum_{x_s \in \Phi_s \cap b(0, \mathcal{R})} \sum_{y_c \in \mathcal{B}^{xs} \cap b(0, \mathcal{R}_3)} P_d h_{y_c} \|x_s + y_c\|^{-\alpha}$.

With description of interference \mathcal{I}_{nm} and \mathcal{I}_{cm} for two classifications of typical MBS user, these interferences at typical user can be characterised. Note that \mathcal{I}_{nm}^m and \mathcal{I}_{cm}^m are functions of distance between typical user and its serving MBS, R_m . As such, the approach is to first condition on R_m to find these conditional interference distributions and then de-condition on R_m at the end. Then the following two Lemmas state the distributions of \mathcal{I}_{nm} and \mathcal{I}_{cm} .

Lemma 4.3. (*Laplace transform of interference for typical user of non-clustered MBS type*) The Laplace transform of the interference \mathcal{I}_{nm} , denoted by $\mathcal{L}_{\mathcal{I}_{nm}}(\mathfrak{s})$, is given by:

$$\mathcal{L}_{\mathcal{I}_{nm}}(\mathfrak{s}) = \mathcal{L}_{\mathcal{I}_{nm}^m}(\mathfrak{s}) \cdot \mathcal{L}_{\mathcal{I}_{nm}^{\text{NDT}}}(\mathfrak{s}) \cdot \mathcal{L}_{\mathcal{I}_{nm}^{\text{CDT}}}(\mathfrak{s}), \quad (4.14)$$

where the terms in (4.14) are defined as follows:

$$\mathcal{L}_{\mathcal{I}_{nm}^m}(\mathfrak{s}) = \int_0^\infty \exp\left(-2\pi\lambda_m \left[\sum_{\bar{n}=1}^{\bar{N}} \Psi_{\bar{n}} Q_1(r_m, t_{\bar{n}}) + \sum_{\bar{l}=1}^{\bar{L}} \Psi_{\bar{l}} Q_2(t_{\bar{l}}) \right]\right) f_{R_m}(r_m) dr_m \quad (4.15)$$

$$\mathcal{L}_{\mathcal{I}_{nm}^{\text{NDT}}}(\mathfrak{s}) = \exp(-2\pi pq \lambda_1 \mathfrak{s} P_d Q_3) \exp\left(-2\pi\lambda_s \int_{\mathcal{R}_2}^\infty (1 - e^{-2pq\lambda_1 \mathfrak{s} P_d f(v, \mathfrak{s})}) v dv\right) \quad (4.16)$$

$$\mathcal{L}_{\mathcal{I}_{nm}^{\text{CDT}}}(\mathfrak{s}) = \exp\left(-2\pi\lambda_s \int_{\mathcal{R}_2}^{\mathcal{R}} (1 - e^{-pq\bar{c}\bar{f}(r, \mathfrak{s})}) r dr\right), \quad (4.17)$$

where $Q_1(r_m, t_{\bar{n}}) = 1 - \frac{1}{1 + s P_m r_m^{-\alpha} t_{\bar{n}}}$, $Q_2(t_{\bar{l}}) = \frac{1}{1 + s P_m \mathcal{R}_1^{-\alpha} t_{\bar{l}}}$, $Q_3 = \sum_{\bar{k}=1}^{\bar{K}} \frac{0.5 \mathcal{R}_3^2 \omega_{\bar{k}} \sqrt{1 - \theta_{\bar{k}}^2} t_{\bar{k}}}{s P_d + (t_{\bar{k}} \mathcal{R}_3)^\alpha}$, $\omega_{\bar{k}} = \frac{\pi}{\bar{K}}$, $t_{\bar{k}} = \frac{1}{2}(\theta_{\bar{k}} + 1)$, $\theta_{\bar{k}} = \cos\left(\frac{2\bar{k}-1}{2\bar{K}}\pi\right)$, $\Psi_{\bar{n}} = \left(1 - C e^{-\frac{2n^2 t_{\bar{n}}^{-\delta}}{\kappa^2}} I_0\left(\frac{4n^2 t_{\bar{n}}^{-\frac{1}{\alpha}}}{\kappa^2}\right)\right) \frac{n^2}{2\alpha}$, $\omega_{\bar{n}} \sqrt{1 - \theta_{\bar{n}}^2} t_{\bar{n}}^{-\delta-1}$, $C \in \left\{e^{-\frac{2r_m^2}{\kappa^2}}, e^{-\frac{2\mathcal{R}_1^2}{\kappa^2}}\right\}$, $\mathbf{n} \in \{r_m, \mathcal{R}_1\}$, $\bar{\mathfrak{N}} \in \{\bar{N}, \bar{L}\}$, $\bar{n} \in \{\bar{n}, \bar{l}\}$, $\theta_{\bar{n}} = \cos\left(\frac{2\bar{n}-1}{2\bar{\mathfrak{N}}}\pi\right)$, $t_{\bar{n}} = \frac{1}{2}(\theta_{\bar{n}} + 1)$, $\omega_{\bar{n}} = \frac{\pi}{\bar{\mathfrak{N}}}$, $\bar{f}(r, \mathfrak{s}) = \int_0^{\mathcal{R}_3} \int_0^{2\pi} \frac{\bar{r}^2 e^{-\bar{r}^2} d\bar{\theta} d\bar{r}}{1 + s P_d (\bar{r}^2 + r^2 - 2\bar{r}r \cos \bar{\theta})^{-\frac{\alpha}{2}}}$, $f(v, \mathfrak{s}) = \int_{v-\mathcal{R}_2}^{v+\mathcal{R}_2} \arccos\left(\frac{r^2 + v^2 - \mathcal{R}_2^2}{2vr}\right) (s P_d + r^\alpha)^{-1} r dr$, $I_0(\cdot)$ is a modified Bessel function of first kind with parameter $\nu = 0$ [77], λ_1 is the baseline homogeneous PPP for Φ_{PHP} and \bar{N}, \bar{L} are the complexity accuracy trade-off parameters.

Proof. See Appendix C. □

Lemma 4.4. (Laplace transform of interference for typical user of clustered MBS type):

The Laplace transform of the interference \mathcal{I}_{cm} , denoted by $\mathcal{L}_{\mathcal{I}_{\text{cm}}}(\mathfrak{s})$, is given by:

$$\mathcal{L}_{\mathcal{I}_{\text{cm}}}(\mathfrak{s}) = \mathcal{L}_{\mathcal{I}_{\text{cm}}^{\text{m}}}(\mathfrak{s}) \cdot \mathcal{L}_{\mathcal{I}_{\text{cm}}^{\text{s}}}(\mathfrak{s}) \cdot \mathcal{L}_{\mathcal{I}_{\text{cm}}^{\text{NDT}}}(\mathfrak{s}) \cdot \mathcal{L}_{\mathcal{I}_{\text{cm}}^{\text{CDT}}}(\mathfrak{s}), \quad (4.18)$$

where $\mathcal{L}_{\mathcal{I}_{\text{cm}}^{\text{m}}}(\mathfrak{s}) = \mathcal{L}_{\mathcal{I}_{\text{nm}}^{\text{m}}}(\mathfrak{s})$, $\mathcal{L}_{\mathcal{I}_{\text{cm}}^{\text{NDT}}}(\mathfrak{s}) = \mathcal{L}_{\mathcal{I}_{\text{nm}}^{\text{NDT}}}(\mathfrak{s})$, and $\mathcal{L}_{\mathcal{I}_{\text{cm}}^{\text{s}}}(\mathfrak{s})$, $\mathcal{L}_{\mathcal{I}_{\text{cm}}^{\text{CDT}}}(\mathfrak{s})$ are:

$$\mathcal{L}_{\mathcal{I}_{\text{cm}}^{\text{s}}}(\mathfrak{s}) = e^{-2\pi s \lambda_s P_s Q_3 |_{\mathcal{R}_3 = \mathcal{R}_2, P_d = P_s}} \quad (4.19)$$

$$\mathcal{L}_{\mathcal{I}_{\text{cm}}^{\text{CDT}}}(\mathfrak{s}) = e^{-2\pi s \lambda_s \int_0^{\mathcal{R}} (1 - e^{-pq\bar{e}\bar{f}(r, \mathfrak{s})}) r dr}. \quad (4.20)$$

Proof. See Appendix D. □

2. When typical user is of SBS type:

In this case, a typical user is always a clustered cellular user because it falls inside the coverage of at least one SBS. Let $\mathcal{I}_s = \mathcal{I}_s^{\text{m}} + \mathcal{I}_s^{\text{s}} + \mathcal{I}_s^{\text{NDT}} + \mathcal{I}_s^{\text{CDT}}$ represents the interference at typical SBS user, where $\mathcal{I}_s^{\text{m}} = \sum_{x_m \in \Phi_m \cap b(0, \mathcal{R}_1)} P_m h_{x_m} \|x_m\|^{-\alpha}$, $\mathcal{I}_s^{\text{s}} = \sum_{x_s \in (\Phi_s \cap \bar{B}(R_s, \mathcal{R}_2)) \setminus z_s^*} P_s h_{x_s} \|x_s\|^{-\alpha}$, $\mathcal{I}_s^{\text{NDT}} = \mathcal{I}_{\text{nm}}^{\text{NDT}}$, and $\mathcal{I}_s^{\text{CDT}}$ represent the interference at typical SBS user from all MBSs, SBSs except the serving SBS, non-clustered DTs, and clustered DTs, respectively. Similar to $\mathcal{I}_{\text{cm}}^{\text{CDT}}$, the interference $\mathcal{I}_s^{\text{CDT}}$ can be found by

first locating the positions of possible interfering cluster centres in $\bar{B}(R_s, \mathcal{R})$ and then considering the interference from all DTs that fall inside $\mathcal{B}^{x_s} \cap b(0, \mathcal{R}_3)$. As a result, the interference $\mathcal{I}_s^{\text{CDT}}$ can be expressed as, $\mathcal{I}_s^{\text{CDT}} = \sum_{x_s \in \Phi_s \cap \bar{B}(R_s, \mathcal{R})} \sum_{y_c \in \mathcal{B}^{x_s} \cap b(0, \mathcal{R}_3)} P_d h_{y_s} \|x_s + y_c\|^{-\alpha}$. Note that \mathcal{I}_s^s and $\mathcal{I}_s^{\text{CDT}}$ are functions of distance between typical user and serving SBS R_s . Therefore, in order to characterise \mathcal{I}_s^s and $\mathcal{I}_s^{\text{CDT}}$, they are first conditioned on R_s to find the conditional distribution of these interference and then de-condition at the end. The following lemma characterises the distribution of interference \mathcal{I}_s .

Lemma 4.5. (*Laplace transform of interference for typical user of SBS type*): *The Laplace transform of the interference, \mathcal{I}_s , denoted by $\mathcal{L}_{\mathcal{I}_s}$, can be derived as follows:*

$$\mathcal{L}_{\mathcal{I}_s}(\mathfrak{s}) = \mathcal{L}_{\mathcal{I}_s^m}(\mathfrak{s}) \cdot \mathcal{L}_{\mathcal{I}_s^s}(\mathfrak{s}) \cdot \mathcal{L}_{\mathcal{I}_s^{\text{NDT}}}(\mathfrak{s}) \cdot \mathcal{L}_{\mathcal{I}_s^{\text{CDT}}}(\mathfrak{s}), \quad (4.21)$$

where $\mathcal{L}_{\mathcal{I}_s^{\text{NDT}}}(\mathfrak{s}) = \mathcal{L}_{\mathcal{I}_{\text{nm}}^{\text{NDT}}}(\mathfrak{s})$, and $\mathcal{L}_{\mathcal{I}_s^m}(\mathfrak{s})$, $\mathcal{L}_{\mathcal{I}_s^s}(\mathfrak{s})$, $\mathcal{L}_{\mathcal{I}_s^{\text{CDT}}}(\mathfrak{s})$ are given as:

$$\mathcal{L}_{\mathcal{I}_s^m}(\mathfrak{s}) = e^{-2\pi\lambda_m \mathfrak{s} P_m Q_3 |_{\mathcal{R}_3=\mathcal{R}_1, P_d=P_m}} \quad (4.22)$$

$$\mathcal{L}_{\mathcal{I}_s^s}(\mathfrak{s}) = \int_0^\infty e^{-2\pi\mathfrak{s}\lambda_s Q_4} f_{R_s}(r_s) dr_s \quad (4.23)$$

$$\mathcal{L}_{\mathcal{I}_s^{\text{CDT}}}(\mathfrak{s}) = \int_0^\infty e^{-2\pi\lambda_s \int_{r_s}^{\mathcal{R}} (1 - e^{-pq\bar{c}\bar{f}(r,s)}) r dr} f_{R_s}(r_s) dr_s, \quad (4.24)$$

where $Q_4 = \sum_{\bar{q}=1}^{\bar{Q}} \frac{0.5(\mathcal{R}_2 - r_s)^2 \omega_{\bar{q}} \sqrt{1 - \theta_{\bar{q}}^2 t_{\bar{q}}}}{s P_s + t_{\bar{q}}^\alpha}$, $\omega_{\bar{q}} = \frac{\pi}{\bar{Q}}$, $\theta_{\bar{q}} = \cos\left(\frac{2\bar{q}-1}{2\bar{Q}}\pi\right)$, $t_{\bar{q}} = \frac{\mathcal{R}_2 - r_s}{2} \theta_{\bar{q}} + \frac{\mathcal{R}_2 + r_s}{2}$, and \bar{Q} is the complexity-accuracy tradeoff parameter.

Proof. See Appendix E □

3. *When typical user is of DR type:*

Similar to a case of MBS, a typical DR can be of types non-clustered and clustered. Hence, under this classification, the interference at typical DR can be defined as follows:

- Denote $\mathcal{I}_{\text{nd}} = \mathcal{I}_{\text{nd}}^{\text{m}} + \mathcal{I}_{\text{nd}}^{\text{NDT}} + \mathcal{I}_{\text{nd}}^{\text{CDT}}$ as the interference at typical DR of non-clustered type, where $\mathcal{I}_{\text{nd}}^{\text{m}} = \mathcal{I}_{\text{s}}^{\text{m}}$, $\mathcal{I}_{\text{nd}}^{\text{NDT}} = \sum_{y_n \in (\Phi_{\text{NDT}} \cap b(0, \mathcal{R}_3)) \setminus y_n^*} P_d h_{y_n} \|y_n\|^{-\alpha}$, and $\mathcal{I}_{\text{nd}}^{\text{CDT}} = \mathcal{I}_{\text{nm}}^{\text{CDT}}$ represent the interference at typical DR from MBSs, non-clustered DTs except its serving DT at y_n^* and, clustered DTs, respectively.
- Denote $\mathcal{I}_{\text{cd}} = \mathcal{I}_{\text{cd}}^{\text{m}} + \mathcal{I}_{\text{cd}}^{\text{s}} + \mathcal{I}_{\text{cd}}^{\text{NDT}} + \mathcal{I}_{\text{cd}}^{\text{CDT}}$ as the interference at typical clustered DR user, where $\mathcal{I}_{\text{cd}}^{\text{m}} = \mathcal{I}_{\text{s}}^{\text{m}}$, $\mathcal{I}_{\text{cd}}^{\text{s}} = \mathcal{I}_{\text{cm}}^{\text{s}}$, $\mathcal{I}_{\text{cd}}^{\text{NDT}} = \mathcal{I}_{\text{cm}}^{\text{NDT}}$, and $\mathcal{I}_{\text{cd}}^{\text{CDT}} = \sum_{y_c \in (\Phi_{\text{CDT}} \cap b(0, \mathcal{R})) \setminus y_c^*} P_d h_{y_c} \|x_s + y_c\|^{-\alpha} = \sum_{x_s \in \Phi_s \cap b(0, \mathcal{R})} \sum_{y_c \in (\mathcal{B}^{x_s} \cap b(0, \mathcal{R}_3)) \setminus y_c^*} P_d h_{y_c} \|x_s + y_c\|^{-\alpha}$ represent the interference at the typical clustered DR from MBSs, SBSs, non-clustered DTs, and clustered DTs except its serving DT at y_c^* .

Now with the description of \mathcal{I}_{nd} and \mathcal{I}_{cd} , the following two lemmas characterise these interference distributions.

Lemma 4.6. *(Laplace transform of interference for typical user of non-clustered DR type): The Laplace transform of the interference \mathcal{I}_{nd} , denoted by $\mathcal{L}_{\mathcal{I}_{\text{nd}}}$, is given by:*

$$\mathcal{L}_{\mathcal{I}_{\text{nd}}}(\mathfrak{s}) = \mathcal{L}_{\mathcal{I}_{\text{nd}}^{\text{m}}}(\mathfrak{s}) \cdot \mathcal{L}_{\mathcal{I}_{\text{nd}}^{\text{NDT}}}(\mathfrak{s}) \cdot \mathcal{L}_{\mathcal{I}_{\text{nd}}^{\text{CDT}}}(\mathfrak{s}), \quad (4.25)$$

where $\mathcal{L}_{\mathcal{I}_{\text{nd}}^{\text{m}}}(\mathfrak{s}) = \mathcal{L}_{\mathcal{I}_{\text{s}}^{\text{m}}}(\mathfrak{s})$, $\mathcal{L}_{\mathcal{I}_{\text{nd}}^{\text{CDT}}}(\mathfrak{s}) = \mathcal{L}_{\mathcal{I}_{\text{nm}}^{\text{CDT}}}(\mathfrak{s})$, and $\mathcal{L}_{\mathcal{I}_{\text{nd}}^{\text{NDT}}}(\mathfrak{s})$ is given by,

$$\mathcal{L}_{\mathcal{I}_{\text{nd}}^{\text{NDT}}}(\mathfrak{s}) = e^{-2\pi p q \lambda_1 s P_d Q_3} e^{-2\pi \lambda_s \int_{\mathcal{R}_2}^{\infty} (1 - e^{-2p q \lambda_1 s P_d f(v, \mathfrak{s})}) v dv}. \quad (4.26)$$

Proof. See Appendix F □

Lemma 4.7. *(Laplace transform of interference for typical user of clustered DR type): The Laplace transform of the interference \mathcal{I}_{cd} , denoted by $\mathcal{L}_{\mathcal{I}_{\text{cd}}}$, is given by:*

$$\mathcal{L}_{\mathcal{I}_{\text{cd}}}(\mathfrak{s}) = \mathcal{L}_{\mathcal{I}_{\text{cd}}^{\text{m}}}(\mathfrak{s}) \cdot \mathcal{L}_{\mathcal{I}_{\text{cd}}^{\text{s}}}(\mathfrak{s}) \cdot \mathcal{L}_{\mathcal{I}_{\text{cd}}^{\text{NDT}}}(\mathfrak{s}) \cdot \mathcal{L}_{\mathcal{I}_{\text{cd}}^{\text{CDT}}}(\mathfrak{s}), \quad (4.27)$$

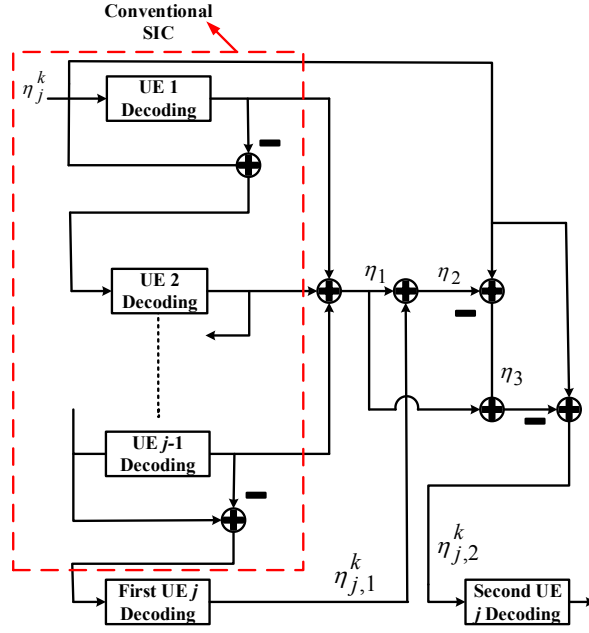


Figure 4.5. Proposed SIE receiver.

where $\mathcal{L}_{\mathcal{I}_{cd}^m}(\mathfrak{s}) = \mathcal{L}_{\mathcal{I}_s^m}(\mathfrak{s})$, $\mathcal{L}_{\mathcal{I}_{cd}^s}(\mathfrak{s}) = \mathcal{L}_{\mathcal{I}_{cm}^s}(\mathfrak{s})$, $\mathcal{L}_{\mathcal{I}_{cd}^{NDT}}(\mathfrak{s}) = \mathcal{L}_{\mathcal{I}_{cm}^{NDT}}(\mathfrak{s})$, and $\mathcal{L}_{\mathcal{I}_{cd}^{CDT}}(\mathfrak{s})$ is given as follows:

$$\mathcal{L}_{\mathcal{I}_{cd}^{CDT}}(\mathfrak{s}) = \mathcal{L}_{\mathcal{I}_{cm}^{CDT}}(\mathfrak{s}) \int_0^{\mathcal{R}^2} e^{-[pq(\bar{c}-1)\bar{f}(r,\mathfrak{s})+r^2]} r dr. \quad (4.28)$$

Proof. See Appendix G □

4.4 Performance Analysis

Based on the association probabilities and interference distributions derived in the previous section, network performance in terms of outage probability and average link throughput are analysed. Further, a SIC with intra-user interference estimation (SIE) receiver is proposed for cellular users, and its performance evaluated against conventional SIC.

4.4.1 Proposed SIE Receiver Design for Cellular Users

Recall that NOMA system is inherently interference limited due to the application of superposition coding, and hence SIC technique is widely adopted for NOMA to minimise intra-user interference. In NOMA, SIC is applied in the order of increasing channel gains, i.e. user j first decodes messages of all $j - 1$ higher-order users and then decodes its own message by considering messages of $j + 1 \dots J$ lower-order users as noise. However, the presence of this intra-user interference from $j + 1 \dots J$ lower-order users increases the SINR threshold for successful decoding. As such, this chapter proposes the SIE receiver design to locally estimate and remove this intra-user interference at j -th user from $j + 1 \dots J$ users to obtain a better estimate of user j message for decoding. The proposed SIE receiver design for j -th NOMA user is shown in Figure 4.5.

The operation of the proposed SIE receiver can be broken down into two steps. First, the estimate of lower-order users $j + 1 \dots J$ is obtained as, $\eta_3 = \eta_j^k - \eta_2 = \sum_{i=j+1}^J \sqrt{\bar{h}_j^k P_k a_i^k} x_i^k - e_1$, where $\eta_j^k = \sum_{i=1}^J \sqrt{\bar{h}_j^k P_k a_i^k} x_i^k$ is the received NOMA signal at user j from tier k (excluding external interference and noise), $\eta_2 = \eta_1 + \eta_{j,1}^k$, $\eta_1 = \sum_{i=1}^{j-1} \sqrt{\bar{h}_j^k P_k a_i^k} x_i^k$ which results in the estimation of higher order users by applying conventional SIC operation, $\eta_{j,1}^k = \sqrt{\bar{h}_j^k P_k a_j^k} x_j^k + e_1$ is the first estimate of user j from tier k , x_i^k is the message signal of i -th user from tier k , $1 \leq i \leq J$, and e_1 is error in estimating $\eta_{j,1}^k$. Second, the intra-user interference estimate η_3 from first step is now used to remove it from η_j^k to obtain second estimation of k -th tier user j as, $\eta_{j,2}^k = \eta_j^k - \eta_3 - \eta_1 + e_2 = \sqrt{\bar{h}_j^k P_k a_j^k} x_j^k + e$, where $e = e_1 + e_2$ and e_2 is the error in obtaining second estimate of k -th tier user j . Finally, $\eta_{j,2}^k$ is used to decode the message signal of user j from tier k . Note that $e = 0$ ($e \neq 0$) refer to perfect (imperfect) estimation of intra-user interference. As such, the performance of proposed SIE receiver is evaluated for both cases of perfect and imperfect intra-user interference estimation in the subsequent sub-sections.

4.4.2 Outage Analysis

Here, the outage probability expressions for typical MBS, SBS and DR users are derived. In each case, the interference PDF is required in order to obtain the outage probabilities. Hence, before proceeding to derive the outage probability expressions, the following Lemma is stated, which is used to obtain the interference PDF from its Laplace transform.

Lemma 4.8. *The PDF $f_{\mathcal{I}}$ of the interference \mathcal{I} can be obtained from its Laplace transform $\mathcal{L}_{\mathcal{I}}(\mathbf{s})$ as [78]:*

$$f_{\mathcal{I}}(\bar{x}) = \frac{e^{v\bar{x}}}{\Theta} \sum_{u=0}^{2U} {}' \Re \left[\mathcal{L}_{\mathcal{I}}(\mathbf{s} = c_u) e^{\frac{\iota\pi\bar{x}}{\Theta}} \right], \quad (4.29)$$

where $c_u = v_0 + \frac{\iota\pi u}{\Theta}$, $v_0 = v_1 - \frac{\log(\varsigma)}{\Theta}$, $v, v_1 > 0$ are real numbers, ς is the desired relative accuracy, Θ is a scaling parameter, $\iota = \sqrt{-1}$, U is the number of terms used to invert the Laplace transform, and the prime term indicates that $u = 0$ summation term is halved.

1. Outage performance of a typical MBS user:

Recall that MBS user can be of clustered or non-clustered type. Hence, at a particular time instant, m -th NOMA MBS user in a representative macro-cell can be of either non-clustered or clustered type (but not both simultaneously). As a result, the following events are defined in order to derive the outage probability for a typical MBS user:

$$\varepsilon_3 = \{\text{user } m \text{ is of non-clustered type}\}$$

$$\varepsilon_4 = \{\text{user } m \text{ is of clustered type}\}$$

$$\varepsilon_5 = \{\text{outage at user } m \text{ given it is of non-clustered type}\}$$

$$\varepsilon_6 = \{\text{outage at user } m \text{ given it is of clustered type}\}$$

Now based on the events $\varepsilon_3 - \varepsilon_6$, the outage probability at a typical MBS user m , denoted as P_m is stated in the following theorem.

Theorem 4.1. *Theorem 1: Considering m -th NOMA MBS user in a representative macro-cell as a typical user, the outage probability of user m can be derived as follows:*

$$P_m^m = p_m P_{\varepsilon_5} + (1 - p_m) P_{\varepsilon_6}, \quad (4.30)$$

where p_m , P_{ε_5} , and P_{ε_6} are the probabilities of events ε_3 , ε_5 and ε_6 , respectively, and P_{ε_5} , and P_{ε_6} are given as follows:

$$P_{\varepsilon_5} = \begin{cases} P_{\varepsilon_5}^{SIC} = \mu_m \sum_{\bar{p}=0}^{M-m} \binom{M-m}{\bar{p}} \frac{(-1)^{\bar{p}}}{m+\bar{p}} \sum_{\bar{s}=1}^{\bar{S}} \Psi_{\bar{s}} \\ \times [F_{h_m}(\varphi_m^{\max} \varrho_{\bar{s}})]^{m+\bar{p}} \sum_{u=0}^{2U} \Re[\mathcal{L}_{\mathcal{I}_{nm}}(c_u) e^{\frac{j\pi g_{\bar{s}}}{\Theta}}] \\ P_{\varepsilon_5}^{SIE} = \int_0^\infty P_{\varepsilon_5}^{SIC} |_{\varphi_m^{\max}=\phi_m^m, \varrho_{\bar{s}}=\varrho_{\bar{s}}+\rho y} f_{|e|^2}(y) dy \end{cases} \quad (4.31)$$

$$P_{\varepsilon_6} = \begin{cases} P_{\varepsilon_6}^{SIC} = P_{\varepsilon_5}^{SIC} |_{\mathcal{L}_{\mathcal{I}_{nm}}(c_u)=\mathcal{L}_{\mathcal{I}_{cm}}(c_u)} \\ P_{\varepsilon_6}^{SIE} = \int_0^\infty P_{\varepsilon_6}^{SIC} |_{\varphi_m^{\max}=\phi_m^m, \varrho_{\bar{s}}=\varrho_{\bar{s}}+\rho y} f_{|e|^2}(y) dy \end{cases} \quad (4.32)$$

where $\Psi_{\bar{s}} = \frac{\varpi_{\bar{s}} e^{(1+v)g_{\bar{s}}}}{\Theta}$, $\varpi_{\bar{s}} = \frac{\Gamma(\bar{S}+1)g_{\bar{s}}}{\bar{S}!(\bar{S}+1)^2 [L_{\bar{S}+1}(g_{\bar{s}})]^2}$, $L_{\bar{S}}(\cdot)$ is a Laguerre polynomial of degree \bar{S} , $g_{\bar{s}}$ are the roots of $L_{\bar{S}}(\cdot)$, $\varrho_{\bar{s}} = 1 + \rho g_{\bar{s}}$, $\rho = \frac{1}{\sigma^2}$, Γ is a gamma function, $\mu_m = \frac{M!}{(M-m)!(m-1)!}$, $\varphi_m^{\max} = \max\{\varphi_1^m, \dots, \varphi_m^m\}$, $\varphi_m^m = \frac{\tau_m^m}{\Upsilon_m (a_m^m - \tau_m^m \sum_{i=m+1}^M a_i^m)}$, $\phi_m^m = \frac{\tau_m^m}{\Upsilon_m a_m^m}$, $\tau_m^m = 2^{\mathbf{v}_m^m} - 1$ is SINR threshold of m -th MBS user, $\Upsilon_m = \frac{P_m}{\sigma^2}$ is the MBS transmit SNR, \mathbf{v}_m^m is the targeted data rate for m -th MBS user, F_{h_m} is the CDF of unordered channel gain for arbitrary MBS user (given in Appendix G), $f_{|e|^2}(y) = \mathcal{G}(\mu_{|e|^2}, \sigma_{|e|^2})$ is assumed to be a Gaussian density with mean $\mu_{|e|^2}$ and variance $\sigma_{|e|^2}$, and e is the error due to imperfect intra-user estimation.

Proof. See Appendix H □

2. Outage performance of a typical SBS user:

The SBS user is always a clustered user. Hence, the outage probability of a user s in representative small-cell is stated in the following theorem.

Theorem 4.2. *Considering s -th NOMA SBS user in a representative macro-cell as a typical user, the outage probability of user s can be derived as:*

$$P_s^s = \begin{cases} P_s^{SIC} = \mu_s \sum_{\bar{p}=0}^{S-s} \binom{S-m}{\bar{p}} \frac{(-1)^{\bar{p}}}{s+\bar{p}} \sum_{\bar{s}=1}^{\bar{S}} \Psi_{\bar{s}} \\ \times [F_{\hat{h}_s}(\varphi_s^{\max} \varrho_{\bar{s}})]^{s+\bar{p}} \sum_{u=0}^{2U} \Re [\mathcal{L}_{\mathcal{I}_s}(c_u) e^{-\frac{u\pi g_{\bar{s}}}{\Theta}}] \\ P_s^{SIE} = \int_0^\infty P_s^{SIC} |_{\varphi_s^{\max}=\phi_s^s, \varrho_{\bar{s}}=\varrho_{\bar{s}}+\rho y} f_{|e|^2}(y) dy, \end{cases} \quad (4.33)$$

where $\mu_s = \frac{S!}{(S-s)!(s-1)!}$, $\varphi_s^{\max} = \max\{\varphi_1^s, \dots, \varphi_s^s\}$, $\varphi_s^s = \frac{\tau_s^s}{\Upsilon_s(a_s^s - \tau_s^s \sum_{i=s+1}^S a_i^s)}$, $\phi_s^s = \frac{\tau_s^s}{\Upsilon_s a_s^s}$, $\tau_s^s = 2^{r_s^s} - 1$ is SINR threshold of s -th SBS user, $\Upsilon_s = \frac{P_s}{\sigma^2}$ is the SBS transmit SNR, r_s^s is the targeted data rate for s -th SBS user, $F_{\hat{h}_s}$ is the CDF of unordered channel gain for arbitrary SBS user defined in a similar way as $F_{\hat{h}_m}$ and is given by $F_{\hat{h}_s}(y) = 2\pi \int_0^{\mathcal{R}_2} (1 - e^{r_s^s y}) f_{R_s}(r_s) dr_s$.

Proof. Based on (4.4), the outage probabilities in decoding s -th SBS user's message using SIC and SIE are given as $P_s^{SIC} = P\left(\frac{\bar{h}_s^s a_s^s P_s}{\bar{h}_s P_s \sum_{i=s+1}^S a_i^s + \mathcal{I}_s + \sigma^2} < \tau_s^s\right) = P(\bar{h}_s^s < \varphi_s^{\max} (1 + \rho \mathcal{I}_s))$ and $P_s^{SIE} = P\left(\frac{\bar{h}_s^s a_s^s P_s}{\mathcal{I}_s + |e|^2 + \sigma^2} < \tau_s^s\right) = P(\bar{h}_s^s < \phi_s (1 + \rho \mathcal{I}_s + \rho |e|^2))$, respectively. Now following similar steps to Theorem 4.1, the results in Theorem 4.2 are obtained. \square

3. Outage performance of a typical DR:

Similar to MBS user, at a particular time instant, a typical DR can be of either non-clustered or clustered type (but not simultaneously). As such, the following events are defined in order to derive the outage probability for a typical DR:

$$\varepsilon_7 = \{\text{DR is of non-clustered type}\}$$

$$\varepsilon_8 = \{\text{DR is of clustered type}\}$$

$$\varepsilon_9 = \{\text{outage at DR given it is of non-clustered type}\}$$

$$\varepsilon_{10} = \{\text{outage at DR given it is of clustered type}\}$$

Now based on the events $\varepsilon_7 - \varepsilon_{10}$, the outage probability at a typical DR, denoted

as P_d is stated in the following theorem.

Theorem 4.3. *The outage probability of a typical DR in the considered network can be derived as follows:*

$$P_d = p_d P_{\epsilon_9} + (1 - p_d) P_{\epsilon_{10}}, \quad (4.34)$$

where p_d , P_{ϵ_9} , and $P_{\epsilon_{10}}$ are the probabilities of events ϵ_7 , ϵ_9 and ϵ_{10} , respectively, and P_{ϵ_9} , and $P_{\epsilon_{10}}$ are given as follows:

$$P_{\epsilon_9} = \sum_{\bar{s}=1}^{\bar{S}} \Psi_{\bar{s}} F_{\bar{h}_{y_c}}(\varphi_d \varrho_{\bar{s}}) \sum_{u=0}^{2U} \Re \left[\mathcal{L}_{\mathcal{I}_{nd}}(c_u) e^{\frac{i\pi g_{\bar{s}}}{\Theta}} \right] \quad (4.35)$$

$$P_{\epsilon_{10}} = P_{\epsilon_9} |_{\mathcal{I}_{nd}(c_u)=\mathcal{I}_{cd}(c_u)}, \quad (4.36)$$

where $F_{\bar{h}_{y_c}}(y) = \frac{2}{\mathcal{R}_3^2} \int_0^{\mathcal{R}_3} (1 - e^{-z^2 y}) z dz$ is the CDF of channel \bar{h}_{y_c} between DT and typical DR which is uniformly distributed inside coverage \mathcal{R}_3 of DT [79], $\varphi_d = \frac{\tau_d}{\Upsilon_d}$, $\tau_d = 2^{\tau_d} - 1$ and τ_d are the SINR threshold and targeted data rate for a typical DR, respectively, and Υ_d is the transmit SNR for a DT.

Proof. Based on (4.5), the outage probability at the typical non-clustered DR is written as, $P_{\epsilon_9} = P\left(\frac{\bar{h}_{y_c} P_d}{\mathcal{I}_{nd} + \sigma^2} < \tau_d\right) = P(\bar{h}_{y_c} < \tau_d (1 + \rho \mathcal{I}_{nd}))$. Now conditioned on \mathcal{I}_{nd} , P_{ϵ_9} can be expressed as, $P_{\epsilon_9} = \mathbb{E}_{\mathcal{I}_{nd}}(F_{\bar{h}_{y_c}}(1 + \rho x)) = \int_0^\infty F_{\bar{h}_{y_c}}(1 + \rho x) f_{\mathcal{I}_{nd}}(x) dx$. Next obtaining \mathcal{I}_{nd} by using (4.29) and then applying Gauss-Laguerre quadrature with similar parameters as were used in (4.31) to derive $P_{\epsilon_5}^{\text{SIC}}$, the result in (4.35) is obtained.

This completes the proof. \square

4.4.3 Link Throughput Analysis

In the previous subsection, the outage probability to evaluate the performance of cellular users and DRs under the considered network setting is derived. A metric of interest that is related to the outage probability is link throughput. Thus, based on the derived outage results from the previous subsection, the average link throughput experienced by a cellular user and DR are analysed.

Definition 4.1. (*Link Throughput*): The effective link throughput between an arbitrary transmitter and receiver, denoted by \mathcal{T} and measured in [bits/s/Hz], is defined as [80]:

$$\mathcal{T} = (1 - P_{out}) \log_2(1 + \tau), \quad (4.37)$$

where P_{out} , τ are the outage probability and SINR threshold of the receiver, respectively.

Now based on Definition 4.1 in (4.37), the average link throughputs for MBS/SBS user and DR are defined as follows:

$$\mathcal{T}_{avg}^m = \frac{\sum_{m=1}^M (1 - P_m^m) \log_2(1 + \tau_m)}{M} \quad (4.38)$$

$$\mathcal{T}_{avg}^s = \frac{\sum_{s=1}^S (1 - P_s^s) \log_2(1 + \tau_s)}{S} \quad (4.39)$$

$$\mathcal{T}_d = (1 - P_d) \log_2(1 + \tau_d). \quad (4.40)$$

Based on (4.38) and (4.39), the average link throughput experienced by an arbitrary cellular (NOMA) user, denoted by \mathcal{T}_{cell} is expressed as:

$$\mathcal{T}_{cell} = \frac{\mathcal{T}_{avg}^m + \mathcal{T}_{avg}^s}{2}. \quad (4.41)$$

Remark 1 (Optimum density of SBSs): Note that there is a clear tradeoff between \mathcal{T}_{cell} and the network interference. While deploying more SBSs potentially improve \mathcal{T}_{cell} ,

it also increases network interference. As a consequence, there exists an optimal SBS density, denoted by, λ_s^* , which can maximise $\mathcal{T}_{\text{cell}}$, and increasing SBS density beyond λ_s^* may result in no improvement in $\mathcal{T}_{\text{cell}}$. As such $\mathcal{T}_{\text{cell}}$ can, in principle, be maximised as:

$$\mathcal{T}_{\text{cell}}^* = \max_{\lambda_s} \mathcal{T}_{\text{cell}} \quad (4.42)$$

By solving this $\mathcal{T}_{\text{cell}}$ optimisation problem numerically, the existence of an optimal SBS density λ_s^* that maximises the $\mathcal{T}_{\text{cell}}$ will be demonstrated in the numerical results section.

4.5 Results and Discussion

This section presents numerical results to analyse the performance of cellular (MBS/SBS) users and DRs under the considered network setting. As shown in Table 4.2, simulation parameters similar to [51] are used unless otherwise stated. In order to generate power allocation coefficients $\{a_j^k\}_{j=1}^J$ using (4.3) for NOMA users, the channel gains $\{\bar{h}_j^k\}_{j=1}^J$ are averaged over 1000 random channel realisations with $\{h_j^k\}_{j=1}^J \sim \mathcal{CN}(0, 1)$ and $\{d_j^k\}_{j=1}^J \sim \mathcal{U}(0, \mathcal{R}_j)$, where $\mathcal{CN}(\cdot)$ and $\mathcal{U}(\cdot)$ represent complex Gaussian and uniform distribution, respectively, and $\mathcal{R}_j \in \{\mathcal{R}_1, \mathcal{R}_2\}$. Further, the performance of NOMA users is evaluated for proposed SIE as well as conventional SIC receivers. The results for MBS and SBS users are shown by averaging over total NOMA users M and S , respectively, and hence they indicate the performance of randomly chosen MBS and SBS users. In addition, as described in the system model, NOMA is applied by BSs for communicating with their downlink cellular users. Consequently, interference may result due to NOMA transmissions from the BSs. Therefore, besides considering the interference from DTs, DR performance is evaluated under potential interference from NOMA based cellular network, unless otherwise stated.

Table 4.2: Simulation parameters

Parameter	Description	Value
M	Total MBS users	3
S	Total SBS users	3
τ_m^m	SINR threshold for user m	$\{0.9, 1.5, 2\}_{m=1}^M$
τ_s^s	SINR threshold for user s	$\{0.9, 1.5, 2\}_{s=1}^S$
τ_d	DR SINR threshold	1
λ_m	Density of Φ_m	10^{-3}
λ_s	Density of Φ_s	10^{-3}
λ_1	Density of Φ_1	10^{-3}
\mathcal{R}_1	MBS coverage radius	1000m
\mathcal{R}_2	SBS coverage radius	200m
\mathcal{R}_3	DT coverage radius	20m
$\Upsilon_m, \Upsilon_s, \Upsilon_d$	Transmit SNRs	[10 – 40]dB
\bar{N}, \bar{L}	Gauss-Chebyshev parameter	5
\bar{S}	Laguerre polynomial degree	2
U	Terms for Laplace inversion	10

1. Average outage comparison and verification of results

The first set of results is presented in Figure 4.6 to compare the average outage performance among MBS user, SBS user, and DR. The results are obtained from the derived outage expressions in (4.30), (4.33) and (4.34). The performance of considered NOMA based network is also compared with that of conventional OMA based network. In addition, Monte Carlo simulations are performed to validate the accuracy of derived outage expressions, which are shown to be in good agreement with the simulations. Several observations can be drawn from Figure 4.6, which are described as follows:

1) It can be observed that NOMA based two-tier cellular network achieves lower outage probability than its OMA counterpart under an interference limited environment. The reason is that in contrast to NOMA based network which serves $M + S$ cellular (MBS and SBS) users in two transmissions, OMA based implementation requires $M + S$ transmissions to serve M MBS and S SBS users, which are hence subject to network interference in every transmission, resulting in overall higher outage probability.

2) The MBS user achieves better outage performance than the SBS user and DR because of the higher MBS transmit power, which results in better SINR for decoding. In addition, DR performs better than SBS user with NOMA-SIC and OMA for SNRs > 25 dB, and 20 dB, respectively. This is because of better SINR as SNR improves and due to smaller pathloss of D2D communication which occurs in short range ($\mathcal{R}_3 < \mathcal{R}_2$). However, at very high SNRs (>37 dB), SBS-NOMA user with SIC again tends to outperform DR due to better removal of intra-user interference. Unlike SBS-NOMA with SIC, the performance of SBS user under proposed SIE is better than DR in all SNR regime because of the estimation and removal of intra-user interference.

Further, at a certain time instant, MBS user and DT can be of clustered or non-clustered type, whereas SBS user is always a clustered user. Having said that, SBS user receives higher interference than MBS user and DR (in average terms) because clustered user experiences interference from $\{\Phi_m, \Phi_s, \Phi_{\text{NDT}}, \Phi_{\text{CDT}}\}$ whereas non-clustered user may receive interference from $\{\Phi_m, \Phi_{\text{NDT}}, \Phi_{\text{CDT}}\}$. This argument coupled with (4.30) and (4.34) may explain another reason for MBS user and DR to achieve lower outage probability than SBS user. One interesting observation is that SBS-NOMA with perfect and imperfect SIE manages to achieve better outage performance than MBS with NOMA-SIC at SNRs > 20 dB, and 25 dB, respectively. This indicates that for NOMA users, the network interference dominantly impacts their performance at low SNRs, whereas the intra-user interference dominantly impacts their performance at high SNRs.

3) It is observed that MBS and SBS users under proposed SIE achieve better outage performance than that achieved with conventional SIC. This is because SIE estimates and removes the intra-user interference from the MBS/SBS user message before final decoding. It is also noted that imperfect SIE achieves better performance than conventional SIC because it manages to partially remove the intra-user interference, whereas SIC makes no attempt to remove it. As a consequence, the results for MBS/SBS NOMA with perfect SIE and conventional SIC can be interpreted as the upper and

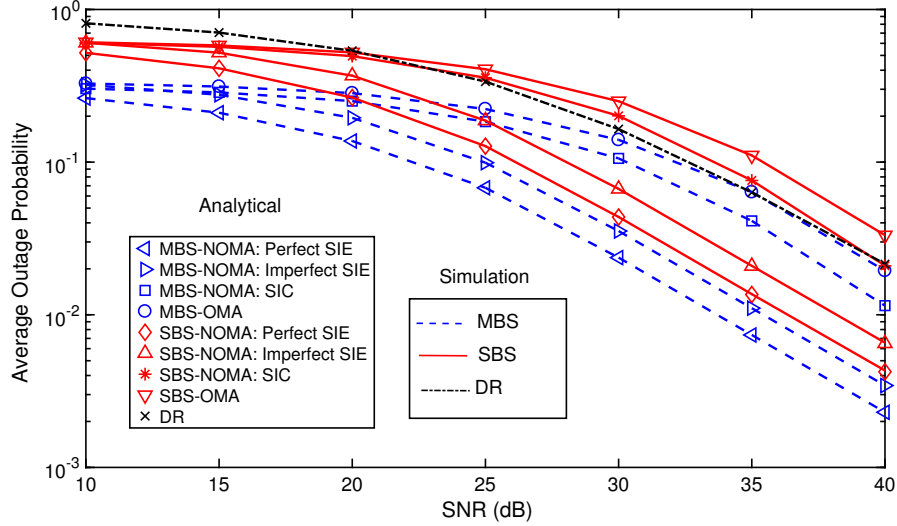


Figure 4.6. Outage comparison among MBS user, SBS user and DR, with $p = q = p_m = 0.5$ and $\bar{c} = 5$.

lower performance bounds for NOMA user, respectively. Hence, any attempt to remove intra-user interference would result in a performance lying between perfect SIE and conventional SIC. This indicates the impact of intra-user interference on the performance of MBS/SBS NOMA user and emphasize the necessity for systematic treatment of intra-user interference from the received NOMA signal.

2. Performance comparison for MBS user and DR of non-clustered and clustered types

In order to gain further insights, Figure 4.7 demonstrates the individual performance of MBS user and DR of non-clustered and clustered type. The results are obtained by using (4.31), (4.32), (4.35) and (4.36). It is found that non-clustered MBS user (DR) outperforms clustered MBS user (DR), respectively. This is intuitively plausible because clustered users (MBS and DR) generally experience greater network interference than their non-clustered counterparts. The reason is that non-clustered users (MBS and DR) experience interference from three transmitter sources ($\Phi_m, \Phi_{\text{NDT}}, \Phi_{\text{CDT}}$), whereas clustered users receive interference from four types of transmitters ($\Phi_m, \Phi_s, \Phi_{\text{NDT}}, \Phi_{\text{CDT}}$). This results in lower SINR at clustered users (MBS

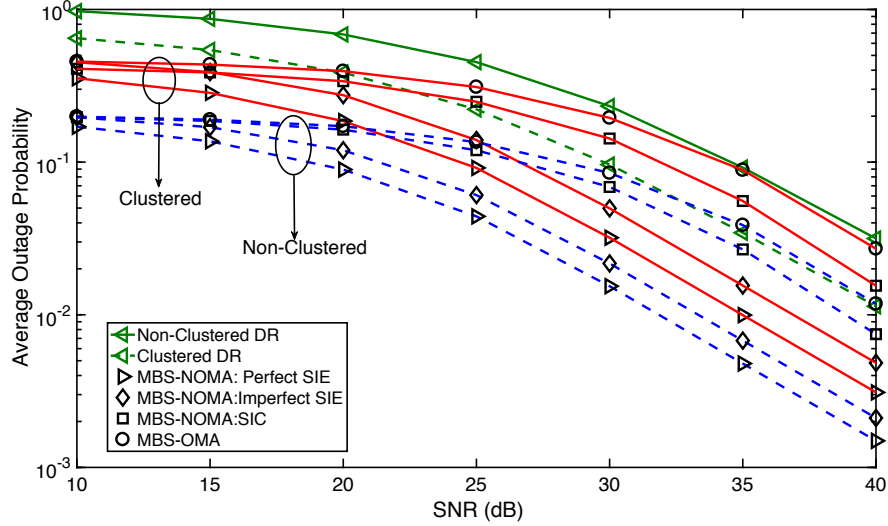


Figure 4.7. Outage comparison among non-clustered and clustered MBS user and DR, with $p = q = p_m = 0.5$ and $\bar{c} = 5$.

and DR) for decoding which translates into higher outage probability. In addition, non-clustered DR outperforms clustered MBS user with NOMA-SIC and OMA at SNRs > 23 dB, and 20 dB, respectively. This can be explained as follows. First, DT and DR are communicating over a shorter link which results in higher SINR due to smaller pathloss. Second, as mentioned, non-clustered DR experiences less network interference than clustered MBS user and MBS with NOMA-SIC does not treat intra-user interference. Consequently, this results in lower SINR available for decoding at clustered MBS user with NOMA-SIC and OMA than non-clustered DR for SNRs > 23 dB, and 20 dB, respectively. However, due to estimation and removal of intra-user interference, clustered MBS user with NOMA-SIE always outperforms non-clustered DR in all SNR regime. Finally, the performance gains of non-clustered/clustered MBS-NOMA over MBS-OMA and MBS with NOMA-SIE over NOMA-SIC can be explained by following similar arguments as were used in the discussion of Figure 4.6.

3. Association Probability

In Figure 4.8, the association probability is plotted as a function of Ω for clustered

cellular user to connect with MBS or SBS in order to exhibit its trend. The results are obtained by plotting (4.12) and (4.13) from Lemma 2. It can be seen that increasing Ω results in larger association probability for clustered cellular user to connect with MBS because its received power from MBS increases. Further, at $\Omega = 1$, the probability of clustered cellular user to associate with MBS or SBS becomes equal. This is intuitively plausible because for $\Omega = 1$, the clustered cellular user is receiving equal amount of powers from MBS and SBS, and thus is equally probable to connect to any BS.

4: Link Throughput

The average link throughput achieved by a randomly chosen cellular user and DR is shown in Figure 4.9 as a function of SNR. The results are obtained by using (4.40) and (4.41). The results in Figure 4.9 demonstrate that an arbitrarily chosen user from NOMA based cellular network achieves superior link throughput than another arbitrarily chosen user from OMA based cellular network and DR. This is because NOMA user achieves overall lower outage probability than DR and OMA user, which is evident from the results of Figs. 4.6 and 4.7. Moreover, NOMA user with SIE obtains better throughput than NOMA with SIC due to superior outage performance of NOMA under SIE. In addition, DR obtains higher throughput than OMA cellular user because of its better outage performance due to smaller pathloss by communicating over short links. In addition, OMA based cellular network shares the available spectrum resources among $M + S$ cellular users, which further translates into a loss in overall link throughput.

5. Optimum number of SBSs

In Figure 4.10, the impact of varying SBS density λ_s on the average link throughput of the cellular user is investigated. The results are obtained by using (4.41) for NOMA and OMA based cellular networks at SNR of 20 dB. Under the considered setting, the results indicate the existence of an optimum value of $\lambda_s = 4 \times 10^{-3}$ beyond which no further improvement in link throughput is achieved. The reason is because deploying more SBSs would also increase network interference and consequently after

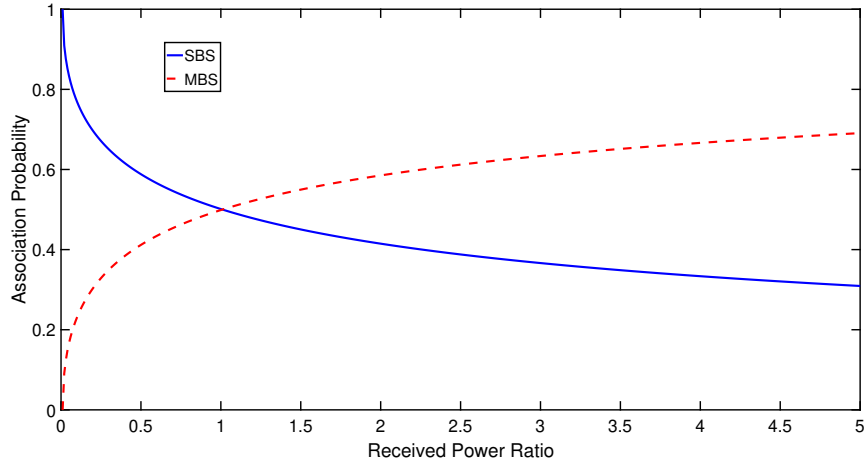


Figure 4.8. Probability of clustered cellular user to connect MBS or SBS.

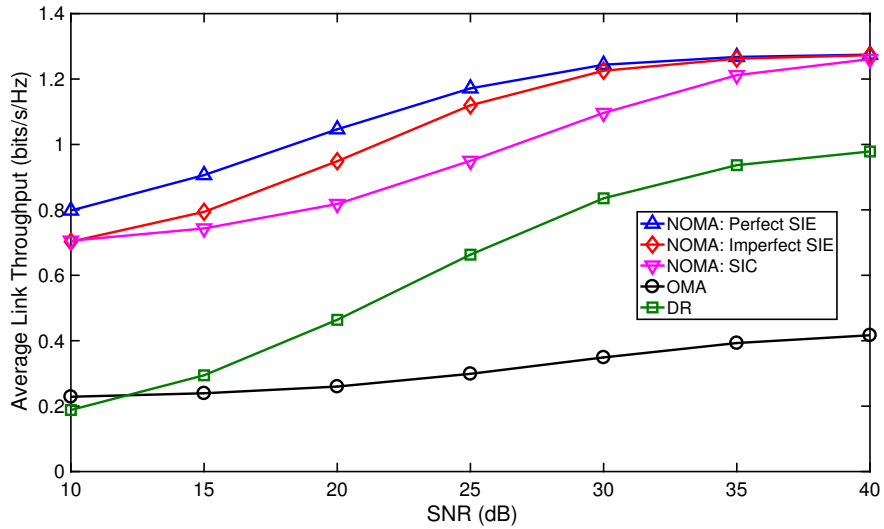


Figure 4.9. Link Throughput comparison among MBS user, SBS user, DR and OMA user.

the optimum λ_s is reached, no further improvement in outage probability of cellular users can be achieved, which translates into a link throughput saturation.

6. Performance of DR under NOMA and OMA networks

Figure 4.11 presents the final set of results where the impact of NOMA or OMA based cellular network on the performance of DR is investigated. It is observed that

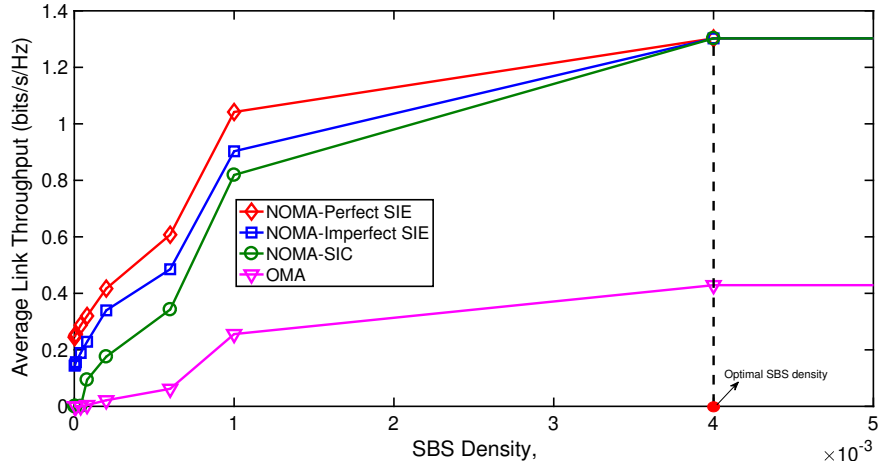


Figure 4.10. Impact of varying SBS density on link throughput of cellular user.

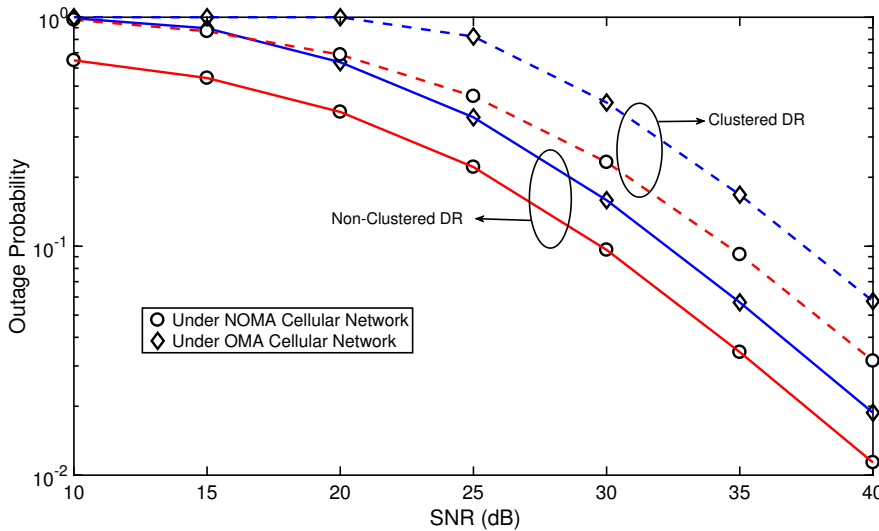


Figure 4.11. Outage of DR under NOMA and OMA networks.

both non-clustered and clustered types of DR achieve lower outage probability when cellular network is using NOMA in both tiers. The reason is that NOMA based cellular network serves $M + S$ users of two-tiers by using only two transmissions, whereas OMA based network requires $M + S$ transmissions to serve $M + S$ users in both tiers. Consequently, a DR experiences more interference under OMA based network than under NOMA based network. Owing to the potential benefits of inband D2D

communication, the results in Figure 4.11 suggest that adopting NOMA for all BS tiers can improve performance of not only cellular users but also DRs as compared to a OMA based network.

4.6 Chapter Summary

In this chapter, a new spatial model has been developed for NOMA based two tier-cellular network with underlay inband D2D communication and randomly deployed BSs and users. In particular, the locations of users are modeled by considering two independent PHP and PCP. Using the developed model, the interference distributions at typical user (cellular/D2D receiver) are first derived by considering contribution from dominant interferers. Further, as the performance of NOMA with SIC is impacted by intra-user interference, a SIE receiver is proposed for cellular users which attempts to locally estimate and remove intra-user interference for better decoding. Based on the interference distributions results, the performance of typical user in terms of outage probability is analysed. Specifically, the performance of typical cellular user is evaluated under conventional SIC and proposed SIE with perfect and imperfect intra-user interference estimation. In addition, using the outage probability results, the average link throughput of typical cellular user and DR are studied. Simulation results are also presented to validate the accuracy of the derived results.

Chapter 5

Quality of Service based NOMA Group D2D Communications

As in the investigation of NOMA in multi-tier cellular networks in the previous chapter, the current literature has paid very little attention to investigate NOMA group D2D communications. Hence, the focus of this chapter is to investigate and analyse the performance of NOMA based group D2D communications under interference limited scenarios.

5.1 Introduction

In this work, in order to capture the key features of D2D communications, i.e., device clustering and spatial separation, the DTs are considered to be randomly distributed over \mathbb{R}^2 according to GPP, while the DRs are assumed to be randomly clustered around DTs. The reason for choosing GPP is that it is a relatively simpler cluster point process that maintains good trade-off between modeling accuracy and analytical tractability. Therefore, in the context of D2D communications, GPP provides more realistic modeling approach against PPP case by capturing the clustering behaviour of D2D devices [81].

Furthermore, the current approach to order users in NOMA group D2D communications is based on the channel gains of the DRs. This ordering approach may not be suitable to D2D communication scenario under which the DRs in the same group are clustered around a common DT and are located in proximity of each other. Hence, the channel conditions of the DRs located in the same D2D group would be very similar. Consequently, this ordering strategy may result in very similar power allocation, which could limit the gains of applying NOMA to D2D communications [6]. In the context of NOMA, there are few works that use QoS based ordering [82–84]. They mainly focused on cellular networks and are limited to the two-user case only. In this chapter, Q-NOMA group D2D communications is proposed and analysed which makes an attempt to fill the aforementioned gaps in literature, and it is the first time that Q-NOMA is proposed and analysed to realise group D2D communications under interference limited scenario.

The main contributions of this chapter are briefly summarised as follows:

- A Q-NOMA group D2D communications is proposed in which D2D users are randomly distributed over the entire two-dimensional plane. Unlike the existing proposals, the DRs in the proposed scheme are ordered according to their QoS requirements, which is more appropriate for the D2D communications scenario.
- The interference distribution at the probe DR is derived by utilizing the results from stochastic geometry. The Laplace transform of interference over GPP is derived in [81], which involves complex double integrals. In order to obtain useful insights, a major step in characterizing the interference is the approximation of integrals in the interference Laplace transform by applying Gaussian–Chebyshev and Gauss–Laguerre quadratures. This approximation results in an interference Laplace transform expression, which is easy to implement.
- Based on the interference approximation results, a closed-form expression for outage probability of the DRs in the proposed Q-NOMA group D2D communications

Table 5.1: Commonly used variables.

Notation	Description
M	Total number of DRs
R_m	Targeted rate of DR m
P_{GT}	Transmit power of GT
β_m	Power allocation coefficient of m -th DR (policy I)
β_m^F	Power allocation coefficient of m -th DR (policy II)
ρ_t	Transmit SNR of GT
d_x	Distance between probe DR and interferer at x
s_m	Message signal of user m
y_m	Received NOMA signal at DR m
\mathcal{I}	Interference at user probe DR
Φ_{GT}	GPP to model DTs locations
λ_{GT}	Intensity of Φ_{GT}
R_D	Coverage radius of GT
N, L	Gaussian-Chebyshev parameters

is derived in order to evaluate the performance.

- Numerical results are presented to validate the accuracy of the derived outage results and compare the performance of the proposed Q-NOMA group D2D with conventional paired D2D communications using OMA.

The rest of this chapter is organised as follows. Sections 5.2 and 5.3 discusses the system model, and proposes the QoS-based NOMA group D2D communications scheme, respectively. Performance analysis is presented in Section 5.4, followed by the numerical results and discussion in Section 5.5. Finally, the chapter is concluded in Section 5.6.

5.2 System Model

Consider inband D2D communications with an overlay cellular network, where a frequency reuse factor of one is assumed among D2D users to achieve better spectrum efficiency. With this setting, every D2D transmission by a DT is subjected to interference

from other active DTs. A composite fading and path loss channel model is considered between every DT and DR. In this chapter, the power fading coefficients are considered to be i.i.d with exponential distribution of unit mean, and a path loss model of $d^{-\alpha}$ is adopted, where d is the distance between the probe DR and test DT, and α is the path loss exponent.

5.2.1 Spatial Distribution of D2D Users

Consider that D2D users are randomly distributed over \mathbb{R}^2 . At any time realization, the D2D users are classified as transmitters or receivers. A group D2D scenario is considered, where each DT is communicating with multiple DRs via a NOMA scheme. A DT which is communicating to multiple D2D devices is referred as a group transmitter (GT). Any D2D user can take a role of GT. It is assumed that the selection of GTs is performed by a BS, and multiple GTs in a given cell can be selected to improve overall system capacity. In addition, multiple GTs are allowed to exist in proximity of each other, where each GT is communicating to its own group of receivers. Hence, at any time realization, each selected GT forms a group/cluster containing DRs. In order to capture both inband and device clustering, the spatial topology of the GTs is modelled by a stationary and isotropic GPP defined on \mathbb{R}^2 , denoted by Φ_{GT} with parent process intensity λ_{GT} . Furthermore, the coverage of each GT is modelled by a disc D with radius R_D . Moreover, the DRs are considered to be clustered around each GT and are assumed to be uniformly distributed inside coverage of GTs. An illustration of NOMA group D2D communication is presented in Figure 5.1. For a quick reference, a list of commonly occurring variables in this chapter is provided in Table 5.1.

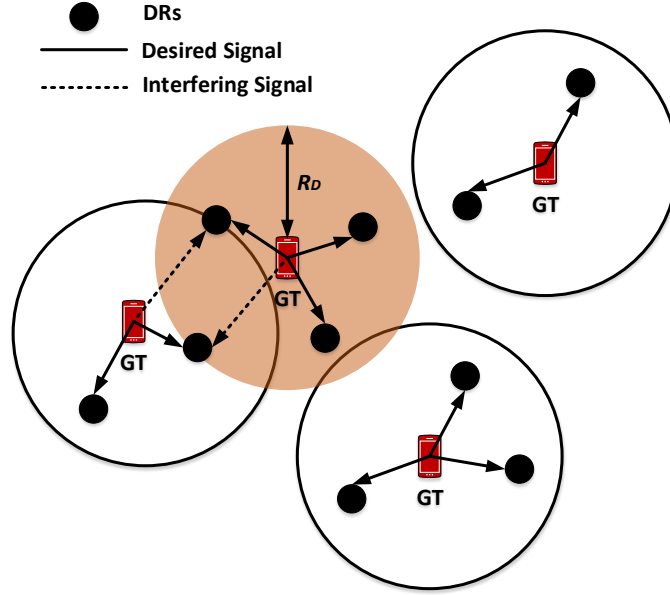


Figure 5.1: Example of inband non-orthogonal multiple access (NOMA) group device-to-device (D2D) communications with overlay cellular network.

5.3 Proposed QoS NOMA Group D2D Communications

Since DRs are clustered around GTs and are located in proximity of each other, therefore, the DRs connected to same GT would have very similar channel conditions. Consequently, in the context of D2D communications, ordering DRs according to their channel conditions to apply NOMA at GT may not achieve the desired multiplexing gains and fairness among DRs. Hence, in this chapter, it is proposed that the DRs for GT are ordered according to their QoS requirements, which are determined by their targeted data rates.

Let there be a total of M DRs distributed inside coverage of a test GT. The probe DR is assumed to be located at the origin, with a desired test GT at $x_0 = (d, 0)$ with $d \neq 0$. Without loss of generality, it can be assumed that the DRs are ordered as $R_1 \leq \dots \leq R_M$, where R_i is the targeted data rate of DR i , $1 \leq i \leq M$. Correspondingly, the power allocation coefficients are sorted as $\beta_1 \geq \dots \geq \beta_M$.

The aforementioned procedure to order DRs of the GT and compute their power allocation coefficients according to users' targeted rates is termed as “*Q-NOMA*”. When it is applied to D2D communications, the communication is referred as “*Q-NOMA group D2D communication*”.

Consider that the NOMA DR m is the probe receiver, then, the received signal from the test transmitter at the probe DR is given as:

$$y_m = h_m \sum_{i=1}^M \sqrt{\beta_i P_{GT}} s_i + n_m, \quad (5.1)$$

where P_{GT} is the transmission power of test GT, s_i is the message signal of DR i and n_m is the AWGN with zero mean and variance σ^2 .

5.3.1 Power Allocation Coefficients Policies

The optimal power and resource allocation improve overall performance and utilise the system resources efficiently. However, the optimum power allocation strategies proposed in existing literature, for example, [85], cannot be directly applied to the current work because of significant difference in system model or underlying transmission method. Therefore, in this sub-section, two simple methods are discussed to compute power allocation coefficients $\{\beta_i\}_{i=1}^M$ that would lead to two possible implementations of Q-NOMA group D2D communications.

Policy I

The Policy I utilises targeted rates of DRs to compute the power allocation coefficients. Similar to [6], the power allocation coefficient for DR i under Policy I is computed as:

$$\beta_i = \frac{1/R_i}{\sum_{j=1}^M \frac{1}{R_j}}. \quad (5.2)$$

The intuition behind Equation (5.2) is that power allocation coefficients could be

utilised to maintain fairness among DRs [5, 86]. In case they are computed in proportion with users' targeted rates, then the highest ordered DR M would result in the highest SIC decoding order with maximum SINR threshold among all ordered DRs. Consequently, all of the lower ordered DRs always require the maximum SINR threshold dictated by the user M , which would result in a biased treatment of lower ordered users (with lower targeted rates). Hence, in order to avoid this biasness, it is proposed to compute the power allocation coefficients as given by Equation (5.2).

Policy II

The concept of F-NOMA was proposed in [13], where the power allocation coefficients are fixed and are computed based on the given user ordering i.e., it does not utilise the actual channel gains to compute $\{\beta_i\}_{i=1}^M$. Similar to [13], a Policy II is adopted to compute $\{\beta_i\}_{i=1}^M$ for conventional NOMA that does not utilise the actual targeted rates of DRs. The power allocation coefficient for DR i under Policy II is computed as:

$$\beta_m^F = \frac{M - m + 1}{\mu}, \quad (5.3)$$

where β_m^F represents the power allocation coefficient of DR m in Policy II and μ is selected in such a way that $\sum_{i=1}^M \beta_i^F = 1$.

5.3.2 Interference Distribution

The reception at the probe DR from the test GT is interfered by the other GTs. The interference at probe DR is given as, $\mathcal{I} = \sum_{x \in \Phi_{GT} \setminus x_0} |g_x|^2 d_x^{-\alpha}$, where g_x and d_x represent the Rayleigh fading channel gain and distance between probe DR and interferer at x , respectively. The following lemma provides the Laplace transform of the interference at probe DR.

Lemma 5.1. *Lemma: Consider a GPP Φ_{GT} with parent process intensity λ_{GT} modeling*

spatial topology of the GTs in a Q-NOMA group D2D communications. Then, the Laplace transform of the interference at the probe DR conditioned at the location of test GT is given by:

$$\mathcal{L}_{\mathcal{I}}(s) = e^{-2\pi\lambda_{GT} \sum_{p=1}^P \Omega_p \frac{\alpha(1-X_1(r_p))+sr_p^{-\alpha}}{1+sr_p^{-\alpha}}} \cdot \Lambda_2(d), \quad (5.4)$$

where $\Omega_p = \omega_p e^{r_p}$, $\omega_p = \frac{\Gamma(P+2)r_p}{P!(P+1)^2(L_{P+1}(r_p))^2}$, $L_P(\cdot)$ is the Laguerre polynomial of degree P , r_p are the roots of $L_P(\cdot)$, $X_1(\cdot)$ and $\Lambda_2(\cdot)$ are given in (I.7) and (I.10), respectively.

Proof. See Appendix I. □

5.4 Outage Analysis

In this section, the outage probability for the DRs in the considered Q-NOMA group D2D communication is derived. Let τ_m and R_m denote the SINR threshold and targeted rate of DR m , respectively, where $\tau_m = 2^{R_m} - 1$. Since each DR employs SIC, the outage at DR m occurs if it does not meet the targeted rate of any higher order DR j , where $1 \leq j < m$. Denote $\zeta_{m \rightarrow j} = \left\{ \tilde{R}_{m,j} < R_j \right\}$ as the outage event at DR m due to decoding of DR j , where $\tilde{R}_{m,j}$ is the achievable rate of user j at DR m . The outage event $\zeta_{m \rightarrow j}$ can be expressed as:

$$\begin{aligned} \zeta_{m \rightarrow j} &= \left\{ \tilde{R}_{m,j} < R_j \right\} \\ &= \left\{ \log_2 \left(1 + \frac{h_m \beta_j P}{h_m P \sum_{i=j+1}^M \beta_i + \mathcal{I} + \sigma^2} \right) < R_j \right\} \\ &= \left\{ h_m < \frac{\varphi_j (\rho \mathcal{I} + 1)}{\rho_t} \right\}, \end{aligned} \quad (5.5)$$

where $\varphi_j = \frac{\tau_j}{\beta_j - \tau_j \sum_{i=j+1}^M \beta_i}$, $\rho = \frac{P_T}{\sigma^2}$, $\rho_t = \frac{P_{GT}}{\sigma^2}$ is the transmit SNR and P_T is the maximum received interference power at the probe DR.

Next, define $\varphi_m^{\max} = \max \{\varphi_1, \dots, \varphi_m\}$. Based on (5.3), the outage probability at the DR m can be given as:

$$\begin{aligned} \mathbb{P}_m &= \Pr \left(h_m < \frac{\varphi_m^{\max}(\rho\mathcal{I} + 1)}{\rho_t} \right) \\ &= \mathbb{E}_{\mathcal{I}} \left[F_{h_m} \left(\frac{\varphi_m^{\max}(\rho x + 1)}{\rho_t} \right) \right], \end{aligned} \quad (5.6)$$

where F_{h_m} is the cumulative distribution function (CDF) of h_m .

Note that the set $\{h_i\}, i = 1, \dots, M$, of channel gains is not ordered because the users are sorted in ascending order of their targeted rates. Since the channel gains are i.i.d. random variables with common CDF F_h , (5.4) can be re-written as:

$$\mathbb{P}_m = \mathbb{E}_{\mathcal{I}} \left[F_h \left(\frac{\varphi_m^{\max}(\rho x + 1)}{\rho_t} \right) \right]. \quad (5.7)$$

Consequently, the outage probability of DR m is provided in the following theorem.

Theorem 5.1. *The outage probability of DR m in the Q -NOMA group D2D communications is derived as:*

$$\mathbb{P}_m = \sum_{l=1}^L b_l e^{-\frac{\varphi_m^{\max} c_l}{\rho_t}} \mathcal{L}_{\mathcal{I}} \left(\frac{\varphi_m^{\max} c_l \rho}{\rho_t} \right), \quad (5.8)$$

where $b_l = \omega_l \sqrt{1 - \phi_l^2} (1 + \phi_l)$, $\omega_l = \frac{\pi}{L}$, $c_l = \left(\frac{R_D}{2} (1 + \phi_l) \right)^\alpha$, $\phi_l = \cos \left(\frac{(2l-1)\pi}{2L} \right)$ and L is the complexity-accuracy trade-off parameter.

Proof. In order to obtain \mathbb{P}_m , F_h is required. Since, all wireless links exhibit Rayleigh fading and the DRs are uniformly distributed inside disc D centered at the location of

test GT, the CDF F_h can be expressed as [79]:

$$F_h(y) = \frac{2}{R_D^2} \int_0^{R_D} (1 - e^{-z^\alpha y}) z dz. \quad (5.9)$$

It is challenging to solve the above integral. As such, it is approximated by applying Gaussian-Chebyshev quadrature as:

$$F_h(y) = \sum_{l=1}^L b_l e^{-c_l y}. \quad (5.10)$$

Based on (5.10), \mathbb{P}_m in (5.5) can be expressed as:

$$\begin{aligned} \mathbb{P}_m &= \int_0^\infty F_h \left(\frac{\varphi_m^{\max}(\rho x + 1)}{\rho_t} \right) f_{\mathcal{I}}(x) dx \\ &= \sum_{l=1}^L \int_0^\infty e^{-\frac{c_l \varphi_m^{\max}(\rho x + 1)}{\rho_t}} f_{\mathcal{I}}(x) dx \\ &= \sum_{l=1}^L b_l e^{-\frac{c_l \varphi_m^{\max}}{\rho_t}} \int_0^\infty e^{-\frac{c_l \varphi_m^{\max} \rho x}{\rho_t}} f_{\mathcal{I}}(x) dx \\ &= \sum_{l=1}^L b_l e^{-\frac{c_l \varphi_m^{\max}}{\rho_t}} \mathcal{L}_{\mathcal{I}} \left(\frac{c_l \varphi_m^{\max} \rho}{\rho_t} \right), \end{aligned} \quad (5.11)$$

where $f_{\mathcal{I}}(x)$ is the PDF of interference \mathcal{I} and the last step follows from the definition of Laplace transform. This proves the result in Theorem 5.1. \square

Note that, due to the presence of interferers in the network, similar to [68, 87], the derived outage probability in (5.8) is a function of variables φ_m^{\max} and interference Laplace transform $\mathcal{L}_{\mathcal{I}}$. This is different from existing works that analyse NOMA wireless systems under no interference where outage probability is mainly a function of φ_m^{\max} . For reference, please see [13, 51, 59]. Furthermore, it is worthy to note that the current outage analysis approach remains valid if more complex cluster models (PCP, and so on.) are adopted for modeling spatial distributions of DTs and DRs. In that

Table 5.2: Simulation parameters.

Parameter	Description	Value
M	Total users	3
$\{R_m\}_{m=1}^M$	Users' targeted rates	$\{0.7, 1.1, 2\}$
R_D	Coverage of GT	10 m
α	Path loss exponent	4
λ_{GT}	Intensity of GTs	10^{-4}
ρ_t	SNR range	(5–40) dB
L, N, V, Q, S	Gaussian-Chebyshev parameters	5
P	Degree of Gauss-Laguerre polynomial	5
d	Distance between probe DR and GT	5 m

case, the $\mathcal{L}_{\mathcal{I}}$ term will be replaced by the Laplace transform of the interference for the adopted model. Intuitively, $\mathcal{L}_{\mathcal{I}}$ is performing a form of scaling in (5.8) and hence the conclusions are expected to remain the same if the spatial distribution model(s) of the DTs and DRs is changed. However, the exact impact on outage probability when more complex cluster processes model is adopted for modeling DT and DR locations would require further study, and hence is considered as a promising future work.

5.5 Numerical Results and Discussion

This section presents the numerical results to evaluate the performance of the considered network as well as to validate the accuracy of the derived expression in (5.8) of Section 5.4. As shown in Table 5.2, simulation parameters used are similar to those in [51], unless otherwise stated. Furthermore, Policy I is considered as a default policy to compute power allocation coefficients, unless otherwise stated.

1. Impact of R_D on Outage Probability

Figure 5.2 presents the impact of varying coverage radius R_D of test GT on the outage probability of ordered DRs as a function of SNR. The derived outage results in (5.8) are shown to be in good agreement with the Monte Carlo simulations.

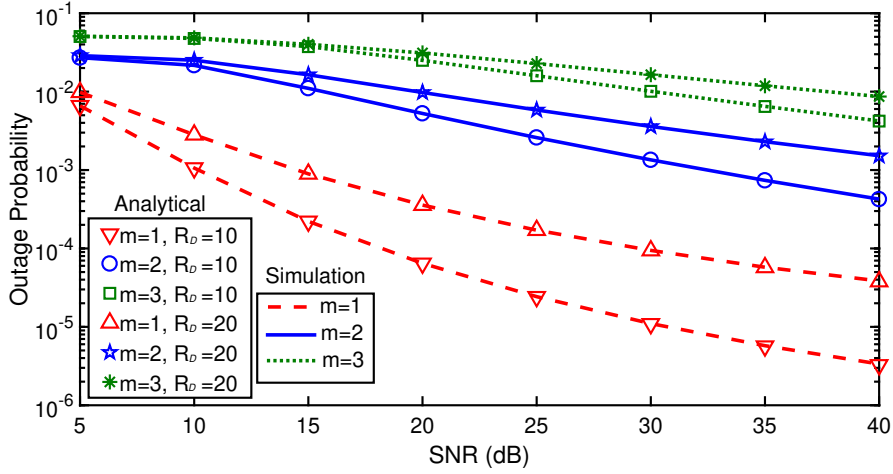


Figure 5.2: Impact of R_D on outage probability.

Several observations can be made from the results in Figure 5.2: (1) increasing the coverage radius of GT results in a higher outage probability because of a larger path loss; (2) different ordered users have distinct decreasing slopes of outage probability because of different targeted rates; (3) the higher order DRs in the proposed Q-NOMA group D2D communications achieve better outage performance because they have smaller targeted rates. This is different from conventional NOMA that orders users based on channel conditions, and where the higher ordered users have larger outage probabilities due to poor channel conditions [13, 87].

2. Impact of d on Outage Probability

The impact of varying distance between probe DR and test GT on the outage performance is investigated in Figure 5.3. It can be observed that varying d has a larger impact on the average achievable outage probability at lower SNR value of 5 dB. This is intuitively plausible because increasing transmission power results in improved SINR at the receiver and hence better outage performance.

3. Comparison between Paired and Grouped D2D Communications

The average outage probability achieved by Q-NOMA group D2D communications under different path loss exponents is shown in Figure 5.4. The performance of paired

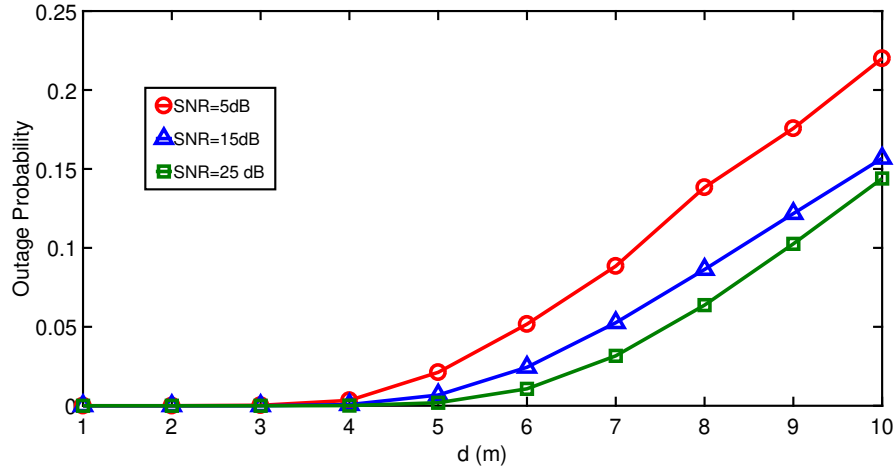


Figure 5.3: Impact of d on outage probability.

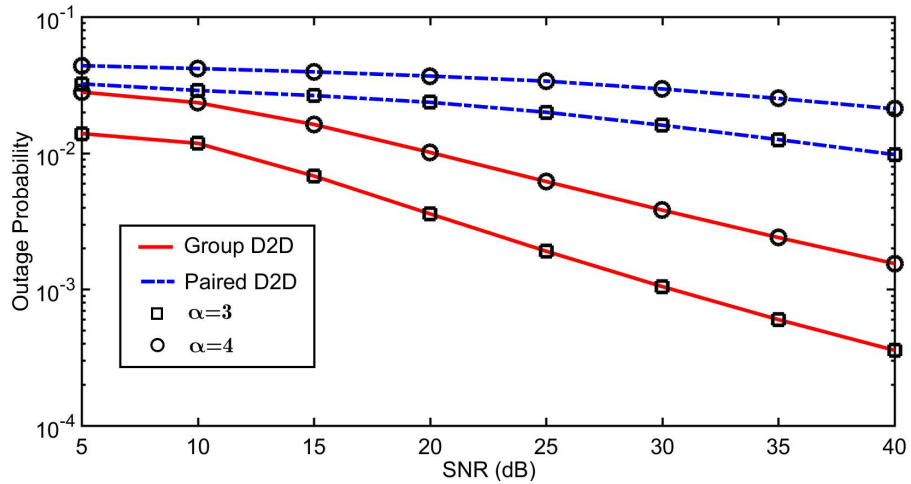


Figure 5.4: Outage comparison between paired and group D2D.

D2D communication based on OMA is also presented in the figure as a benchmark for comparison. It can be observed that Q-NOMA group D2D achieves overall lower outage probability than the paired D2D communication for different values of path loss. This is because, as opposed to paired D2D, Q-NOMA group D2D communication uses only single transmission, which results in better SINR at the DRs under an interference limited scenario.

4. Comparison between Two Implementations of Q-NOMA Group D2D Communications In this section, the performance of two possible implementations of Q-NOMA group D2D communications based on power allocation coefficients Policies I and II is compared. The results for Q-NOMA group D2D communication under Policy I are also obtained by utilising (5.8), with the exception that $\{\varphi_m^{\max}\}_{m=1}^M$ are computed by using fixed power allocation coefficients $\{\beta_m^F\}_{m=1}^M$. For this comparison, five different cases are considered for users' targeted rates which are utilised to compare the outage probabilities achieved by the Q-NOMA group D2D communications under Policies I and II at an SNR of 25 dB. Table 5.3 summarizes the outage comparison between these two implementations of the group D2D communications. The power allocation coefficients for Policy I are derived as $\beta_m^F = \{0.5, 0.33, 0.17\}_{m=1}^M$, whereas those for Policy II are calculated using (5.2) based on users' targeted rates and are shown in Table 5.3.

It is observed from the results in Table 5.3 that Q-NOMA under Policy I achieves lower outage probability in cases 1 and 2, whereas it obtains better outage performance in cases 4 and 5 for Policy II. In addition, the results in case 3 indicate the importance of proper power and rate allocation to avoid situations of complete outage. Moreover, it can be observed that the Q-NOMA group D2D communication under Policy I performs better in cases where the users' targeted rates are significantly apart. This is more suitable to D2D communication scenarios where different users may have diverse QoS requirements.

Table 5.3: Average outage comparison between two implementations of quality of service based non-orthogonal multiple access (Q-NOMA) group device-to-device (D2D) communications.

Case	Targeted Rates, $\{R_m\}_{m=1}^3$	Power Allocation Coefficients, $\{\beta_m\}_{m=1}^3$	Policy I	Policy II
1.	{1, 2.5, 3}	{0.58, 0.24, 0.18}	0.04	1
2.	{1, 1.5, 2}	{0.47, 0.3, 0.23}	0.002	0.04
3.	{0.5, 1.5, 2}	{0.63, 0.21, 0.16}	1	1
4.	{0.9, 1, 2}	{0.42, 0.38, 0.2}	1	0.001
5.	{0.2, 2, 2.2}	{0.85, 0.08, 0.07}	0.006	0.002

Table 5.4: Average outage comparison between paired device-to-device (D2D) and quality of service based non-orthogonal multiple access (Q-NOMA) group D2D communications ($M > 3$).

Total Users, M	Q-NOMA Policy I	Q-NOMA Policy II	Paired D2D
5	0.003	0.07	0.08
7	0.007	0.06	0.12
9	0.01	0.1	0.3

In order to extend the analysis beyond the case of $M > 3$ users, the average outage comparison between paired D2D and Q-NOMA group D2D communications (based on power allocation coefficients Policies I and II) is further presented in Table 5.4. These results are obtained by considering $M = 5, 7, 9$ with $R_m \sim \mathcal{U}(0.1, 2)$, $\forall m \in M$ and $\rho_t = 25$ dB, where $\mathcal{U}(\cdot, \cdot)$ represents the random uniform distribution function. It can be observed that the results in Table 5.4 are consistent with those presented in Figure 5.4, for example, Q-NOMA group D2D communications consistently achieve lower outage probability than paired D2D communications.

5.6 Chapter Summary

In this chapter, a Q-NOMA group D2D communications is proposed. In order to study the performance of the proposed network, the Laplace transform of the interference is

first derived, based on which the closed-form expression for outage probability to analyse the performance of the DRs in the proposed Q-NOMA group D2D communications is derived. The results show that the proposed Q-NOMA group D2D achieves overall lower outage probability than its counterpart paired D2D communication. Furthermore, based on two power allocation coefficient policies, the comparison between two possible implementations of the proposed Q-NOMA group D2D communications is presented. Due to the similar channel conditions and diverse QoS requirements of DRs, the results show that the proposed Q-NOMA implementation based on Policy I is more realistic and suitable than one based on Policy II for group D2D communications.

Chapter 6

NOMA for Ubiquitous Wireless Sensor Networks

The application of NOMA is well-studied in the context of cellular networks. However, no formal studies have been done in literature to explore the potentials of applying NOMA for UWSNs. This motivates the investigation and analysis of utilising NOMA for UWSNs in this chapter.

6.1 Introduction

Although originally proposed for cellular systems, NOMA exhibits strengths that are considered as highly relevant to addressing the deployment challenges of UWSNs, i.e. large-scale networks of wireless sensors densely deployed for ubiquitous monitoring of physical environments. Specifically, for a given spectrum bandwidth, NOMA can enable more simultaneous connections than existing approaches without the overheads of coding and spreading to facilitate the separation of users' signals at the receiver [12]. This is particularly attractive to supporting massive connectivity without requiring more

spectrum resources in UWSNs. NOMA can be applicable to both uplink (sensors-to-sink) and downlink (sink-to-sensors) communication where powerful sink nodes can perform the equivalent role of BSs for the tasks of user grouping and transmission power allocation. In UWSN, however, there is a greater motivation and challenge to apply NOMA in the downlink.

Firstly, UWSNs with large geographic coverage typically use short-range multi-hop communication in order to conserve energy [88]. The size of the routing table at each node increases with the number of destinations. Unlike in uplink communication where the sink node is the main destination of all sensors' outgoing traffic, the routing table size for DL communication can grow prohibitively with a massive number of sensors as destinations [89]. In this case, NOMA can offer a practical solution by enabling direct DL transmissions from sink node to multiple sensors simultaneously. DL transmissions are initiated when sink node queries a specific sensor or group of sensors for some information [90,91], or communicates information essential for their operations such as sleep-wake schedules [92]. Further, unlike 5G, most UWSNs operate in unlicensed spectrum where sensors also experience CT interferences [93] from other devices sharing the same spectrum.

To date, NOMA has been investigated only in the context of cellular networks. The use of NOMA for UWSN has not been proposed in literature, and the reported performance gains of NOMA over its counterparts cannot be straightforwardly claimed for UWSN. This is because unlike in cellular network, the sink node in a UWSN has no control over all transmitters within its coverage, including sensors and sinks of other UWSNs under different administrative domains or CT nodes that share the same spectrum such as WiFi and Bluetooth devices. Hence, it is important to investigate the performance of a UWSN employing NOMA under interference-limited scenario.

The main novelty and contributions of this paper are summarised as follows.

- For the first time, NOMA is proposed as a spectrum efficient means of supporting massive connectivity in UWSNs, and its performance in a downlink scenario where sink transmits to a group of sensors using NOMA under CT and other interferences is investigated using stochastic geometry [34]. The sensors, sinks and CT nodes can reside randomly and independently of each other in a 2D plane. Hence, their spatial topologies can be modeled with three different homogeneous PPPs.
- In order to evaluate the performance, the closed-form expression for the outage probability at probe receiver's location is derived. In addition, the diversity order achieved by a probe receiver is also analysed. Further, the average link throughput and energy consumption efficiency analysis are also presented to gain better understanding of applying NOMA to UWSN and benchmark the performance against conventional OMA.
- Numerical results are shown to validate the accuracy of the performed analysis as well as compare the outage, throughput and energy efficiency performances between the NOMA and OMA based UWSNs. Moreover, a computational complexity analysis is performed to evaluate the complexity required by SIC units of sensor receivers to decode NOMA message signals.

The rest of this chapter is organised as follows. Section 6.2 describes the network model. Section 6.3 and 6.4 provide the outage and diversity analysis, and the throughput and energy consumption efficiency analysis, respectively. The results and discussion are presented in Section 6.5, followed by the chapter summary in Section 6.6.

Table 6.1: Commonly used variables in Chapter 6.

Notation	Description
α	Path loss exponent
β_j	Power allocation coefficient of j -th user
ϖ_j	Target SINR threshold for j -th user
P_{out}^m	Outage probability of the m -th user
$\phi(\cdot; \cdot; \cdot)$	Confluent hyper-geometric function
$\Lambda_{m \rightarrow j}$	SINR at m -th user to decode j -th user message
Λ_m	SINR at m -th user to decode its own message
κ	Average interference level
\mathcal{X}	Average system SNR
d_m	Distance between test transmitter and m -th user
d_0	Guard zone radius around each sensor receiver
h_m	Channel between m -th NOMA user and test transmitter
M	Total number of NOMA users
$L_S(\cdot)$	Laguerre polynomial of degree s
N, T	Gaussian-Chebyshev parameters
P	Transmit power of test transmitter
P_c	Constant power consumption of circuits
R	Radius of disc A
TP_m	Average link throughput of user m
ς	Overall energy consumption efficiency

6.2 Network Model

Consider a UWSN comprising of sensor and sink nodes, which are randomly distributed in an infinite 2D plane. Further, it is assumed that the CT nodes are also co-located with sensor and sink nodes. These CT nodes are not a part of UWSN but are operating in the same frequency band, and hence cause interference to the reception of probe receiver. The spatial topology of the sensor, sink and CT transmitter nodes is modeled by three homogenous PPPs, denoted by, Φ_{SK} , Φ_{SE} , and Φ_{CT} with intensities λ_{SK} , λ_{SE} , and λ_{CT} , respectively. A realisation of these transmitter processes is shown in Figure 6.1

In this chapter, a downlink transmission scenario is considered where a sink node communicates with sensor nodes using NOMA. In order to avoid ambiguity, the sensor receivers are referred to as *users*. In addition, the probe sink node is termed as a test

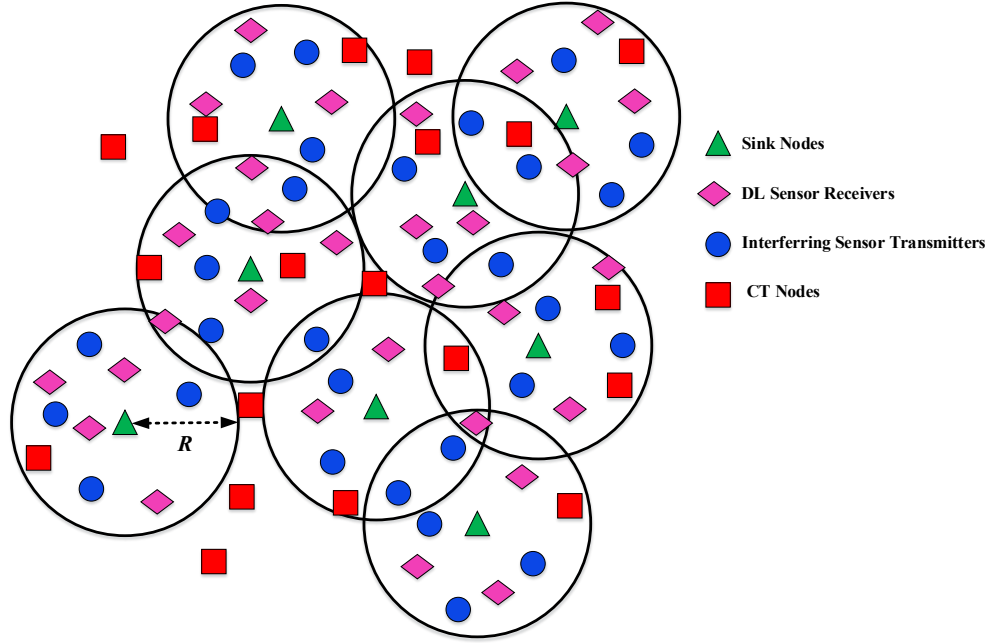


Figure 6.1: A realisation of Φ_{SE} , Φ_{SK} , and Φ_{CT} transmitter processes.

transmitter, which is considered to be located at the centre of a disc A with radius R . The M NOMA users are considered to be uniformly distributed inside disc A , as shown in Figure 6.2. Further, the probe receiver always means the m -th NOMA user.

All communication links in the network follow a composite Rayleigh fading and distance dependent path-loss channel model. The channel between the m -th user and test transmitter is given by $h_m = \hat{h}_m (1 + d_m^\alpha)^{-\frac{1}{2}}$, where \hat{h}_m and d_m represent the Rayleigh fading channel gain, and distance between the test transmitter and m -th user, respectively, and α is the path loss exponent. In addition, a bounded path loss model is considered to avoid the issue of singularity at small distances [13, 34]. Without loss of generality, it is assumed that NOMA users' channel gains are ordered as $|h_1|^2 \leq \dots \leq |h_M|^2$. Consequently, the power allocation coefficients under NOMA are sorted as $\beta_1 \geq \dots \geq \beta_M$ with $\sum_{i=1}^M \beta_i$. The test transmitter sends a superimposed

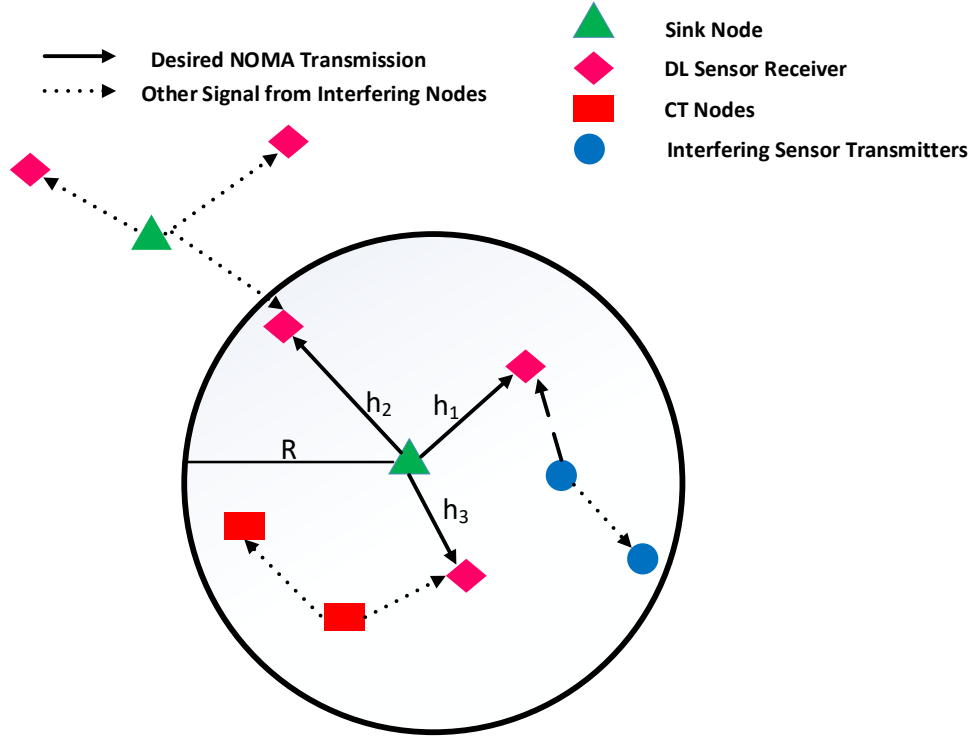


Figure 6.2: An illustration of sink-to-sensors communication using NOMA under interference of other sink, sensor and CT nodes.

signal to all NOMA users and the received signal at the m -th user is given as:

$$r_m = h_m \sum_{i=1}^M \sqrt{\beta_i P} s_i + n_m, \quad (6.1)$$

where P is the transmission power of test transmitter, s_i is the message signal of i -th sensor node, and n_m is the AWGN with zero mean and variance σ^2 .

For each NOMA user, there are two types of interference that interfere the reception of desired signal. First is the intra-user interference that is present due to the superposition of multiple users in NOMA, and the second is due to the transmission of undesired transmitters in the network. SIC is employed at each user receiver to mitigate the intra-user interference. The optimal decoding order of SIC is in the sequence of

increasing channel gains. Therefore, m -th user decodes the message signals of all j users, $j < m$, before decoding its own message, and treats the message signals of the users $j > m$ as noise.

For the second type, consider that the interference links among unwanted transmitters and probe NOMA receiver are dominated by path loss. Assume the probe receiver is located at origin of the coordinate system i.e., $d_m = (x_0, 0)$ with $x_0 = 0$ then the total interference at probe user's location can be written as, $\mathcal{I} = \sum_{w \in \Phi_{SE}} (1 + d_w^{-\alpha})^{-1} + \sum_{x \in \Phi_{SK}} (1 + d_x^{-\alpha})^{-1} + \sum_{y \in \Phi_{CT} \setminus x_0} (1 + d_y^{-\alpha})^{-1}$, where d_w , d_x , and d_y represent the distances between undesired transmitting sensors, sinks, CT nodes and the probe receiver, respectively. Further, sensors and sinks operate on very low power levels, the NOMA users may experience excessive interference from a nearby transmitter(s) leading to a situation of complete outage. To avoid this, a guard zone of radius d_0 is considered around each NOMA user within which no unwanted transmitter is allowed to transmit [94].

A list of commonly used variables in this chapter is summarized in Table 6.1.

Let $\Lambda_{m \rightarrow j}$ represents the SINR at the m -th NOMA user to decode the message signal of j -th user, $j < m$, then, $\Lambda_{m \rightarrow j}$ can be computed as follows:

$$\Lambda_{m \rightarrow j} = \frac{|h_m|^2 \beta_j \mathcal{X}}{|h_m|^2 \mathcal{X} \sum_{i=j+1}^M \beta_i + \kappa \mathcal{I} + 1}, \quad (6.2)$$

where $\mathcal{X} = \frac{P}{\sigma^2}$ is the average system SNR, $\kappa = \frac{P_T}{\sigma^2}$ is the average interference level, and P_T is the common maximum transmission power available to sink, sensor and CT nodes.

If all the $j < m$ users are decoded and removed successfully by the m -th user from

its observation signal , then SINR required to decode its own message is given by:

$$\Lambda_{m \rightarrow m} = \frac{|h_m|^2 \beta_m \mathcal{X}}{|h_m|^2 \mathcal{X} \sum_{i=m+1}^M \beta_i + \kappa \mathcal{I} + 1}, \quad (6.3)$$

6.3 Outage and Diversity Analysis

In this section, an exact analysis of the outage probability for m -th user under the considered network setting is presented. Let ϖ_j and R_j represent the target SINR, and the rate for user j , respectively, where $1 \leq j \leq M$ and $\varpi_j = 2^{R_j} - 1$. To simplify notation, define as $\nabla_{m,j} = \{\Lambda_{m \rightarrow j} < \varpi_j\}$ the outage event at m -th user when it fails to decode the message of j -th user, $1 \leq j \leq m$. Consequently, the outage probability for m -th user, denoted by P_{out}^m can be written as follows:

$$P_{\text{out}}^m = 1 - \text{Pr}(\nabla_{m,1}^c \cap \dots \cap \nabla_{m,m}^c), \quad (6.4)$$

where $\nabla_{m,j}^c$ is the complement event of $\nabla_{m,j}$. In order to proceed further, rewrite $\nabla_{m,j}^c$ as:

$$\begin{aligned} \nabla_{m,j}^c &= \{\Lambda_{m \rightarrow j} > \varpi_j\} \\ &= \left\{ \frac{|h_m|^2 \beta_j \mathcal{X}}{|h_m|^2 \mathcal{X} \sum_{i=j+1}^M \beta_i + \kappa \mathcal{I} + 1} > \varpi_j \right\} \\ &= \left\{ |h_m|^2 \mathcal{X} \left(\beta_j - \varpi_j \sum_{i=j+1}^M \beta_i \right) > \varpi_j (\kappa \mathcal{I} + 1) \right\} \\ &\stackrel{(a)}{=} \{|h_m|^2 > \tau_j (\kappa \mathcal{I} + 1)\} \end{aligned} \quad (6.5)$$

where $\tau_j = \frac{\varpi_j}{\mathcal{X}(\beta_j - \varpi_j \sum_{i=j+1}^M \beta_i)}$. Step (a) provides the following essential condition to keep NOMA operational:

$$\text{C1} : \beta_j - \varpi_j \sum_{i=j+1}^M \beta_i > 0. \quad (6.6)$$

When condition C1 is violated, the m -th user will always suffer outage, irrespective of the channel SNR. Further, by defining $\tau_m^* = \max\{\tau_1, \dots, \tau_m\}$, P_{out}^m can be written as:

$$P_{\text{out}}^m = 1 - P_r(|h_m|^2 > \tau_m^* (\kappa \mathcal{I} + 1)). \quad (6.7)$$

To proceed forward, it can be noticed that $|h_m|^2$ are the ordered channel gains. Then, the ordered and unordered channel $|\tilde{h}|^2$ have following relationships [95]:

$$F_{|h_m|^2}(t) = \mu_m \sum_{q=0}^{M-m} \binom{M-m}{q} \frac{(-1)^q}{m+q} \left[F_{|\tilde{h}|^2}(t) \right]^{m+q} \quad (6.8)$$

$$f_{|h_m|^2}(t) = \mu_m \sum_{q=0}^{M-m} \binom{M-m}{q} (-1)^q \left[F_{|\tilde{h}|^2}(t) \right]^{m+q-1}, \quad (6.9)$$

where $\mu_m = \frac{M!}{(M-m)!(m-1)!}$. To this end, the following theorem presents the exact expression for P_{out}^m .

Theorem 6.1. *The outage probability of the m -th NOMA user under the considered*

network setting can be derived as:

$$\begin{aligned}
 P_{out}^m &= \frac{1}{\Theta} \sum_{s=1}^S \Psi_s e^{vg_s} \left\{ \sum_{k=0}^{2K}{}' \Re \left[e^{-\lambda\pi \left[\left(e^{-c_k d_0^{-\alpha}} - 1 \right) d_0^{2+c_k \sum_{t=1}^T \eta_t e^{-u_t c_k d_0^{-\alpha}} \right] + \frac{\iota\pi g_s}{\Theta}} \right] \right. \\
 &\times \left[\mu_m \sum_{q=0}^{M-m} \binom{M-m}{q} (-1)^q \sum_{n=1}^N \psi_n [\phi(\delta, 1+\delta; -a_n(\kappa g_s + 1)) + \right. \\
 &\left. \left. \varepsilon\phi(1+\delta, 2+\delta; -a_n(\kappa g_s + 1))] [1 - e^{-\tau_m^*(\kappa g_s + 1)t_n} \phi(\delta, 1+\delta; -a_n(\kappa g_s + 1))]^{m+q-1} \right] \right\}, \tag{6.10}
 \end{aligned}$$

where $\Psi_s = w_s e^{g_s}$, $w_s = \frac{\Gamma(S+1)g_s}{S!(S+1)^2[L_{S+1}(g_s)]^2}$, $L_S(\cdot)$ is the Laguerre polynomial of degree S , g_s are the roots of $L_S(\cdot)$, $c_k = v_0 + \frac{\iota\pi k}{\Theta}$, $v_0 = v_1 - \frac{\log(\varsigma)}{\Theta}$, $v, v_1 > 0$ are real numbers, ς is the desired relative accuracy, Θ is a scaling parameter, $\iota = \sqrt{-1}$, K is the number of terms used to invert the Laplace transform, and the prime term indicates that $k = 0$ summation term is halved, $\lambda = \lambda_{SE} + \lambda_{SK} + \lambda_{CT}$, $\eta_t = \frac{1}{2}d_0^{2-\alpha}\omega_t\sqrt{1-\varphi_t^2}u_t^{-\alpha}$, $\omega_t = \frac{\pi}{T}$, $u_t = \frac{(1+\varphi_t)}{2}$, $\varphi_t = \cos\left(\frac{2t-1}{2T}\pi\right)$, $\psi_n = \omega_n\sqrt{1-\theta_n^2}\tau_m^*(\kappa z + 1)e^{-\tau_m^*(\kappa z + 1)t_n}$, $\theta_n = \cos\left(\frac{2n-1}{2N}\pi\right)$, $\omega_n = \frac{\pi}{N}$, $t_n = \frac{(1+\theta_n)}{2}$, $a_n = \tau_m^*t_nR^\alpha$, $\delta = \frac{2}{\alpha}$, $\varepsilon = \delta(1+\delta)^{-1}R^\alpha$, T, N are the complexity-accuracy tradeoff parameters, and $\phi(\cdot; \cdot; \cdot)$ is a confluent hyper-geometric function.

Proof. See Appendix J □

6.3.1 Diversity Analysis

In this sub-section, the diversity analysis for the ordered NOMA users in high SNR regime is presented. The diversity order of the m -th user outage probability is defined as:

$$D = - \lim_{\mathcal{X} \rightarrow \infty} \frac{\log P_{out}^m}{\log \mathcal{X}}. \tag{6.11}$$

In order to obtain D , it can be observed from (6.7) that the asymptotic outage

probability in high SNR regime, denoted as P_m^∞ , can be expressed as:

$$P_m^\infty = P_r (|h_m|^2 < t^*), \quad (6.12)$$

where $t^* = \frac{\tilde{\tau}_m \kappa \mathcal{I}}{\mathcal{X}}$, $\tilde{\tau}_m = \max \{\bar{\tau}_1, \dots, \bar{\tau}_m\}$ and $\bar{\tau}_m = \frac{\varpi_m}{(\beta_m - \varpi_m \sum_{i=m+1}^M \beta_i)}$. Next, when, $\mathcal{X} \rightarrow \infty$, $t^* \rightarrow 0$ and similar to (6.8), the CDF of the ordered channel is expressed as:

$$F_{|h_m|^2}^\infty (t^*) = \mu_m \sum_{q=0}^{M-m} \binom{M-m}{q} \frac{(-1)^q}{m+q} \left[F_{|\tilde{h}|^2}^\infty (t^*) \right]^{m+q} \quad (6.13)$$

In high SNR regime, note that in the CDF expression for the unordered channel in Appendix J, $e^{-t^*} \approx 1 - t^*$ and $\phi(\delta, 1 + \delta; -t^* R^\alpha) \rightarrow 1$ and . Hence, $F_{|\tilde{h}|^2}^\infty (t^*)$ in (6.13) can be approximated as:

$$F_{|\tilde{h}|^2}^\infty (t^*) \approx t^*. \quad (6.14)$$

Substituting (6.14) into (6.13), $F_{|h_m|^2}^\infty (t^*)$ can be expressed as:

$$F_{|h_m|^2}^\infty (t^*) \approx \vartheta (\tilde{\tau}_m \kappa \mathcal{I} \mathcal{X}^{-1})^m + o \left[(\tilde{\tau}_m \kappa \mathcal{I} \mathcal{X}^{-1})^m \right], \quad (6.15)$$

where $\vartheta = \frac{\mu_m}{m}$. Based on (6.15), P_m^∞ in (6.12) is given as:

$$P_m^\infty \approx \frac{1}{\mathcal{X}^m} \int_0^\infty \vartheta (\tilde{\tau}_m \kappa z)^m f_{\mathcal{I}}(z) dz. \quad (6.16)$$

It can be observed that the integral in (6.16) is constant. Hence, P_m^∞ can be expressed as follows:

$$P_m^\infty \approx A \mathcal{X}^{-m} + o(\mathcal{X}^{-m}). \quad (6.17)$$

Finally, substituting (6.17) into (6.11), the diversity order experienced by the m -th

user is found to be m . It can be observed from (6.16) that interference in integral is independent of \mathcal{X} and hence the factor \mathcal{X}^{-m} dominates in (6.16) under high SNR. This indicates that the interference-limited NOMA based UWSN becomes equivalent to an interference-free network. This result on diversity order can be interpreted as follows. First, the m -th user avails exactly m chances to decode its own message. Second, the m -th user has $(m-1)$ interferences from the higher order users that need to be cancelled out by applying SIC. Hence, it obtains a diversity of m .

6.4 Throughput and Energy Consumption Efficiency Analysis

6.4.1 Link Throughput Efficiency

The link throughput efficiency between the m -th user and the test transmitter, denoted by TP_m and measured in [bits/s/Hz] is defined as [80]:

$$TP_m = (1 - P_{\text{out}}^m) \log_2(1 + \varpi_m) \quad (6.18)$$

Correspondingly, the average link throughput efficiency of the network is:

$$TP_{\text{avg}} = \frac{\sum_{m=1}^M TP_m}{M}. \quad (6.19)$$

6.4.2 Energy Consumption Efficiency

NOMA is used by the sink node to communicate with the sensors. Since NOMA is typically applied on top of an underlying access technology to better reuse the transmission resources, e.g. time slots, frequency channels, or spreading codes, an additional SIC unit is required at the sensors to decode the desired message. It is

thus important to analyze the overall energy consumption efficiency ζ of the NOMA based UWSN. The total energy consumption along the signal path (communication and circuits) can be decomposed into three main components [96]: the power consumed by power amplifiers P_a , the power consumed by SIC unit to process information P_s , and the power consumed by all other circuit units (filters, mixers, frequency synthesizer, etc.) P_c . Hence, the overall ζ in Joules/bit can be expressed as:

$$\zeta = \frac{P_a + MP_c + P_s}{R_b}, \quad (6.20)$$

where $R_b = W \cdot TP_{avg}$ is the bit rate, W is the channel bandwidth in Hz, $P_a = \nu P$, $\nu = \frac{\nu_2}{\nu_1}$, ν_1 is the drain efficiency of the power amplifier, and ν_2 is the peak-to-average ratio.

The P_c is considered as a constant, and P_s can be regarded as the average power consumed by SIC units of all scheduled sensor receivers. In order to find P_s , the power consumed by m -th sensor, denoted by P_m , to process $N_b = |W TP_m|$ bits is required. The first step in this regard is to express P_m in terms of the required computational complexity C_m . To proceed forward, a power consumption model for the sensor device is required. Considering the sensor as CMOS device, the power consumed during computation in a static CMOS device is given as [97]:

$$P_m = C_{eff} V_m^2 \hbar_m, \quad (6.21)$$

where where C_{eff} , V_m , and \hbar_m are the effective switching capacitance, supply voltage, and clock frequency of m -th sensor, respectively. Further, V_m and \hbar_m are directly related as:

$$\hbar_m = \partial V_m, \quad (6.22)$$

where ϑ is a design parameter that takes a value of $O(W)$ [98]. Dynamic voltage scaling (DVS) is a standard technique for conserving power in CMOS devices through dynamically adjusting the clock frequency by scaling the voltage according to processing load [99]. For a given N_b , V_m can be scaled to match \hbar_m with C_m/s . Based on (6.21) and (6.22), P_m can be expressed as:

$$P_m = C_{eff} \left(\frac{C_m}{\vartheta} \right)^3. \quad (6.23)$$

and C_m is given in terms of number of floating point operations (FLOP) per bit decision [46] as:

$$C_m = N_b \left[2N_s M + 5M + 8 \sum_{m=1}^{M-1} m + (M-1)(5 + 2N_s) \right] + 2MN_s(M-1) + 2MN_b + M + M \log_2(M), \quad (6.24)$$

where N_s is the number of samples to represent one bit. Finally, based on (6.23) and (6.24), substituting $P_s = \frac{\sum_{m=1}^M P_m}{M}$ into (6.20) obtains the overall ζ .

6.5 Results and Discussion

This section presents results to verify the accuracy of outage probability, link throughput and energy consumption analysis for a UWSN which uses NOMA for downlink (sink-to-source) transmission. The coefficients β_m are calculated according to the power allocation scheme proposed for NOMA in [13], with $\beta_m = \frac{M-m+1}{\mu}$ where μ is selected such that $\sum_{m=1}^M \beta_m = 1$. In all the simulations, the specific parameter values are summarised in Table 6.2 unless otherwise stated.

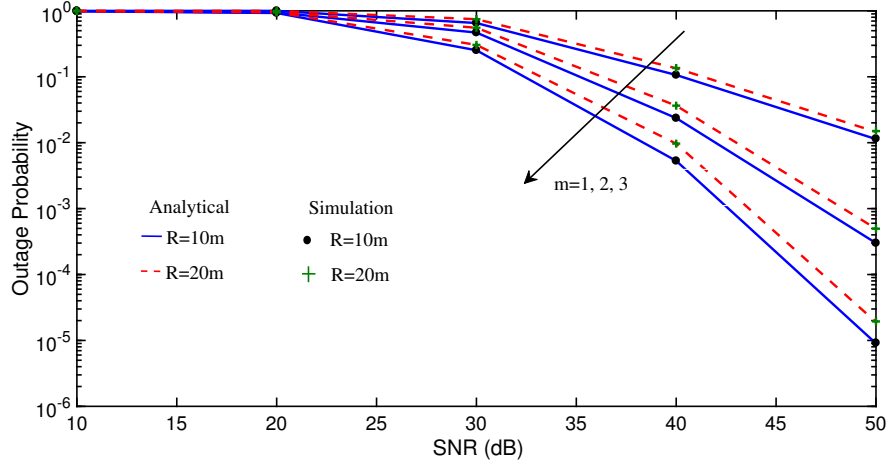
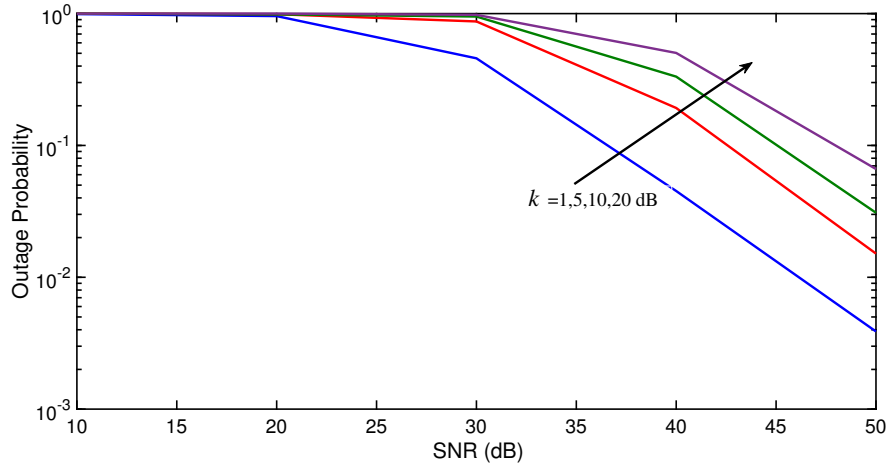
Figure 6.3 shows the outage probability of each m -th user under the impact of different transmission radius R of the sink node. The solid and dashed curves are

Table 6.2: Simulation parameters.

Parameter	Description	Value
α	Path loss exponent	4
β_m	Power allocation coefficient of m -th user	$\{0.6, 0.3, 0.1\}_{1,2,3}$
ϖ_m	SINR threshold for m -th user	$\{0.9, 1.5, 2\}_{1,2,3}$
λ_{SE}	Intensity of Φ_{SE}	10^{-3}
λ_{SK}	Intensity of Φ_{SK}	10^{-4}
λ_{CT}	Intensity of Φ_{CT}	10^{-3}
κ	Average interference	1 dB
σ^2	Noise power	-90 dBm
\mathcal{X}	Average system SNR	[10 to 50] dB
K	Fourier series terms	10
M	Total NOMA users	3
N	Gaussian-Chebyshev parameter	3
P	Test transmitter transmission power	[-10 to 30] dBm
R	Transmission radius of test transmitter	10 m
S	Degree of Laguerre polynomial	2
T	Gaussian-Chebyshev parameter	5

analytical results obtained by plotting (6.10), while simulation results are shown in "•" and "+" to validate the derived analytical expressions. It can be observed that increasing R results in higher outage probability due to increased path loss. Further, the ordered NOMA users have different outage performance, as each has a different channel condition.

Figure 6.4 demonstrates the average outage probability under different interference levels κ , defined immediately after (6.2). Reducing κ expectedly lowers the outage probability. Figure 6.5 further shows the outage probability of each m -th user under the impact of different path loss α . The results show that NOMA achieves lower outage probability than OMA for different values of α . The link throughput efficiency of each m -th user with increasing transmit power of test transmitter (sink node) are shown in Figure 6.6. It can be seen that NOMA achieves better throughput efficiency than OMA, as all the ordered NOMA users have lower outage probability than their OMA counterparts. Figure 6.7 shows the energy consumption efficiency ζ comparison


 Figure 6.3: Impact of different R on outage probability.

 Figure 6.4: Impact of κ on average outage probability.

between NOMA and OMA as a function of transmit power P . The results are obtained by considering 2 and 3 users. The power allocation coefficients and SINR thresholds for $M = 3$ are given in Table 6.2. For $M = 2$, they are chosen as $\beta_m = \{0.8, 0.2\}_{m=1,2}$, and $\varpi_m = \{0.9, 1.5\}_{m=1,2}$ respectively. Further, $C_{eff} = 2 \times 10^{-15}$ Farads for 70 nm CMOS technology [100], channel bandwidth $W = 3$ MHz, $N_s = 4$ samples to represent one bit, and circuit power consumption $P_c = 20$ dBm. Overall, NOMA achieves better ς than OMA due to a lower outage probability which results in larger R_b in (6.20)

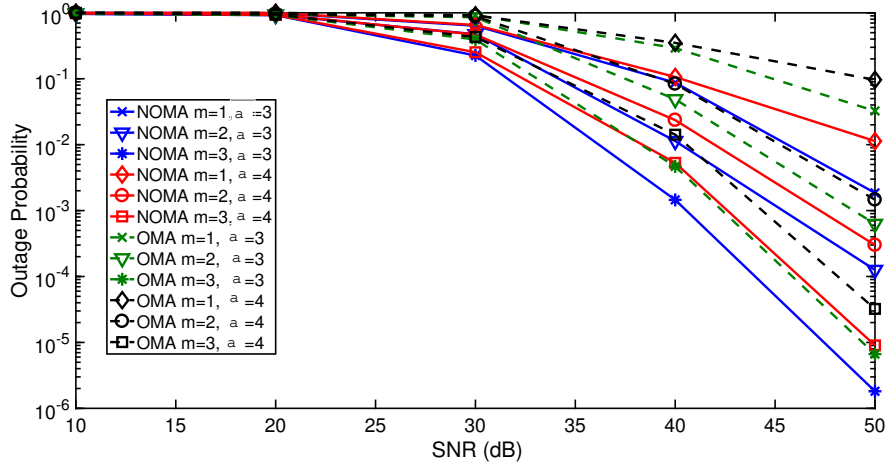


Figure 6.5: Impact of α on outage probability.

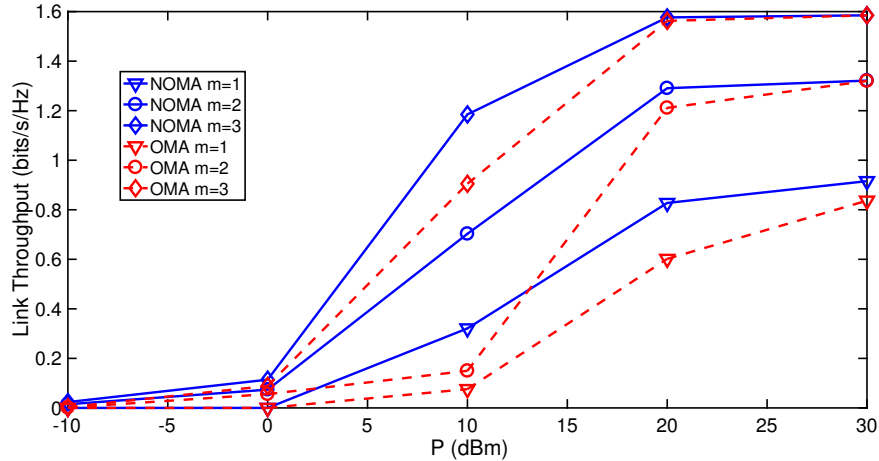


Figure 6.6: Link throughput efficiency comparison between NOMA and OMA.

and consequently higher ζ . However, the ζ of both schemes are comparable beyond a transmit power of 15 dBm, which indicates the importance of optimizing the power and rate allocation in NOMA based UWSNs.

Since sensors have limited processing capacity, it is necessary to also analyze the complexity requirements of NOMA for these sensors. For downlink (sink-to-sensors) communication, the required complexity for the scheduled sensor receivers will be the complexity of their SIC units to process the received NOMA message. Figure 6.8

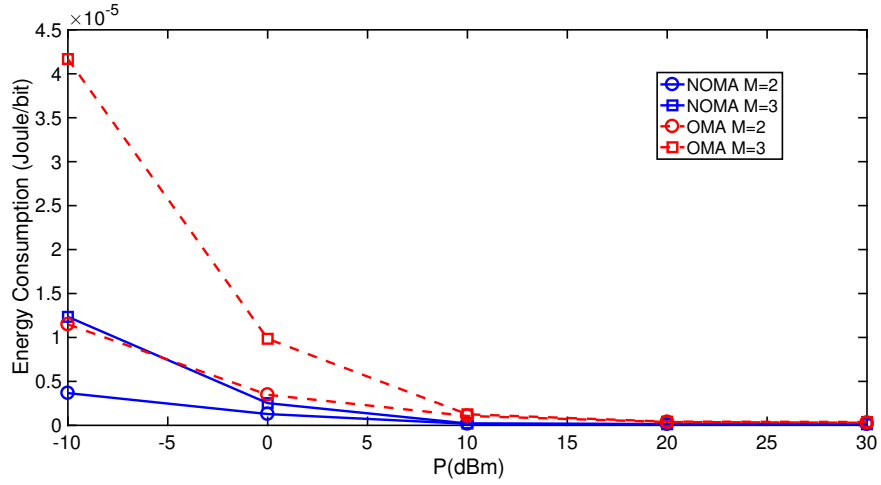


Figure 6.7: Energy consumption efficiency comparison between NOMA and OMA.

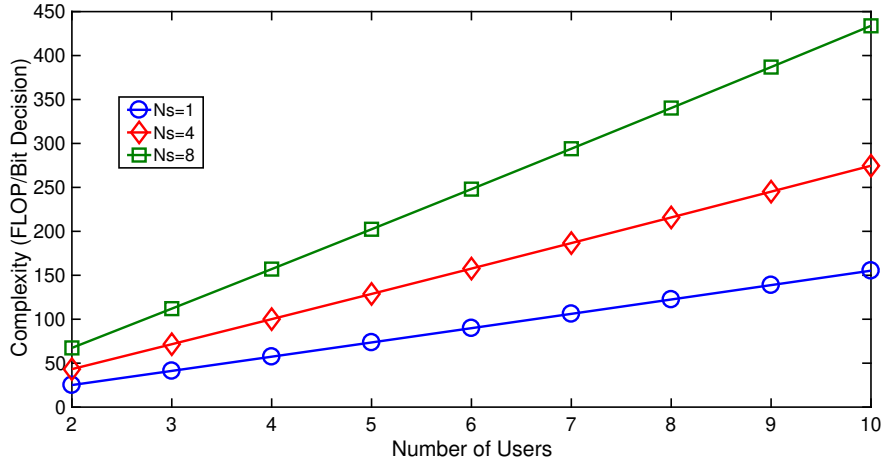


Figure 6.8: Computational complexity of NOMA receivers.

shows the computation complexity in terms of the FLOPs per bit decision, i.e. the number of FLOPs needed to decode one bit, obtained by using (6.24), under different M ordered users and N_s samples used to represent one bit. The results expectedly show the receiver's complexity increases with M and N_s .

In order to evaluate whether the current sensor platforms can implement the SIC unit for NOMA in UWSNs, ARM Cortex-M3 and Cortex-M7 processors are considered, which are widely used processors for current lower-, and higher-end sensor platforms,

Table 6.3: Computational time per bit decision by SIC unit

Processor	Capacity (MFLOPS)	Time (μs)	Time (μs)
		$M = 3$	$M = 9$
ARM Cortex-M3	0.618	113	405
ARM Cortex-M7	22.1	3.2	11.2

respectively. Based on their specified capacity in terms of MFLOPS [101], the required computational time per bit decision is computed for $M = 3$ and $M = 9$ users with $N_s = 4$ samples, as shown in Table 6.3. Consider a maximum payload size of 127 bytes (or 1016 bits) widely used in low-powered UWSNs, the computational time per message with $M = 3 \sim 9$ users can range between 115 \sim 411 ms, and 3.3 \sim 11.5 ms for Cortex-M3, and Cortex-M7 processor, respectively.

6.6 Chapter Summary

In this chapter, NOMA for UWSNs is proposed and its performance is evaluated. Different from cellular use-case, NOMA in UWSNs are further subject to interferences from cross-technology nodes operating in the same unlicensed spectrum as the sensors. Focusing on the downlink (sink-to-sensors) scenario, a new closed-form expression for outage probability is derived at the probe receiver's location by utilizing stochastic geometry and order statistics. Numerical analysis shows that NOMA achieves lower outage probability, resulting in higher average throughput and better energy consumption efficiency than conventional OMA, suggesting that NOMA is very attractive for interference-limited UWSNs. Further, the computational time complexity for NOMA message decoding is within acceptable limits when using current and upcoming generations of processors for UWSNs.

Chapter 7

Hybrid Multiple Access with Channel Gain Stretching

From the literature review and research conducted in Chapters 4-6, it is observed that the performance gain of NOMA over OMA is insignificant in low SNR regime. In addition, the performance of NOMA is impacted under similar channel conditions among different users. In order to address these two problems, a novel HMA with CGS is proposed and analysed in this chapter.

7.1 Introduction

NOMA is inherently more interference limited than conventional OMA due to superposition coding. Hence, NOMA requires a higher SINR for successful decoding. Furthermore, previous studies showed that NOMA has no significant gain over OMA in low SNR regime [13], which makes it less attractive for those users with low SNR. This trend is also demonstrated by the numerical results of chapters 4, 5, and 6.

As such, this shortcoming motivates us to propose a downlink HMA which dynamically schedules some users for OMA and others for NOMA while satisfying a

necessary condition, to be presented in Section 7.2, which is derived according to the transmit SNR and user targeted rate. The proposed HMA is flexible to be applied to any NOMA group size and aims to achieve a better overall system performance than pure NOMA and OMA. The main contributions of this chapter are:

- A necessary condition on users' channel gains under which the proposed HMA can outperform pure NOMA or OMA is derived.
- An optimisation problem is formulated, which is solved numerically to obtain the K for G_2 that results in the optimal throughput for the proposed HMA system.
- A CGS scheme to apply NOMA effectively in HMA under similar channel conditions is proposed.
- A CGS scheme to apply NOMA effectively in HMA under similar channel conditions is proposed.
- The exact closed-form expression for the outage probability of HMA is derived.
- Numerical results are provided to validate the accuracy of the analytical expression, and compare the performance among HMA, NOMA and OMA.

The rest of this chapter is organised as follows. Section 7.2 describes the system model, while Section 7.3 introduces the proposed scheme. The outage analysis is provided in Section 7.4, followed by the results and discussion in Section 7.5. Finally, Section 7.6 summarises the chapter.

7.2 System Model

Consider a downlink multi-user transmission scenario with single BS located at the centre of a disc D , with radius r . The total communication bandwidth is considered to

be W Hz. Let there be a total number of M users uniformly distributed inside D and are ordered according to channel gains as $h_1 \leq \dots \leq h_M$, where $h_m = |\hat{h}_m|^2(1 + d_m^\alpha)^{-1}$ denotes the channel gain between user m and BS. Here, \hat{h}_m is Rayleigh fading gain, d_m represents the distance between user m and BS, and α is the path loss exponent.

In NOMA, decoding is performed in ascending order of channel gains. Therefore, the rate of user m under NOMA is given by [50]:

$$\tilde{R}_m = \log_2 \left(1 + \frac{\Upsilon a_m h_m}{1 + \Upsilon h_m \sum_{i=m+1}^M a_i} \right), \quad (7.1)$$

where $\Upsilon = \frac{P}{\sigma^2}$ is the transmit SNR, P is the total transmission power of the BS, σ^2 is the power of the additive noise, a_m is the power allocation coefficient for user m such that $\sum_{i=1}^M a_i = 1$ and $a_m = \frac{P_m}{P}$.

It is well known that NOMA achieves higher capacity than OMA under suitable SINR conditions [6]. If OMA is adopted over NOMA, the rate of user m should at least degrade by ξ_m bits per channel use, where ξ_m represents the minimum rate loss of user m , which is given by:

$$\xi_m \leq \tilde{R}_m - \bar{R}_m, \quad (7.2)$$

where $\bar{R}_m = \frac{1}{M} \log_2(1 + \Upsilon h_m)$ is the rate of user m when OMA is applied [50].

Furthermore, the target rate for user m , denoted as R_m , can still be ensured with OMA if and only if:

$$\bar{R}_m \geq R_m. \quad (7.3)$$

It should be noted that (7.3) acts as a constraint to the rate loss in (7.2) i.e. the rate loss should not exceed an amount such that R_m is not met. By solving inequalities (7.2)

Table 7.1: Commonly used variables.

Notation	Description
M	Total number of users
R_m	Targeted rate of user m
\tilde{R}_m	Achievable rate of user m under NOMA
\bar{R}_m	Achievable rate of user m under OMA
a_j	Power allocation coefficient of j -th user
Υ	Transmit SNR range
W	Available system bandwidth
N	Gaussian-Chebyshev parameter

and (7.3), the necessary condition on the channel gain of user m is obtained as follows:

$$h_m \geq \max \left\{ \frac{\kappa_m}{X_m}, Y_m \right\}, \quad (7.4)$$

where $\kappa_m = 2^{R_m + \xi_m} - 1$, $X_m = \Upsilon \left(a_m - \kappa_m \sum_{i=m+1}^M a_i \right) > 0$ and $Y_m = (2^{MR_m} - 1) \Upsilon^{-1}$.

Condition (7.4) states that user m can still meet R_m even if it is scheduled for OMA. Hence, in the next section, a HMA scheme is proposed in which users who satisfy condition (7.4) can be (but not necessarily) scheduled for OMA. A list of commonly used variables in this chapter is summarised in Table 7.1.

7.3 Proposed Scheme

Consider a system with total users $M > 1$. Let v denotes the number of users that satisfy (7.4). When total users $M = 2$ or $v = 0$, then conventional NOMA must be utilized for transmission. Consider a case when $M > 2$ and $v > 0$. Then the proposed HMA can be applied, which is expressed as follows:

Step 1) In order to dynamically schedule some users for OMA and others for NOMA, at a certain time instant, BS computes κ_m , X_m and Y_m . Then, based on (7.4), the BS divides total M users into two groups G_1 and G_2 that contain K and J users,

respectively, where $M = K + J$. Accordingly, the channel of users in G_1 and G_2 are given as $\{h_k\}_{k=1}^K$ and $\{h_j\}_{j=1}^J$, respectively.

Step 2) In order to apply NOMA for users in G_2 , the power allocation coefficients are computed for J ordered users ($a_1 \geq \dots \geq a_J$) with $\sum_{i=1}^J a_i = 1$.

Step 3) The BS allocates bandwidths W_1 and W_2 ($W = W_1 + W_2$) to groups G_1 , and G_2 , respectively. By using a control channel, the BS then informs G_1 and G_2 users to receive using OMA, and NOMA, respectively.

The proposed HMA scheme divides the total users in groups G_1 and G_2 . Therefore, it is important to find the maximum number of users that can be scheduled for OMA leading to optimum throughput, power and bandwidth allocations. As such, the following optimisation problem is formulated to obtain optimal throughput.

7.3.1 Optimal Throughput and Group Size

$$\max_{P, \omega, W} \sum_{k=1}^K \omega_k \log_2 \left(1 + \frac{P_k h_k}{\sigma^2} \right) + W_2 \sum_{j=1}^J \log_2 \left(1 + \frac{P_j h_j}{h_j \sum_{i=j+1}^J P_i + \sigma^2} \right) \quad (7.5)$$

subject to

$$\mathbf{C1:} \quad \omega_k \log_2 \left(1 + \frac{P_k h_k}{\sigma^2} \right) > R_k, \quad 1 \leq k \leq K$$

$$\mathbf{C2:} \quad W_2 \left(1 + \frac{P_j h_j}{h_j \sum_{i=j+1}^J P_i + \sigma^2} \right) > R_j, \quad 1 \leq j \leq J$$

$$\mathbf{C3:} \quad W_1 + W_2 \leq W$$

$$\mathbf{C4:} \quad \sum_{k=1}^K \omega_k \leq W_1$$

$$\mathbf{C5:} \quad 2 \leq J \leq M - 1$$

$$\mathbf{C6:} \quad K = J - M$$

$$\mathbf{C7:} \quad k \in \{1, 2, \dots, K\}$$

$$\mathbf{C8:} \quad j \in \{1, 2, \dots, J\}$$

$$\mathbf{C9:} \quad \sum_{k=1}^K P_k + \sum_{j=1}^J P_j \leq P$$

Insights into the Optimisation Problem

The optimisation problem in (7.5) aims to find the number of users K that can be scheduled for OMA group which optimises the overall throughput of the proposed HMA scheme subject to the constraints **C1-C9**. The constraints **C1, C2** ensure that the achievable rates of G_1 and G_2 users meet their targeted rates. The constraint **C3** optimises the bandwidth allocations W_1 and W_2 for the groups G_1 , and G_2 , respectively. The condition **C4** further optimises the bandwidth allocation among K OMA users of

group G_1 . The constraints **C5-C8** impose that group size K and J are integers. Finally, the constraint **C9** optimises the power allocation for G_1 and G_2 users and also ensures that the allocated power to both groups cannot exceed the total available power at the BS.

It can be observed that the problem in (7.5) is a mixed-integer non-linear programming (MINLP) problem whose solution has a combinatorial nature. That being said, the maximum size K for group G_2 leading to the optimal throughput requires exhaustive search, whose computational complexity for practical systems becomes infeasible with large number of users [49]. Consequently, it is very challenging to obtain the analytical solution of the formulated problem in (7.5). As such, this problem is numerically solved with the MatLab optimisation solvers for the HMA to obtain optimal throughput. In the rest of this chapter, the allocated powers P_j and P_k refer to the optimal powers obtained upon solving the problem (7.5) numerically.

Since HMA creates two user groups, a situation may arise when G_2 users have similar channel conditions. In order to apply NOMA more effectively under such situations, CGS scheme is further proposed in next sub-section that artificially generates a difference among channel gains of G_2 users.

7.3.2 Channel Gain Stretching Method for G_2 Users in HMA

CGS Method 1

The situation of comparable channel conditions for NOMA users in G_2 is equivalent to the pixels in a digital image having very similar intensities. The visual appearance of the digital image can be enhanced by applying gamma transformation that maps a narrow ambit of intensities into a wider intensity range [102]. Inspired by gamma transformation, a CGS scheme is proposed that maps the channel h_j of the j -th user in

G_2 to a new value, \bar{h}_j , which is given as:

$$\bar{h}_j = c_j(h_j + \eta_j)^{\Gamma_j}, \quad (7.6)$$

where c_j , η_j and Γ_j are positive constants, and are selected in such a way to achieve a significant difference among power allocations $\{P_j\}_{j=1}^J$.

Example 1: Consider that $J = 2$ and $(h_1, h_2) = (0.87, 0.9)$. Now using (7.6) with $c_1 = 0.5$, $c_2 = 3$, $\eta_1 = \eta_2 = 0.1$, $\Gamma_1 = 1$ and $\Gamma_2 = 0.1$, the stretched channel gains are obtained as $(\bar{h}_1, \bar{h}_2) = (0.485, 3)$. Now based on stretched gains (\bar{h}_1, \bar{h}_2) , the new power allocations (P_1, P_2) could be obtained with significant difference by solving the problem (7.5).

CGS Method 2

Under situations of similar channel conditions, a following transformation is proposed to artificially generate channel gain difference among NOMA users:

$$\bar{h}_j = k_{1,j}(h_j)^{k_{2,j}}, \quad (7.7)$$

where \bar{h}_j is the transformed channel gain of user j and $k_{1,j} > 0$, $k_{2,j} > 0$ are positive constants for user j and are selected in such a way to achieve a significant difference among channel gains of users.

Example 2: Consider a case of two users with $(h_1, h_2) = (0.87, 0.9)$. Now applying (7.7) with $k_{1,1} = k_{2,1} = 0.5$, $k_{1,2} = 3$, $k_{2,2} = 3.5$ results in stretched coefficients as $(\bar{h}_1, \bar{h}_2) = (0.46, 2)$. The power allocation P_j is then computed by solving problem (7.5) for a given targeted rate constraints.

7.4 Outage Analysis

It is important to investigate the outage performance of the HMA users. As such, the exact expression for the outage probability of users in HMA is stated in the following theorem.

Theorem 7.1. *The closed-form expression for the outage probability of user $q \in \{j, k\}$ from group $G \in \{G_1, G_2\}$ can be derived as:*

$$\begin{aligned} P_q = \mu_q \sum_{l=0}^{Q-q} \binom{Q-q}{l} (-1)^l \left\{ \sum_{n=1}^N \Psi_n [\Phi(\delta, 1 + \delta; -b_n) \right. \\ \left. + \rho \Phi(1 + \delta, 2 + \delta; -b_n)] \right. \\ \left. \times [1 - \delta e^{-\tau_q^* s_n} \mathbf{B}(1, \delta) \Phi(\delta, 1 + \delta; -b_n)]^{q+l-1} \right\}, \end{aligned} \quad (7.8)$$

where $\mu_q = (Q-1)! / [(Q-q)!(q-1)!]^{-1}$, $Q \in \{J, K\}$, $\rho = \delta(1+\delta)^{-1} r^\alpha$, $\delta = \frac{2}{\alpha}$, $b_n \in \{b_n^{G_1}, b_n^{G_2}\}$, $\Psi_n \in \{\Psi_n^{G_1}, \Psi_n^{G_2}\}$, $\tau_q^* \in \{\tau_j^*, \tau_k^*\}$, $\mathbf{B}(\cdot, \cdot)$ is a beta function, $\Phi(\cdot, \cdot; \cdot)$ is a confluent hypergeometric function and N is complexity-accuracy trade-off parameter.

Subsequently, the terms defining the variables in (7.8) can be described as follows. $b_n^{G_1} = \tau_k^* s_n r^\alpha$, $b_n^{G_2} = \tau_j^* s_n r^\alpha$, $\tau_k^* = 2^{KR_k} - 1$, $\tau_j^* = \max\{\tau_1 \dots \tau_j\}$, $\tau_j = \varepsilon_j \left[\Upsilon \left(a_j - \varepsilon_j \sum_{i=j+1}^J a_i \right) \right]^{-1}$, $\varepsilon_j = 2^{R_j} - 1$, $s_n = \frac{1}{2}(1 + \theta_n)$, $\theta_n = \cos(\frac{2n-1}{2N}\pi)$, $\Psi_n^{G_1} = \delta \omega_n \sqrt{1 - \theta_n^2} \mathbf{B}(1, \delta) \tau_k^* e^{-\tau_k^* s_n}$, $\Psi_n^{G_2} = \delta \omega_n \sqrt{1 - \theta_n^2} \mathbf{B}(1, \delta) \tau_j^* e^{-\tau_j^* s_n}$, $\omega_n = \frac{\pi}{N}$ and R_j and R_k are the target rates for users j and k , respectively.

Proof. The outage at the j -th user in G_2 for decoding any of the higher order user u ,

where $1 \leq u < j$ is given as:

$$\begin{aligned} P_{j \rightarrow u} &= \Pr \left[\log_2 \left(1 + \frac{\Upsilon a_u h_j}{1 + \Upsilon h_j \sum_{i=u+1}^J a_i} \right) < R_u \right] \\ &= \Pr (h_j < \tau_u) \end{aligned} \quad (7.9)$$

The overall outage probability of user j is given as:

$$\begin{aligned} P_j &= \Pr (h_j < \tau_j^*) \\ &\stackrel{(a)}{=} \mu_j \sum_{l=0}^{J-j} \binom{J-j}{l} (-1)^l \int_0^{\tau_j^*} \left[F_{|\hat{h}|^2}(x) \right]^{j+l-1} f_{|\hat{h}|^2}(x) dx, \end{aligned} \quad (7.10)$$

where (a) is obtained by analysing order statistics [95], $F_{|\hat{h}|^2}$ and $f_{|\hat{h}|^2}$ are the CDF, and PDF of the unordered channel gain, respectively. The CDF $F_{|\hat{h}|^2}$ is given as [79]:

$$\begin{aligned} F_{|\hat{h}|^2}(x) &= \frac{2}{r^2} \int_0^r (1 - e^{-(1+z^\alpha)x}) z dz \\ &\stackrel{(b)}{=} 1 - \delta e^{-x} \mathbf{B}(1, \delta) \Phi(\delta, 1 + \delta; -xr^\alpha), \end{aligned} \quad (7.11)$$

where (b) is obtained by first making a change of variable from $z^\alpha \rightarrow y$ and then applying Eq. 3.383 of [77]. Taking the derivative of (7.11) to obtain $f_{|\hat{h}|^2}$ and substituting $F_{|\hat{h}|^2}$ and $f_{|\hat{h}|^2}$ into (7.10), P_j can be re-written as:

$$\begin{aligned} P_j &= \mu_j \sum_{l=0}^{J-j} \binom{J-j}{l} (-1)^l \int_0^{\tau_j^*} \delta \mathbf{B}(1, \delta) e^{-x} [\Phi(\delta, 1 + \delta; -xr^\alpha) \\ &\quad + \rho \Phi(1 + \delta, 2 + \delta; -xr^\alpha)] \\ &\quad \times [1 - \delta e^{-x} \mathbf{B}(1, \delta) \Phi(\delta, 1 + \delta; -xr^\alpha)]^{j+l-1} dx. \end{aligned} \quad (7.12)$$

The approximation of P_j is obtained by applying Gaussian-Chebyshev quadrature

as:

$$\begin{aligned}
 P_j = \mu_j \sum_{l=0}^{J-j} \binom{J-j}{l} (-1)^l & \left\{ \sum_{n=1}^N \Psi_n^{G_2} [\Phi(\delta, 1 + \delta; -b_n^{G_2}) \right. \\
 & \left. + \rho \Phi(1 + \delta, 2 + \delta; -b_n^{G_2})] \right. \\
 & \left. \times [1 - \delta e^{-\tau_j^* s_n} \mathbf{B}(1, \delta) \Phi(\delta, 1 + \delta; -b_n^{G_2})]^{j+l-1} \right\}. \quad (7.13)
 \end{aligned}$$

This gives the result of outage probability for any j -th user in G_2 . Following the similar steps to (7.13), the outage probability of user k in G_1 can be similarly obtained as:

$$\begin{aligned}
 P_k &= \Pr \left[\frac{1}{K} \log_2 (1 + \Upsilon h_k) < R_k \right] = \Pr (h_k < \tau_k^*) \\
 &= P_j |_{j=k, J=K, \Psi_n^{G_2} = \Psi_n^{G_1}, b_n^{G_2} = b_n^{G_1}, \tau_j^* = \tau_k^*}. \quad (7.14)
 \end{aligned}$$

Finally, combining the results in (7.13) and (7.14) proves the result in Theorem 7.1. \square

Corollary 8.1. *The outage probability of user j in G_2 under the application of CGS scheme 1 is given as:*

$$\bar{P}_j = P_q |_{q=j, \Psi_n = \Psi_n^{G_2}, b_n = b_n^{G_2}, \tau_q^* = \tau_j^*, \tau_j^* = \varphi_j^*}, \quad (7.15)$$

where $\varphi_j^* = \max \{\varphi_1, \dots, \varphi_j\}$ and $\varphi_j = \left(\frac{\tau_j}{c_j} \right)^{\frac{1}{\Gamma_j}} - \eta_j$.

Proof: In case of CGS method 1, the outage at j -th user in G_2 for decoding any of the higher order user $u, 1 \leq u < j$, is given as, $\bar{P}_{j \rightarrow u} = \Pr (\bar{h}_j = \tau_u) = \Pr [c_j (h_j + \eta_j)^{\Gamma_j} < \tau_u] = \Pr (h_j < \varphi_u)$. By defining $\varphi_j^* = \max \{\varphi_1, \dots, \varphi_j\}$, the overall outage probability at j -th user under CGS is given as, $\bar{P}_j = \Pr (h_j < \varphi_j^*)$. Now following the same steps as of Theorem 7.1 proves the result in (7.15). \square

Corollary 8.2. *The outage probability of user j in G_2 under the application of CGS*

Table 7.2: Simulation parameters.

Parameter	Description	Value
M	Total users	3
N	Gaussian-Chebyshev parameter	5
ε_m	SINR threshold of user m	$(0.9, 1.5, 2)_{m=1,2,3}$ dB
r	Radius of disc D	20m
α	Path loss exponent	4
Υ	Transmit SNR range	[10 – 40] dB

scheme 2 is given as:

$$\bar{P}_j = P_q |_{q=j, \Psi_n = \Psi_n^{G_2}, b_n = b_n^{G_2}, \tau_q^* = \tau_j^*, \tau_j^* = \vartheta_j^*}, \quad (7.16)$$

where $\vartheta_j^* = \max \{\vartheta_1, \dots, \vartheta_j\}$ and $\vartheta_j = \left(\frac{\tau_j}{k_{1,j}} \right)^{k_{2,j}}$.

Proof: In case of CGS method 2, the outage at j -th user in G_2 for decoding any of the higher order user $u, 1 \leq u < j$, is given as, $\bar{P}_{j \rightarrow u} = \Pr(\bar{h}_j = \tau_u) = \Pr \left[h_j < \left(\frac{\tau_u}{k_{1,u}} \right)^{k_{2,u}} \right] = \Pr(h_j < \vartheta_u)$. By defining $\vartheta_j^* = \max \{\vartheta_1, \dots, \vartheta_j\}$, the overall outage probability at j -th user under CGS method is given as, $\bar{P}_j = \Pr(h_j < \vartheta_j^*)$. Now following the same steps as of Theorem 7.1 proves the result in (7.16). \square

It should be noted that under similar channel conditions, the application of proposed CGS methods reduce SINR threshold for successful decoding from τ_j^* to φ_j^* or ϑ_j^* , which improves outage performance as demonstrated in numerical results section.

7.5 Results and Discussion

As shown in Table 7.2, simulation parameters similar to those in [51] are used, unless otherwise stated. 1000 random realizations of $\hat{h}_m \sim \mathcal{CN}(0, 1)$, $d_m \sim \mathcal{U}(0, r)$ and $\xi_m \sim \mathcal{U}(0, 0.05)$ are generated where $\mathcal{CN}(\cdot, \cdot)$ and $\mathcal{U}(\cdot, \cdot)$ represent complex Gaussian and uniform distribution, respectively. Further, the outage and throughput results are

averaged over all M users.

Figure 7.1 compares the average outage performance of proposed HMA with conventional NOMA and OMA as a function of SNR. It can be observed that HMA achieves lower average outage probability than NOMA and OMA and improves it by 38.8 – 79.8% and 40 – 93% respectively in the considered SNR range. This better performance of HMA results in due to less intra-user interference as $J = 2$ users perform NOMA in HMA compared to $M = 3$ in conventional NOMA. In addition, Monte Carlo simulations are also performed to validate the accuracy of derived outage results in (7.8) which are shown to be in good agreement with the simulations.

Figure 7.2 and 7.3 demonstrate the benefits of applying the proposed CGS methods 1 and 2 to G_2 HMA users under comparable channel gain parameters as used in Examples 1 and 2 of Section 7.3.2-A. The results show that the average outage performance of G_2 HMA users can be enhanced with the proposed CGS by 32 – 85% in the considered SNR range. This is because with CGS, users' power allocation coefficients would be computed with significant difference under similar channel conditions, which then results in better SIC operation at users. In addition, it can also be observed from Figure 7.3 that the performance of both ordered users is also improved under application of CGS method, whereas the performance of both users become comparable for conventional NOMA without CGS.

Figure 7.3 further shows the outage performance among NOMA system with CGS method 2 and OMA. It can be observed that NOMA under proposed CGS method 2 scheme outperforms NOMA without CGS and OMA. Further, both $m = 1, 2$ users have similar channel conditions, therefore, application of OMA results in same performance for both users, and hence only one result for OMA scheme is presented.

The average throughput comparison among HMA, NOMA and OMA systems is presented in Figure 7.4. The results are obtained by numerically solving the problem (7.5) using the 'fmincon' solver of MatLab software, with $\{R_k\}_{k=1}^K = \{R_j\}_{j=1}^J = 1$

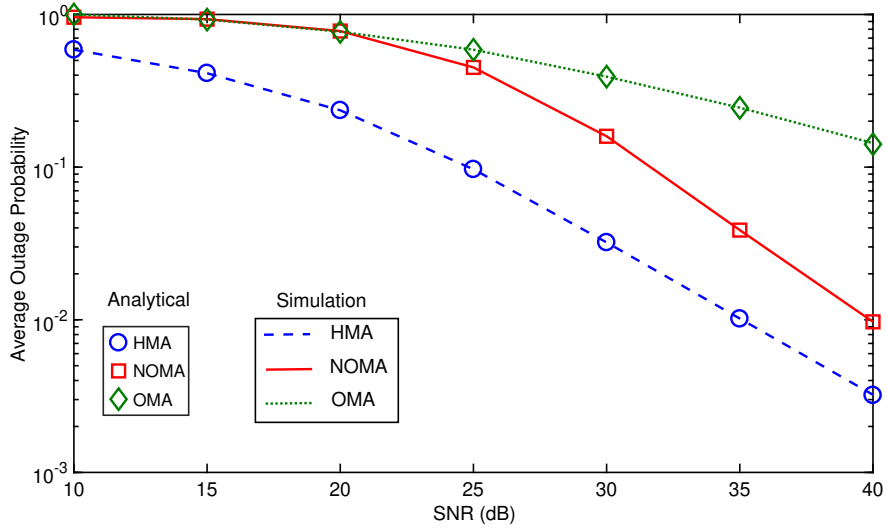


Figure 7.1. Outage comparison among HMA, NOMA and OMA.

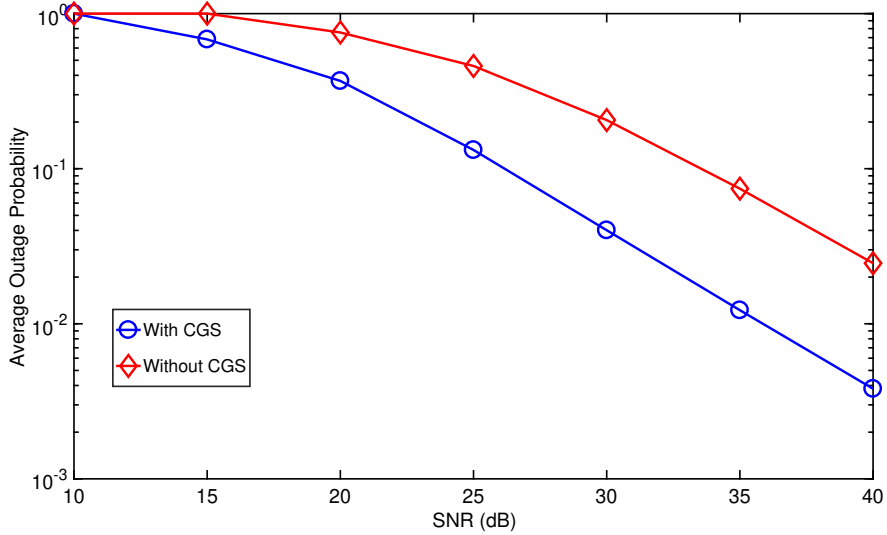


Figure 7.2. Outage comparison of G_2 HMA users with and without CGS under CGS method 1.

Mbps and $W = 10$ MHz which is most commonly used in single-input single-output long term evolution (LTE) downlink systems. It can be observed that HMA achieves higher average throughput than OMA for all considered values of M . In addition, the group size K for G_2 yielding an optimal throughput in HMA system is also shown in

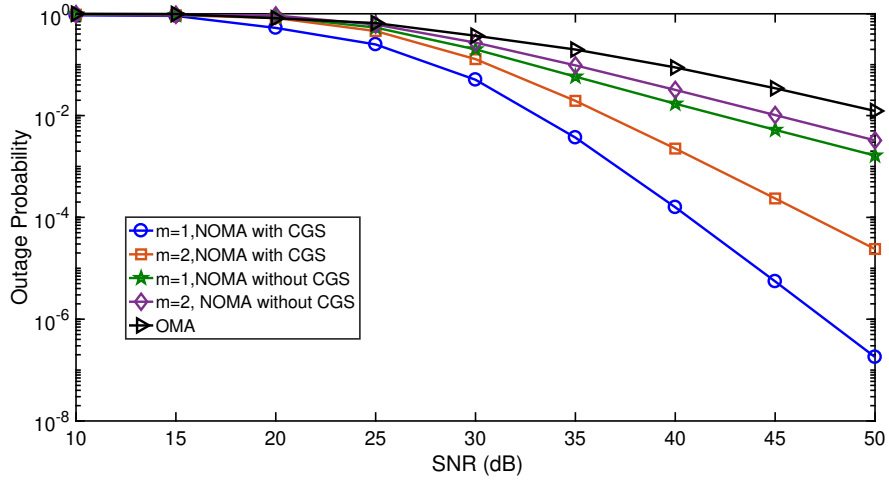


Figure 7.3. Outage performance comparison of G_2 HMA users with and without CGS and OMA under CGS method 2.

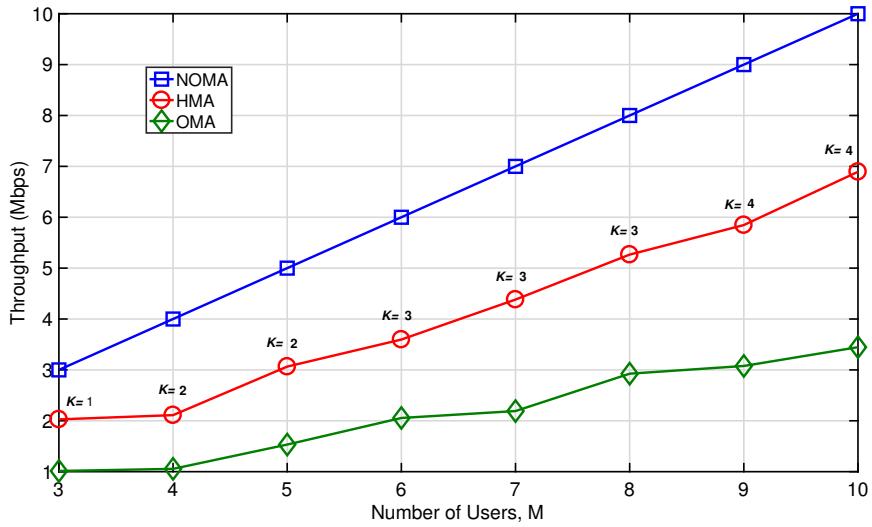


Figure 7.4. Throughput comparison among HMA, NOMA and OMA.

Figure 7.4. This group size can be viewed as the maximum number of users that can be scheduled for OMA in HMA while obtaining the optimal throughput. Further, it can be observed that there is a throughput loss in HMA compared to NOMA because entire W is not accessible by all users in HMA, and as opposed to better outage of HMA users in Figure 7.1, the throughput is influenced more by available bandwidth than intra-user

Table 7.3: Average outage probability (for $M > 3$)

Performance Metric	Total Users, M	HMA	NOMA	OMA
Average	5	0.46	0.79	0.81
Outage Probability	7	0.62	0.82	0.87
	9	0.75	0.88	0.9

interference and noise. However, the proposed HMA has superior outage performance and offers a more balanced tradeoff between decoding reliability and system throughput. As a result, the proposed scheme is particularly suited for systems that operate in low SNRs with moderate throughput requirements. Table 7.3 extends the outage probability results to cases of $M > 3$, where $\Upsilon = 20\text{dB}$, $M = \{5, 7, 9\}$ and $\{\varepsilon_m \sim \mathcal{U}(0.1, 1)\}_{m=1}^M$, $\forall m \in M$. It should be noted that the results remain generally consistent with those in Figure 7.1.

7.6 Chapter Summary

This chapter proposes a novel downlink HMA scheme based on NOMA and OMA. A necessary condition on the users' channel gains under which HMA can outperform pure NOMA or OMA is derived. An optimisation problem is formulated which is solved numerically to achieve maximum size K for group G_2 , resulting in the optimal throughput for the proposed HMA system. Furthermore, a CGS scheme is proposed for applying NOMA more effectively in HMA when users' channel conditions are similar. The exact closed-form expression for the outage probability is derived. Numerical results are presented to compare the average outage and throughput performance of HMA with conventional NOMA and OMA.

Chapter 8

PIC-based Receiver Structure for NOMA

Existing works and the previous chapters have assumed SIC as the baseline receiver for NOMA in order to mitigate the intra-user interference. However, there are some inherent issues of SIC that can limit the NOMA performance. In order to alleviate the problems related to the use of SIC with NOMA, this chapter proposes an alternate PIC-based receiver design for NOMA.

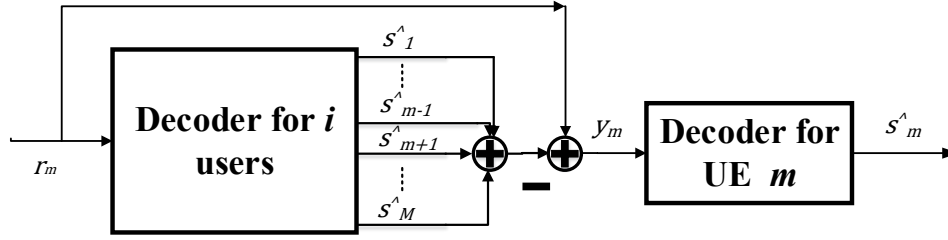
8.1 Introduction

There are several potential issues with SIC receivers which can adversely affect the performance of NOMA. The first drawback is that it is power sensitive. This means that its performance will degrade dramatically if two or more UEs have similar or same power [14, 46]. For example, if two or more UEs have comparable channel gains, then NOMA scheme will assign same power allocation coefficients to them, and thus the performance of SIC will degrade. The second shortcoming of the SIC is that its performance is highly dependent on the correct decoding of the first UE. In case the first

UE is not decoded correctly, this error in decoding will propagate successively to lower order UEs and hence deteriorate the system performance [6, 14]. More specifically, at any stage of decoding, if UE k is not decoded correctly, the performance of all the UEs having decoding order less than k will be affected badly. The third weakness of the SIC receiver is that for a large group of UEs in NOMA, the decoding delay for lower order UEs will be increased due to successive decoding nature of SIC. In order to reduce decoding delays, NOMA has to group small number of UEs having significant difference in channel gains, thus limiting the system capacity [6]. Finally, the users that are served by NOMA transmission scheme achieve unequal rates because the NOMA protocol is based on the order of SIC. This issue is extremely important in situations having strict fairness constraints [5].

The aforementioned critical performance limiting factors for SIC motivate us to propose an alternate PIC-based receiver design for NOMA downlink. The main motivation of this chapter is to study PIC-based receiver structure for downlink NOMA and to compare it with NOMA-SIC. In particular, the main contributions of this work are briefly summarise as follows:

- A PIC-based receiver structure is proposed for downlink NOMA and discuss some design considerations for it.
- Considering intra-user interference as one of the important design consideration for proposed PIC-based receiver, an equivalent transmission model is proposed for downlink NOMA. Based on the proposed transmission model, stochastic geometry tools are utilised to model the intra-user interference in downlink NOMA signal.
- Based on modeling results, an algorithm is proposed to estimate the intra-user interference in downlink NOMA signal, which is then removed prior to decoding.

Figure 8.1: Proposed receiver structure for UE m

- The closed form expression for outage probability is derived in order to evaluate the performance of the NOMA system under proposed intra-user interference estimation and cancellation technique.
- Simulation results are presented to justify the proposal of PIC-based receiver for downlink NOMA. In addition, numerical results for intra-user interference estimation and outage analysis probability for NOMA under proposed algorithm are also presented.

The rest of this chapter is organised as follows. Section 8.2 presents the proposed PIC-based receiver design for NOMA. Section 8.3 introduces the modeling and estimation of intra-user interference in NOMA signal. Results and discussion are presented in Section 8.4, followed by the chapter summary in Section 8.5.

8.2 Proposed PIC-based Receiver Design for NOMA

This section describes the structure and operation of the proposed PIC based receiver at UE for 5G downlink NOMA transmissions. The block diagram of the proposed PIC-based receiver for UE is shown in Figure 8.1.

Based on (2.2), (6.1), the received composite signal at the m -th UE can be expressed

as:

$$r_m = h_m \sum_{i=1}^M \sqrt{\beta_i P_t} s_i, \quad (8.1)$$

where P_t is the transmission power of BS, $h_m = \hat{h}_m d_m^{-\frac{\alpha}{2}}$ with $h_1 \leq \dots \leq h_M$, \hat{h}_m and d_m represent the Rayleigh fading channel gain, and distance between the BS and m -th user, respectively, α is the path loss exponent, β_i is the power allocation coefficient of user i with $\sum_{i=1}^M \beta_i = 1$ and $\beta_1 \geq \dots \geq \beta_M$, s_i is the message signal of i -th UE, P_t is the transmit power of BS with maximum available power P_B , and n_m is the AWGN with zero mean and variance σ^2 .

The proposed PIC-based receiver will perform decoding in two steps. In the first step, the proposed receiver will remove the intra-user interference caused by the transmission from users $1, \dots, m-1, m+1, \dots, M$. In contrast to SIC, the proposed receiver will mitigate the intra-user interference in a parallel fashion. After removing the interference from other users, at the second step, the receiver will decode the message of UE m .

In order to illustrate the intra-user interference cancellation procedure, consider an example of UE m with received signal r_m . Let \hat{s}_i be the estimate of message signal for UE i after decoding, then, an estimate of the message signal for UE m is obtained by subtracting the summation of all estimates $\hat{s}_i, i \neq m$ from the original received signal r_m . Hence, the signal at the input of the decoder for UE m can be written as:

$$y_m = r_m - \sum_{i=1}^M \hat{s}_i, \quad i \neq m. \quad (8.2)$$

The decoder of UE m will perform decoding on y_m to get the estimate of the message signal for UE m . A list of commonly used variables in this chapter is provided in Table 8.1

Table 8.1: Commonly used variables.

Notation	Description
M	Total number of users
R_m	Targeted rate of user m
P_t	Transmit power of BS
P_B	Maximum available power at BS
β_m	Power allocation coefficient of m -th user
ρ_t	Transmit SNR of BS
d_m	Distance between user m and BS
s_m	Message signal of user m
r_m	Received NOMA signal at user m
\mathcal{I}_m	Intra-user interference at user m
Φ	Marked point process
λ	Intensity of MPP Φ
\mathcal{R}_D	Coverage radius of BS
N, L	Gaussian-Chebyshev parameters

8.2.1 Filter Bank Design for Decoder of Users

Filter bank design is one of the possible approaches for implementing a block for decoder of i UEs to cancel the intra-user interference in a parallel manner. The composite signal r_m is fed into the matched filter input of each UE i , where $i = 1, \dots, m-1, m+1, \dots, M$. The output from each matched filter is then used to get the estimate of the transmitted message signal for that UE. The resulting probability of bit error at the receiver of UE m , denoted as, P_{BER} in an AWGN channel is given as [46]:

$$P_{\text{BER}} = Q \left(\left[\frac{N_0}{2E_b} \left(\frac{1 - \left(\frac{M-1}{K}\right)^{S+1}}{1 - \frac{M-1}{K}} \right) + \frac{1}{K^{S+1}} \left(\frac{(M-1)^{S+1} - (-1)^{S+1} \sum_{j=1}^K P_j}{M P_m} + (-1)^{S+1} \right) \right]^{-\frac{1}{2}} \right) \quad (8.3)$$

where P_j is the received power for UE j , M is the total number of UEs, K is a processing gain, S are the number of PIC stages, N_0 is the one sided noise power spectral density of the AWGN, E_b is the energy per bit and $Q(\cdot)$ is a standard Q function.

The proposed PIC-based receiver solves the problems of decoding failure in SIC due to equal or comparable power allocation for two or more NOMA downlink UEs, successive error propagation, decoding delay and dependency on the correct decoding of the first UE. All of these characteristics of the proposed receiver make it a stronger choice to adopt for the receiver side of UE in 5G downlink NOMA transmissions

8.2.2 Design Challenges for Proposed Receiver

1. Upper limit on the number of UEs in a decoder block

The receiver of a UE has a limited processing capability and power, which hinders one from processing and removing the interference from all the $N - 1$ UEs simultaneously, though it is theoretically feasible to do so. Furthermore, by increasing the number of UEs, the corresponding complexity of the UE receiver will also increase. Therefore, there exists a maximum value for the number of UEs to be processed at a receiver in order to attain a good tradeoff between receiver complexity and system capacity.

2. Estimate of user i message signal at UE n receiver

The estimate \hat{s}_i of the message signal for user i depends on its matched filter output at the receiver of UE n . For the proposed PIC-based receiver, unbiased or nearly fair estimate of the UE message signal, i.e. $\hat{s}_i \approx s_i$ was assumed. Unfortunately, in reality this estimate is biased after cancellation and it will increase with system loading [14]. Hence, for practical deployment of this receiver for NOMA downlink, this issue must be considered and requires further study.

3. Power Control

Power control is a vital component of a cellular network which is used to manage interference, energy and connectivity by maintaining the received SNR in both uplink and downlink. Therefore, it is of interest in understanding how NOMA transmission

protocol will be integrated with the existing power control strategies (both in uplink and downlink). In particular, having implemented uplink power control, the problem is how the NOMA transmission scheme will allocate different power to the downlink UEs in order to exploit power domain for multiplexing. One possible solution to solve this problem is requiring the UE to send to the BS its local noise information, based on which the NOMA protocol will allocate different power levels to the users. Further, it is of interest to investigate how the power control will help in reducing the intra-user interference at the proposed PIC based receiver. Hence, the investigation of integrating power control with NOMA and its impact on the proposed receiver structure can be an interesting research topic in NOMA.

4. Channel Estimation

In all real time scenarios, the assumption of perfect channel information will not be valid and hence the channel is estimated before performing any further processing. Due to the random nature of wireless channels, the estimate can never be accurate. Therefore, to make the receiver design more practical, it is necessary to analyze the performance of the PIC-based receiver under imperfect channel estimation in the context of 5G NOMA downlink

Note that downlink NOMA transmission is inherently interference limited due to superposition coding. As such, it is important to model and estimate the intra-user interference in downlink NOMA signal. This could also aid to improve the estimate of user i message at UE n receiver for proposed PIC-based receiver. As a result, the rest of this chapter focuses on modeling and estimating the intra-user interference in downlink NOMA signal.

8.3 Modeling and Estimation of Intra-User Interference in NOMA Signal

In this section, a novel equivalent transmission model for downlink NOMA system is presented, which is then utilised to model and estimate the intra-user interference. Based on these results, a closed-form expression for outage probability is derived to analyse the performance of NOMA under proposed intra-user interference estimation algorithm.

8.3.1 Equivalent Transmission Model for NOMA

Consider a cellular network with M NOMA users randomly distributed inside a disc \mathcal{D} of radius $\mathcal{R}_{\mathcal{D}}$ which represents the coverage of a BS located at the centre of $\mathcal{R}_{\mathcal{D}}$. Based on (8.1), the received NOMA signal r_m at UE m can be decomposed into two parts as:

$$r_m = h_m \sqrt{\beta_m P_t} s_m + h_m \underbrace{\sum_{i=1, i \neq m} \sqrt{\beta_i P_t} s_i}_{G_m} + n_m, \quad (8.4)$$

where the first term on RHS represents the faded version of the m -th user's message, the second term G_m is the superposition of remaining $M - 1$ users' messages, and the interference at m -th user can be defined as $\mathcal{I}_m = |G_m|^2$. This decomposition facilitates to propose an equivalent transmission model for DL NOMA in a novel way as shown in Figure 8.2, which is explained as follows.

Consider the case of a m -th user. From the second term G_m in (8.4), it can be observed that there are $M - 1$ interfering message signals present in r_m . One can visualize this as having imaginary transmitters located on a disc of radius d_m with the m -th user located at its centre, and the BS is the desired transmitter of m -th user only. Each imaginary transmitter i communicates with its intended (imaginary) receiver by transmitting a

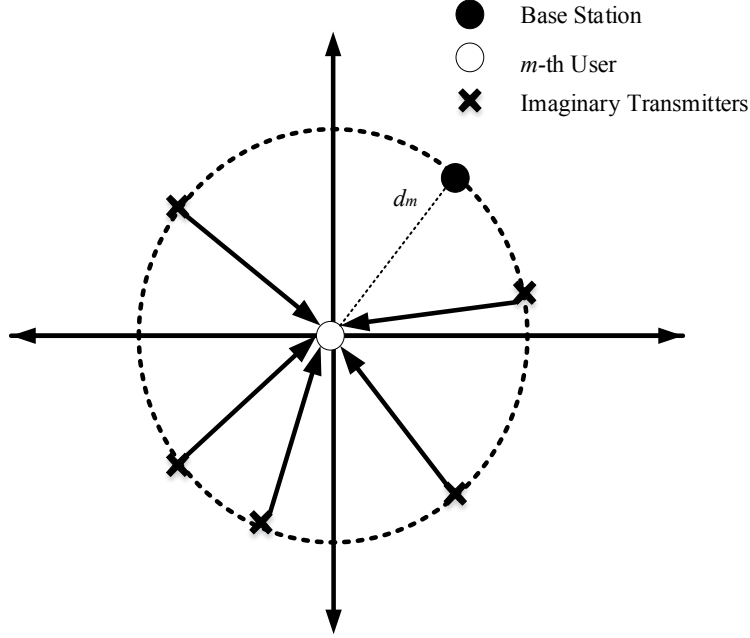


Figure 8.2: Equivalent Transmission Model for DL NOMA.

signal of power $\beta_i P_t$. Thus, each imaginary transmission is received at the m -th user with power $|h_m|^2 \beta_i P_t$, which in turn interferes with its reception of the desired signal from BS.

8.3.2 Intra-User Interference Modeling and Estimation

Intra-user interference modeling Consider a MPP Φ defined over $\mathbb{R}^2 \times \mathbb{K}$, where \mathbb{R}^2 denotes a 2D Euclidean space, and \mathbb{K} represents a mark space. Let ξ be a purely atomic random counting measure with finite atoms to describe the process. The locations of the atoms $\{x_i : i = 1, \dots, M\}$ and their associated marks $\{k_i : i = 1, \dots, M\}$ are considered as i.i.d with distributions $\pi_1(\cdot)$, and $\pi_2(\cdot)$, respectively.

Under the proposed equivalent transmission model, x_1 and $k_1 = \beta_1 P_t$ represent the BS's location, and transmission power, respectively, while the sets $\{x_i\}$ and ,

where $\{k_i\}$, represent the imaginary transmitters' locations, and transmission powers, respectively, i.e. each imaginary transmitter is uniquely defined by a combination of its location and mark. With this description, a realization of ξ can be represented by a set $\{(x_i, k_i : i = 1, \dots, M)\}$ consisting of i.i.d pairs $(x_i, k_i : i = 1, \dots, M)$ on $\mathbb{R}^2 \times \mathbb{K}$, having distribution $\Psi(d(x, k)) = \pi_1(dx) \pi_2(dk)$ [35].

Consider that the m -th user is located at origin of the coordinate system, then the interference at the m -th user, which is caused only by imaginary transmissions (since BS is the desired transmitter) is given by $\mathcal{I}_m = \sum_{(x,k) \in \Phi \setminus (x_1, k_1)} k |\hat{h}_x|^2 d_x^{-\alpha}$, where \hat{h}_x and d_x represent the Rayleigh fading channel gain, and distance between m -th user and an imaginary transmitter, respectively, at location x .

Having proposed the equivalent transmission model along with the conditional process $\Phi \setminus (x_1, k_1)$, the following Lemma states the distribution of the interference power.

Lemma 8.1. *Consider i.i.d marks at imaginary transmitters are uniformly distributed over a range $[P_{\min}, P_{\max}]$, where P_{\min} and P_{\max} represent the minimum, and maximum transmission powers, respectively. Then the Laplace transform of the interference \mathcal{I}_m at m -th user is given by:*

$$\mathcal{L}_{\mathcal{I}_m}(s) = C_M e^{-\Omega s^\delta}, \quad (8.5)$$

where $C_M = \frac{1}{P^{M-1}}$, $\Omega = \frac{\lambda_g \pi (P_{\max}^{1+\delta} - P_{\min}^{1+\delta}) \Gamma(1+\delta) \Gamma(1-\delta)}{(1+\delta)P}$, λ_g is the intensity for the ground process of Φ , $\delta = \frac{2}{\alpha}$, $P = P_{\max} - P_{\min} > 0$, and $\Gamma(\cdot)$ is a gamma function.

Proof. This lemma can be easily verified by standard arguments from stochastic geometry, i.e. conditioning on the fading and applying Eq. (13.1.15) of [35] will result in (8.5). \square

Remark: Under the proposed equivalent transmission model, the interference at the

Algorithm 1: Procedure to estimate \mathcal{I}_m

1. Generate a stable RV \mathcal{S} .
 2. Normalise r_m to obtain \bar{r}_m
 3. Apply adaptive LMS filter with r_m and $Y = \mathcal{S}\bar{r}_m$ as input signal and desired signal, respectively.
 4. The output of the LMS filter gives estimate \hat{G}_m of G_m .
 5. Compute power of \hat{G}_m to obtain estimate $\hat{\mathcal{I}}_m$.
-

-th user due to DL NOMA transmissions can be modeled as a stable random variable (Slivnyak's theorem) with its Laplace transform given by (8.5).

Intra-user Interference Estimation

A simple procedure for the -th user to estimate the interference from received signal is given in Algorithm 1.

8.3.3 Outage Analysis

The application of Algorithm 1 provides \hat{G}_m , which subtracted from r_m yields:

$$r_m - G_m = h_m \sqrt{\beta_m P_t} s_m + (1 - \kappa) G_m + n_m, \quad (8.6)$$

where $0 < \kappa \leq 1$ with $\kappa = 1$ representing ideal estimation of G_m .

The received SINR for the m -th user is given by $\zeta_m = \frac{|h_m|^2 \beta_m P_t}{(1-\kappa)^2 \mathcal{I}_m + \sigma^2}$. The outage occurs when $\zeta_m < \tau_m$, where $\tau_m = 2^{R_m} - 1$ and R_m is the targeted data rate for the m -th user. Therefore, the outage probability at the m -th user can be expressed as:

$$P_{\text{out}}^m = P_r \left(\frac{|h_m|^2 \rho_t}{\rho \mathcal{I}_m + 1} < \varphi_m \right) = F_{T_m}(\varphi_m), \quad (8.7)$$

where $\varphi_m = \frac{\tau_m}{\beta_m}$, $T_m = \frac{|h_m|^2 \rho_t}{\rho \mathcal{I}_m + 1}$, $\rho_t = \frac{P_t}{\sigma^2}$, $\rho = \frac{(1-\kappa)^2}{\sigma^2}$ and F_{T_m} is the CDF of T_m .

Unlike NOMA with SIC [13, 87], NOMA is not sensitive to choices of β_m and R_m (for all m) under the proposed approach due to SINR threshold condition φ_m . In order

to obtain P_{out}^m , F_{T_m} is required. Following a similar approach in [87], and conditioned on \mathcal{I}_m and ρ_t , and based on (8.7), F_{T_m} can be obtained as:

$$F_{T_m|\mathcal{I}_m, \rho_t}(\varphi_m) = F_{|h_m|^2} \left(\frac{\varphi_m (\rho z + 1)}{u} \right), \quad (8.8)$$

where $F_{|h_m|^2}$ is the CDF of h_m . Let \tilde{h} denotes the unordered channel gain. By applying order statistics [95], the CDFs of the unordered and ordered channel gains are related by the following relationship:

$$F_{|h_m|^2}(t) = \mu_m \sum_{q=0}^{M-m} \binom{M-m}{q} \frac{(-1)^q}{m+q} [F_{|\tilde{h}|^2}(t)]^{m+q}, \quad (8.9)$$

where $\mu_m = \frac{M!}{(M-m)!(m-1)!}$. Since the users are random uniformly distributed within a disc \mathcal{D} of radius $\mathcal{R}_{\mathcal{D}}$, and the fading is Rayleigh distributed, $F_{|\tilde{h}|^2}$ can be expressed as [79]:

$$F_{|\tilde{h}|^2}(t) = \frac{2}{\mathcal{R}_{\mathcal{D}}^2} \int_0^{\mathcal{R}_{\mathcal{D}}} (1 - e^{-r^{\alpha t}}) r \, dr. \quad (8.10)$$

The integral in (8.10) is very challenging to solve for $\alpha > 2$ (beyond free space path loss), and hence it is approximated by applying Gaussian-Chebyshev quadrature [103] as follows:

$$F_{|\tilde{h}|^2}(t) \approx \sum_{n=0}^N a_n e^{-b_n t}, \quad (8.11)$$

$a_0 = -\sum_{n=1}^N a_n$, $a_n = -\omega_n \sqrt{1 - \theta_n^2} (1 + \theta_n)$, $\omega_n = \frac{\pi}{N}$, $b_n = \left(\frac{\mathcal{R}_{\mathcal{D}}}{2} (1 + \theta_n)\right)^\alpha$, $\theta_n = \cos\left(\frac{2n-1}{2N}\pi\right)$ and N is a complexity-accuracy tradeoff parameter. Substituting (8.11)

into (8.9) and applying multinomial theorem, (8.11) can be expressed as:

$$\begin{aligned}
 F_{|h_m|^2}(t) &= \\
 \mu_m \sum_{q=0}^{M-m} \binom{M-m}{q} \frac{(-1)^q}{m+q} \sum_{r_0+\dots+r_N=m+q} \binom{m+q}{r_0+\dots+r_N} \left(\prod_{n=0}^N a_n^{r_n} \right) e^{-\sum_{n=0}^N r_n b_n t},
 \end{aligned} \tag{8.12}$$

where $\binom{m+q}{r_0+\dots+r_N} = \frac{(m+q)!}{r_0! \dots r_N!}$, and $\{r_i\} 0 \leq i \leq N$ are non-negative integers. Based on (8.12) and (8.8), P_{out}^m can now be expressed as:

$$\begin{aligned}
 P_{\text{out}}^m &= \int_0^\infty \int_0^\infty F_{|h_m|^2} \left(\frac{\varphi_m(\rho z + 1)}{u} \right) f_{\mathcal{I}_m}(z) f_{\rho_t}(u) dz du \\
 &= \mu_m \sum_{q=0}^{M-m} \binom{M-m}{q} \frac{(-1)^q}{m+q} \sum_{r_0+\dots+r_N=m+q} \binom{m+q}{r_0+\dots+r_N} \left(\prod_{n=0}^N a_n^{r_n} \right) \\
 &\quad \times \int_0^\infty \int_0^\infty e^{-\sum_{n=0}^N \frac{r_n b_n \varphi_m(\rho z + 1)}{u}} f_{\mathcal{I}_m}(z) f_{\rho_t}(u) dz du \\
 &= \mu_m \sum_{q=0}^{M-m} \binom{M-m}{q} \frac{(-1)^q}{m+q} \sum_{r_0+\dots+r_N=m+q} \binom{m+q}{r_0+\dots+r_N} \left(\prod_{n=0}^N a_n^{r_n} \right) \\
 &\quad \times \int_0^\infty \int_0^\infty e^{-\sum_{n=0}^N \frac{r_n b_n \varphi_m}{u}} \mathcal{L}_{\mathcal{I}_m} \left(\sum_{n=0}^N \rho \frac{r_n b_n \varphi_m}{u} \right) f_{\rho_t}(u) dz du \\
 &= C_M \mu_m \sum_{q=0}^{M-m} \binom{M-m}{q} \frac{(-1)^q}{m+q} \sum_{r_0+\dots+r_N=m+q} \binom{m+q}{r_0+\dots+r_N} \left(\prod_{n=0}^N a_n^{r_n} \right) \\
 &\quad \times \int_0^\infty e^{-\sum_{n=0}^N \frac{r_n b_n \varphi_m}{u} - \frac{\Omega(\sum_{n=0}^N \rho r_n b_n \varphi_m)}{u^\delta}} f_{\rho_t} du.
 \end{aligned} \tag{8.13}$$

In order to obtain P_{out}^m , f_{ρ_t} is required, which is provided in the following theorem.

Theorem 8.1. *Consider a downlink NOMA transmission scenario with a composite path loss and Rayleigh fading channel model, the PDF of transmit SNR of BS is given*

by:

$$\begin{aligned}
 f_{\rho_t}(u) &= \eta_m e^{-\eta_m \Upsilon\left(\delta, \frac{\varepsilon}{u}\right) u^\delta} \left(\delta u^{\delta-1} \Upsilon\left(\delta, \frac{\varepsilon}{u}\right) - e^{-\frac{\varepsilon}{u}} \varepsilon^\delta u^{-1} \right) U(\rho_B - u) \\
 &\quad + \Delta(u - \rho_B) e^{-\eta_m \Upsilon\left(\delta, \frac{\varepsilon}{u}\right) u^\delta},
 \end{aligned} \tag{8.14}$$

where $\Delta(\cdot)$, $U(\cdot)$, and $\Upsilon(\cdot)$ are the impulse function, step function, and lower incomplete gamma function, respectively, $\rho_B = \frac{P_B}{\sigma^2}$, $\varepsilon = c\mathcal{R}_D^\alpha$ where $c > 0$, $\eta_m = \frac{\lambda\delta\pi}{c^\delta}$, and λ is the intensity of a thinned homogeneous PPP.

Proof. See Appendix K. □

Substituting (8.14) into (8.13) and applying the Gaussian-Chebyshev quadrature, the outage probability at the m -th user is obtained as:

$$\begin{aligned}
 P_{\text{out}}^m &= C_M \mu_m \sum_{q=0}^{M-m} \binom{M-m}{q} \frac{(-1)^q}{m+q} \sum_{r_0+\dots+r_N=m+q} \binom{m+q}{r_0+\dots+r_N} \left(\prod_{n=0}^N a_n^{r_n} \right) \\
 &\quad \times \left[e^{-\frac{\sum_{n=0}^N r_n b_n \varphi_m}{\rho_B} - \frac{\Omega\left(\sum_{n=0}^N \rho r_n b_n \varphi_m\right)^\delta}{\rho_B^\delta} - \eta_m \Upsilon\left(\delta, \frac{\varepsilon}{\rho_B}\right) \rho_B^\delta} \right. \\
 &\quad \left. + \sum_{l=1}^L \Psi_l e^{-\frac{\sum_{n=0}^N r_n b_n \varphi_m}{\rho_B t_l} - \frac{\Omega\left(\sum_{n=0}^N \rho r_n b_n \varphi_m\right)^\delta}{\rho_B^\delta t_l^\delta} - \eta_m \Upsilon\left(\delta, \frac{\varepsilon}{\rho_B t_l}\right) \rho_B^\delta t_l^\delta} \right],
 \end{aligned} \tag{8.15}$$

where $\Psi_l = \frac{\omega_L}{2} \sqrt{1 - \theta_l^2} \eta_m \left(\delta \rho_B^\delta t_l^{\delta-1} \Upsilon\left(\delta, \frac{\varepsilon}{\rho_B t_l}\right) - e^{-\frac{\varepsilon}{\rho_B t_l}} \varepsilon^\delta t_l^{-1} \right)$, $\omega_L = \frac{\pi}{L}$, $t_l = \frac{1}{2}(1 + \theta_l)$, $\theta_l = \cos\left(\frac{2l-1}{2L}\pi\right)$, and L is the complexity-accuracy tradeoff parameter.

8.4 Results and Discussion

1. PIC-based receiver for downlink NOMA results.

In this sub-section, the analytical performance comparisons between PIC and SIC are presented. Apart from the fact that PIC solves the problems posed by SIC, the

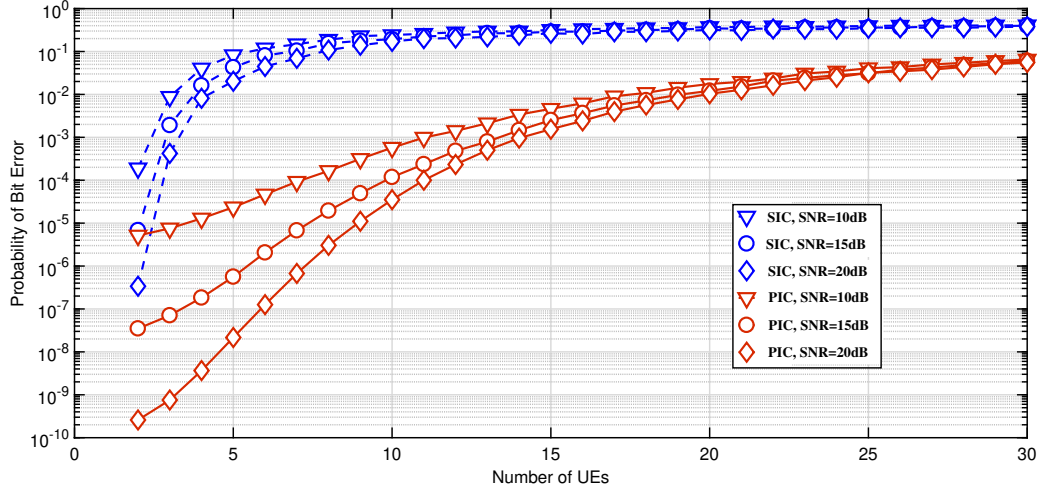


Figure 8.3: Probability of bit error and number of UEs

analysis also serves to promote the proposed PIC-based receiver structure as an alternate of SIC for 5G downlink NOMA based on its better performance.

The first comparison is presented between probability of bit error and number of UEs, as shown in Figure 8.3. The results are obtained with 30 UEs for both SIC and PIC. Each set of results is collected by keeping constant SNR of 10, 15 and 20 dB. The results show that by increasing the number of UEs beyond 5, there is negligible impact of increasing SNR for SIC receiver, while for PIC, the performance gain is appreciable up to 15 users for all three considered values of SNR.

The second set of results is presented in terms of probability of bit error and SNR, as shown in Figure 8.4. This figure shows the analytical bit error rate (BER) performance of SIC and PIC along with simulation results for NOMA with SIC and PIC receivers for the case of three users. The power allocation coefficients $\beta_m, m = 1, 2, 3$ for three NOMA UEs are considered to be random variables (due to the random nature of the channel), uniformly distributed between (0,1) with $\sum_{m=1}^3 \beta_m = 1$. In this way, the case of equal or comparable power allocation is also incorporated for two or more NOMA users in the simulations, as there exists a finite probability that two or all three NOMA users can be allocated with same power coefficient, which implies that they have

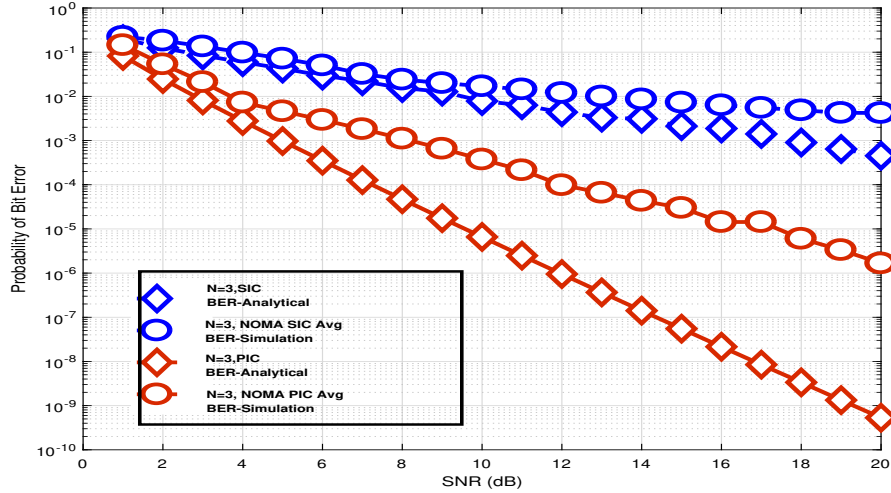


Figure 8.4: Downlink NOMA BER performance for 3 UEs

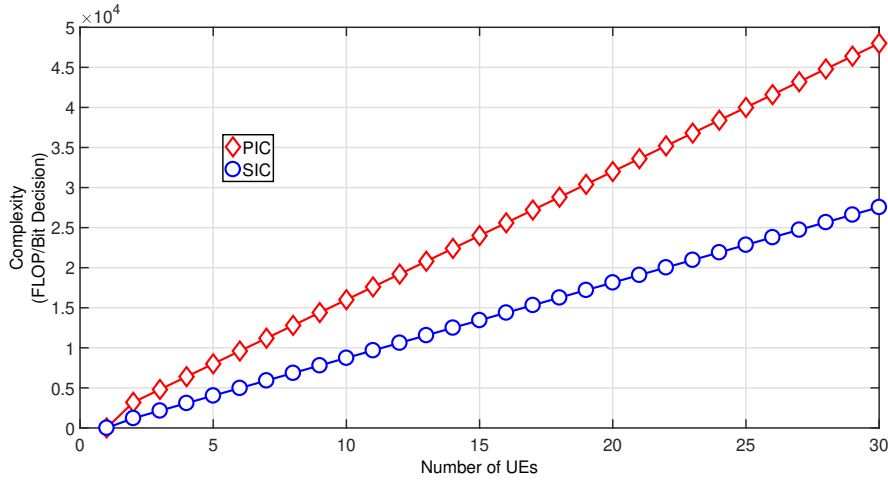


Figure 8.5: Computational complexity and number of UEs

same or comparable channel quality. This choice for considering the power allocation coefficient as random variable makes it more realistic and general for comparison. The analytical results for SIC and PIC receivers provide a performance bound for NOMA simulation. The simulation results show that NOMA with PIC receiver at UE performs better than NOMA with SIC in all SNR regions.

The final set of comparison between SIC and PIC techniques is presented in terms

Table 8.2: Simulation parameters.

Parameter	Description	Value
N_b	Number of bits	100
N_s	Number of samples per bit	10
\bar{L}	Number of multipath signals	10
M	Number of UEs	30
S	Number of PIC stages	3

of computational complexity, measured in FLOP, and is shown in Figure 8.5. A FLOP can be an operation implementing a multiplication or addition, while more complex operations can be regarded as multiple operations. For analysis purpose, the computational complexity derived for SIC and PIC receivers in [46] is utilised to process a frame of N_b bits, which is given by:

$$C_{\text{SIC}} = N_b \bar{L} \left[2N_s M + 5M + 8 \sum_{m=1}^{M-1} m + (M-1)(5 + 2N_s) \right] + 2M \bar{L} N_s (M \bar{L} - 1) + 2M N_b + M + M \log_2(M) \quad (8.16)$$

$$C_{\text{PIC}} = M \bar{L} N_b [S(6N_s + 7) - 4N_s - 1], \quad (8.17)$$

where C_{SIC} and C_{PIC} are computational complexities in terms of number of FLOP required for decoding N_b bits using SIC, and PIC receiver, respectively, \bar{L} is the maximum number of multipath signals processed by correlators at the receiver, and N_s is the number of samples per bit.

The computational complexity is computed for the parameters stated in Table 8.2. The increased computational complexity for PIC, as depicted in Figure 8.5 is due to the parallel structure of this receiver. The performance gains in Figures 8.3 and 8.4 were achieved at the cost of higher computational complexity.

In order to evaluate whether the processing power of current smartphone (UE) has a capability to implement the PIC receiver with this expected complexity, a certain

Table 8.3: Computational time of PIC for each mobile SoC.

SoC	MFLOP/sec	T μs
Samsung Exynos 3110	17.7	2800
Nvidia Tegra 2	54.4	900
Texas Instruments OMAP 4460	75	653
Qualcomm Snapdragon 600	540	90.7
Samsung Exynos 5 Octa 5410	627	78
Qualcomm Snapdragon 800	1034	47.3

system-on-chip (SoC) that is used in some smartphones with a capability to process X FLOP/sec is considered. The processing power in MFLOP/sec (10^6 FLOP/sec) of different popular mobile SoCs is listed in Table 8.3 [104–106].

The equivalent computational time T (in μs) per bit of decision for PIC is calculated for each mobile SoC. The maximum considered computational complexity for PIC with $M = 30$ is approximately 4.9×10^4 FLOP, as shown in Figure 8.5. The results of T show that the current and upcoming generations of smartphones should have the capability to implement PIC based receiver for 5G downlink NOMA.

2. Intra-user interference estimation results.

In this sub-section, numerical results on the accuracy of the proposed interference estimation and outage performance of NOMA are presented. Figure 8.6 shows the comparison between the actual (\mathcal{I}_m) and estimated ($\hat{\mathcal{I}}_m$) interferences. These results are obtained by applying Gaussian pulse shaping filter and a set of parameters similar to [87], i.e. $M = 3$, $\alpha = 4$, $R_1 = R_2 = R_3 = 0.1$ BPCU (bits per channel use), $\beta_1 = 0.4$, $\beta_2 = 0.35$ and $\beta_3 = 0.25$. Results show that the interference can be estimated with a small mean-squared-error (MSE) of approximately 1.5×10^{-3} .

For outage performance analysis, $N = 5$, $L = 2$, $\lambda = 10^{-3}$, $\rho = 20$ dB are considered and other parameters remain unchanged. Figure 8.7 shows the outage probability of m -th user under impact of different \mathcal{R}_D . Results obtained from Monte-Carlo simulations show good agreement with those obtained from (8.15). It is observed

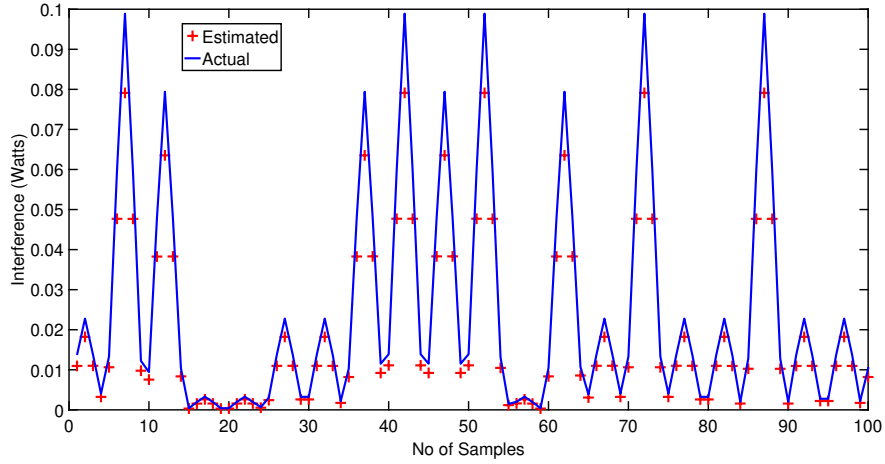
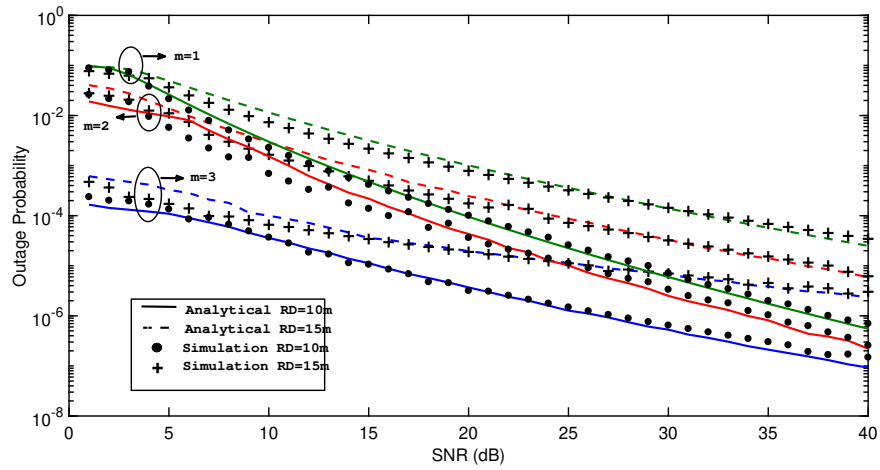


Figure 8.6: Estimation of interference.


 Figure 8.7: Impact of different \mathcal{R}_D on outage probability of m -th user.

that reducing \mathcal{R}_D expectedly decreases outage probability due to a smaller path loss, which is consistent with previous studies [13, 87]. Figure 8.8 further shows the outage probability of m -th user under impact of different α . As a representative case, a similar set of parameters from [13] are assumed, i.e. $M = 2$, $R_1 = R_2 = 2$ BPCU, $\beta_1 = 0.7$, $\beta_2 = 0.3$ and $\mathcal{R}_D = 5m$. It can be verified that with these choices of $R_1 = R_2 = 2$, $\beta_1 = 0.7$, and $\beta_2 = 0.3$, NOMA with SIC will suffer complete outage due to violation of the SNIR threshold condition in [13, 87]. On the other hand, NOMA

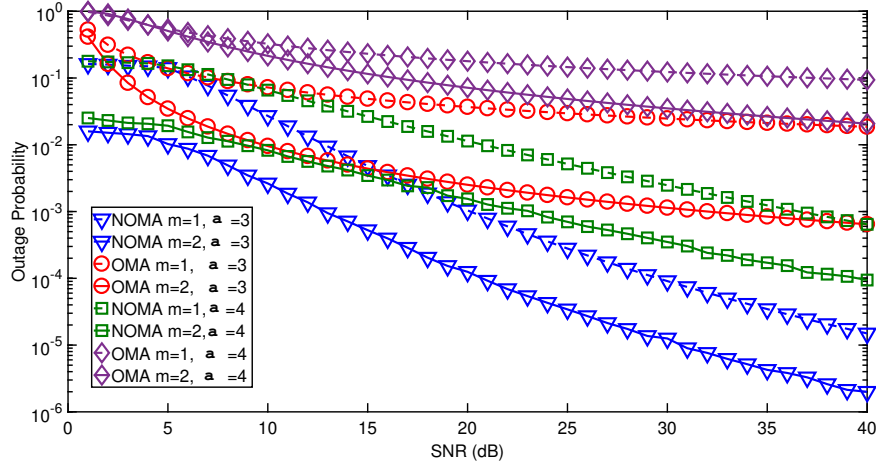


Figure 8.8: Impact of different α on outage probability of m -th user.

with the proposed interference model (for downlink users to estimate and remove interference) continues to operate with lower outage probability than conventional OMA for the considered values of α .

Finally, Figure 8.9 presents the outage probability comparison between NOMA under the proposed approach (for modeling, estimating, and cancelling interference) and NOMA with SIC. The results are obtained by using the same parameters as those for Figure 8.8, except $R_1 = R_2 = 1$ BPCU. It is clear that NOMA under the proposed approach has lower outage as compared to NOMA with SIC.

8.5 Chapter Summary

In this chapter, firstly, some of the critical performance limiting factors related to SIC are highlighted, which can result in the performance degradation of NOMA. In particular, NOMA with SIC requires a careful choice of target rates and power allocation coefficients in order to keep NOMA operational. In order to alleviate the problems posed by SIC, an alternate receiver structure for downlink NOMA based on parallel interference cancellation technique is proposed, along with some design consideration

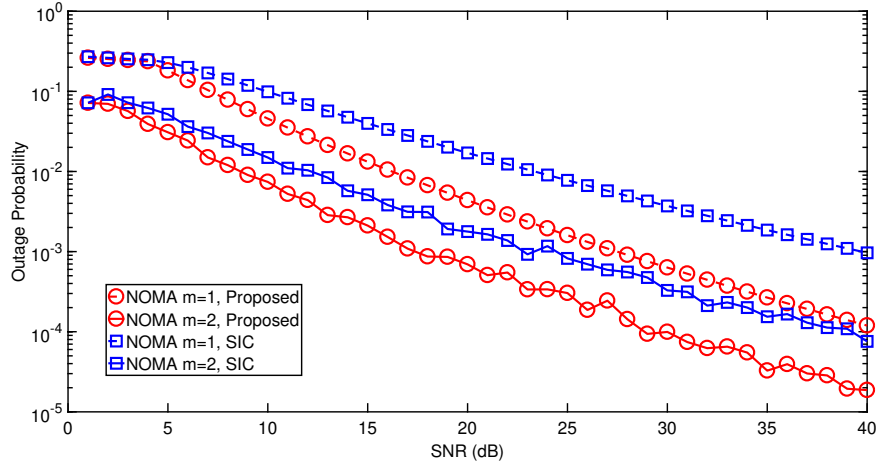


Figure 8.9: Performance comparison between NOMA under proposed approach and NOMA with SIC.

factors. Considering, intra-user interference in downlink NOMA as one of the important design aspect for the proposed receiver, the downlink NOMA system is represented in a novel way by proposing an equivalent transmission model, which is then utilized for intra-user interference modeling and estimation using stochastic geometry. In order to evaluate the performance, the closed-form expression of outage probability is derived for NOMA under proposed intra-user interference estimation and cancellation technique. Numerical simulations are conducted in the following two parts: 1) To justify the PIC-based receiver proposal for downlink NOMA, and 2) To evaluate the performance of NOMA under proposed intra-user interference estimation and cancellation algorithm. The numerical results prove the superiority of proposed PIC based receiver over SIC and hence is a promising receiver choice for UE in 5G downlink NOMA. In addition, the results demonstrate that with the proposed interference model and its application to estimate and remove the interference in the downlink signal before decoding, NOMA not only outperforms its OMA counterpart, but also manages to continue operating under conditions where NOMA with conventional SIC receiver suffers complete outage.

Chapter 9

Conclusion and Future Work

The research conducted in this thesis has been divided into two main parts. The first part primarily investigated the application of NOMA for multi-tier cellular networks, D2D communication, and WSNs. A persistent issue herein is accurate modeling and analysis of the considered network(s) with randomly distributed nodes (users, BSs, sensors and so on) over the entire 2D plane. In particular, it is important to investigate the performance of a typical user in a network under interference limited environment where spectral resources are utilised in an aggressive fashion. The investigation has three major components: 1) Selecting appropriate PP(s) to accurately model the spatial locations of the network nodes which possess relevant properties to capture their real deployment trends; 2) Interference characterisation at the typical user; and 3) Derivation of appropriate performance metrics based on the modeling approach and obtained interference distributions. Hence, comprehensive and analytically tractable frameworks have been developed for NOMA based multi-tier cellular networks, group D2D communication, and ubiquitous WSNs. For each of these networks, the interference at typical user is characterised by deriving its Laplace transform, which is then utilised to derive the outage probability expressions for performance analysis. The second part of this thesis addressed two objectives related to downlink NOMA: 1) To improve the system

performance in low SNR regime by utilising both NOMA and OMA in an optimal way; and 2) To alleviate the SIC related issues that can degrade the performance of downlink NOMA significantly. To this end, a summary of original contributions presented from Chapter 4 to Chapter 8 of this thesis along with some promising directions for future work are discussed in the rest of this chapter.

9.1 Summary of Contributions

In Chapter 4, a comprehensive and tractable framework is developed for analysis of two-tier cellular networks with underlay D2D communications, where NOMA is utilised by both MBSs and SBSs for communication with their cellular users. The MBS users and DRs are further classified as of non-clustered or clustered type. Stochastic geometry tools are used to evaluate the performance of typical MBS user, SBS user and DRs in terms of outage probability. The performance of NOMA based cellular network is also benchmarked against that of its conventional OMA counterpart. The results demonstrate that NOMA network users achieve lower outage probability than that of OMA. Further, in an interference limited environment, an arbitrary MBS user always achieve better performance than the SBS user and DR.

Moreover, it is observed that non-clustered type MBS user and DR outperform their clustered counterparts as more network interference is experienced by the latter than the former. It is also observed that an arbitrary NOMA user achieves higher average link throughput than DR and OMA user. More importantly, the performance of cellular users under the proposed SIE is always better than conventional SIC due to SIE's estimation and removal of intra-user interference. A pivotal conclusion is that adopting NOMA as a baseline transmission scheme in multi-tier cellular network not only improves the performance of cellular users but also that of DRs in the underlying D2D network. This is because DRs experience less interference under NOMA based cellular network than

what they receive under OMA based network.

The aforementioned analysis reveals several interesting design insights. The most important amongst them is the impact of intra-user interference on performance of NOMA users. It is noticed that at low SNRs, the network interference predominantly influence the performance while at high SNRs, the impact of intra-user interference is dominant. This necessitates a need for systematic treatment of intra-user interference in the system design to improve the performance of NOMA users. As a consequence, a SIE receiver is proposed to locally estimate and remove intra-user interference. The resulting analysis reveals that any attempt to remove intra-user interference would result in a performance lying between NOMA with perfect SIE and conventional SIC.

Chapter 5 proposes the Q-NOMA scheme for group D2D communications. In order to study its performance, the Laplace transform of the interference expression is firstly obtained, based on which the closed-form expression for the outage probability is derived. The results show that the proposed Q-NOMA group D2D achieves overall lower outage probability than its counterpart paired D2D communication. Further, a comparison between two implementations of the proposed scheme based on two power coefficient allocation policies is presented. Due to similar channel conditions and diverse QoS requirements of the DRs, it is shown that the proposed Q-NOMA implementation based on Policy I is more realistic and suitable than one based on Policy II for group D2D communications.

The chapter 6 investigates the application and performance of NOMA in UWSNs. Different from cellular use-case, NOMA in UWSNs are further subject to interferences from cross-technology nodes operating in the same unlicensed spectrum as the sensors. Focusing on downlink (sink-to-sensors) scenario, a new closed-form expression for outage probability at the probe receiver's location is derived by utilising stochastic geometry and order statistics. Numerical analysis shows that NOMA achieves lower outage probability, higher average throughput and better energy efficiency than conventional

OMA, hence is an attractive enabling technology for massive machine connectivity in interference-limited UWSNs. Further, the computational time complexity for NOMA message decoding is within acceptable limits when using current and upcoming generations of processors for UWSNs.

In Chapter 7, a novel HMA with CGS scheme is proposed and analysed for its average outage and throughput performances. In addition, an optimisation problem is formulated, which is solved numerically to obtain the K for G_2 that results in the optimal throughput for the proposed HMA system. The results show that the HMA scheme achieves overall superior outage performance than NOMA and OMA in the considered SNR range. Further, it is shown that the outage performance of G_2 users can be enhanced with CGS under similar channel conditions. In terms of throughput, HMA always outperforms OMA, whereas suffers throughput loss compared to NOMA. Consequently, it is capable of yielding a more balanced trade-off between outage performance and system throughput.

Finally, in Chapter 8, some limitations related to SIC that can degrade the performance of NOMA scheme in downlink are highlighted. In order to alleviate the problems posed by SIC, an alternate receiver structure based on PIC for downlink NOMA is proposed. The results prove the superiority of proposed receiver in terms of bit error rate performance over conventional SIC at the cost of higher computational complexity, which is still however within the processing capability of current and upcoming generations of smartphones. Hence, it can be considered as a promising receiver choice for UE in future 5G downlink NOMA.

9.2 Future Work

Based on the findings obtained in this thesis, some potential directions for future research are suggested as follows:

- The analysis in Chapter 4 reveals the existence of a maximum number of SBSs beyond which no further performance enhancement for cellular users is achieved. Thus, a possible future design consideration is to optimise the number of SBSs subject to a given set of performance and resource constraints.
- From an application perspective, the results of Chapter 4 can be extended to analyse cache enabled networks in terms of hit probability and caching throughput [107, 108]. In addition, the developed analytical framework in Chapter 4 can be utilised to study other performance metrics such as ergodic sum rate and bit error rate.
- An interesting extension of work on Q-NOMA group D2D communications in Chapter 5 is to allow inter-group D2D communications, where GTs relay message of source DR to destination DR in a multi-hop fashion. How to establish a communication link between source and destination DRs, while keeping propagation delay to minimum is a major challenge.
- In the context of UWSNs, minimising node energy consumption is critical. As such, the developed spatial model in Chapter 6 can be integrated with optimal power and rate allocation strategies for NOMA to maximise the battery life of the sensors.
- One promising future extension for the proposed HMA with CGS scheme in Chapter 7 is to design it for MIMO systems and evaluate its performance in terms of the diversity and ergodic sum-rate achieved. The optimisation of user groupings using machine learning is yet another possible extension of this work.
- The decoding performance of proposed PIC receiver in Chapter 8 can be improved by applying the intra-user interference estimation and cancellation technique in Chapter 8 to cancel the residual interference that results from parallel UE

CHAPTER 9. CONCLUSION AND FUTURE WORK

decodings. Integrating power control in downlink NOMA with PIC receiver is another potential direction for future work.

Appendix A

Proof of Lemma 4.1

$$\begin{aligned}\mathcal{A}_s &= \mathbb{P} \left\{ \mathbf{1} \left(\arg \max_{k \in \{m, s\}} P_k R_k^{-\alpha} = s \right) \right\} \\ &= \mathbb{P} \left(R_s^{-\alpha} P_s > R_m^{-\alpha} P_m \right) \\ &= \mathbb{P} \left(R_m > \Omega^{\frac{1}{\alpha}} R_s \right) \\ &= \int_0^\infty \left[1 - F_{R_m} \left(\Omega^{\frac{1}{\alpha}} r_s \right) \right] f_{R_s} (r_s) dr_s. \tag{A.1}\end{aligned}$$

Based on (A.1), the association probability \mathcal{A}_m is obtained by using $\mathcal{A}_m + \mathcal{A}_s = 1$. This proves the results in Lemma 4.1.

Appendix B

Proof of Lemma 4.2

The CDF F_{R_m} in (4.7) can be expressed as [37]:

$$\begin{aligned}
F_{R_m}(r_m) &= 1 - \sum_{n=0}^{\infty} \frac{(-1)^n}{n!} \int_{(B(0,r_m))^n} \det \left(K(x_{m_i}, x_{m_j}) \right)_{1 \leq i, j \leq n} dx_{m_1} \dots dx_{m_n} \\
&\stackrel{(a)}{\approx} 1 - \sum_{n=0}^{\infty} \frac{(-1)^n}{n!} \int_{(B(0,r_m))^n} \prod_{i=1}^n K(x_{m_i}, x_{m_i}) dx_{m_1} \dots dx_{m_n} \\
&= 1 - \sum_{n=0}^{\infty} \frac{(-1)^n}{n!} \left[\int_{B(0,r_m)} K(x_{m_i}, x_{m_i}) dx_{m_i} \right]^n \\
&= 1 - e^{-\int_{B(0,r_m)} K(x_m, x_m) dx_m} \\
&\stackrel{(b)}{=} 1 - e^{-\lambda_m \int_{B(0,r_m)} dx_m} \\
&\stackrel{(c)}{=} 1 - e^{-2\pi\lambda_m r_m^2}, \tag{B.1}
\end{aligned}$$

where (a) results in by applying diagonal approximation [109], (b) is obtained by simplifying the Gauss DPP kernel defined after (4.9) and (c) follows by converting from Cartesian to polar coordinates.

Now based on (4.8) and (B.1), the association probability \mathcal{A}_s in (4.10) can be

expressed as:

$$\begin{aligned}
 \mathcal{A}_s &\approx 2\pi\lambda_s \int_0^\infty e^{-\pi r_s^2 (\lambda_s + 2\lambda_m \Omega^\delta)} r_s \mathrm{d}r_s \\
 &= 2\pi\lambda_s \int_0^\infty e^{-\pi r_s^2 \lambda_s (1 + 2\beta \Omega^\delta)} r_s \mathrm{d}r_s \\
 &\stackrel{(a)}{=} \pi\lambda_s \int_0^\infty e^{-\pi \lambda_s (1 + 2\beta \Omega^\delta) t} \mathrm{d}t \\
 &= (1 + 2\beta \Omega^\delta)^{-1}, \tag{B.2}
 \end{aligned}$$

where (a) is obtained by a change of variable from $r_s^2 \rightarrow t$. Finally, based on (B.2), the approximation to association probability \mathcal{A}_m in (4.13) is obtained in a straightforward manner. This completed the proof of Lemma 4.2.

Appendix C

Proof of Lemma 4.3

In order to prove this Lemma, $\mathcal{L}_{\mathcal{I}_{nm}^m}$, $\mathcal{L}_{\mathcal{I}_{nm}^{\text{NDT}}}$ and $\mathcal{L}_{\mathcal{I}_{nm}^{\text{CDT}}}$ are required. First, start by deriving $\mathcal{L}_{\mathcal{I}_{nm}^m}(\mathfrak{s})$. Condition on $R_m = r_m$, the conditional distribution of \mathcal{I}_{nm}^m is written

as,

$$\begin{aligned}
 \mathcal{L}_{\mathcal{I}_{\mathbb{m}}^m | R_m = r_m}(\mathfrak{s}) &= \mathbb{E}_{\Phi_m} \left[\prod_{\mathbf{x}_m \in (\Phi_m \cap \bar{B}(r_m, \mathcal{R}_1)) \setminus \mathbf{x}_s^*} \mathbb{E}_{h_{\mathbf{x}_m}} \left(\exp -\mathfrak{s} P_m h_{\mathbf{x}_m} \|\mathbf{x}_m\|^{-\alpha} \right) \right] \\
 &\stackrel{(a)}{=} \frac{\sum_{n=0}^{\infty} \frac{(-1)^n}{n!} \int_{(\mathbb{R}^2)^n} \det \left(K_{z_m^*}^! \left(\mathbf{x}_{m_{\bar{i}}}, \mathbf{x}_{m_{\bar{j}}} \right) \right)_{1 \leq \bar{i}, \bar{j} \leq n} \prod_{\bar{i}=1}^n \left(1 - \frac{\mathbf{1}_{r_m \leq |\mathbf{x}_{m_{\bar{i}}}| \leq \mathcal{R}_1}}{1 + \mathfrak{s} P_m \|\mathbf{x}_{m_{\bar{i}}}\|^{-\alpha}} \right) d\mathbf{x}_{m_1} \dots d\mathbf{x}_{m_n}}{\sum_{n=0}^{\infty} \frac{(-1)^n}{n!} \int_{(b(0, r_m))^n} \det \left(K_{z_m^*}^! \left(\mathbf{x}_{m_{\bar{i}}}, \mathbf{x}_{m_{\bar{j}}} \right) \right)_{1 \leq \bar{i}, \bar{j} \leq n} d\mathbf{x}_{m_1} \dots d\mathbf{x}_{m_n}} \\
 &\stackrel{(b)}{=} \frac{\sum_{n=0}^{\infty} \frac{(-1)^n}{n!} \int_{(\mathbb{R}^2)^n} \prod_{\bar{i}=1}^n K_{z_m^*}^! \left(\mathbf{x}_{m_{\bar{i}}}, \mathbf{x}_{m_{\bar{i}}} \right) \left(1 - \frac{\mathbf{1}_{r_m \leq |\mathbf{x}_{m_{\bar{i}}}| \leq \mathcal{R}_1}}{1 + \mathfrak{s} P_m \|\mathbf{x}_{m_{\bar{i}}}\|^{-\alpha}} \right) d\mathbf{x}_{m_1} \dots d\mathbf{x}_{m_n}}{\sum_{n=0}^{\infty} \frac{(-1)^n}{n!} \int_{(b(0, r_m))^n} \prod_{\bar{i}=1}^n K_{z_m^*}^! \left(\mathbf{x}_{m_{\bar{i}}}, \mathbf{x}_{m_{\bar{i}}} \right) d\mathbf{x}_{m_1} \dots d\mathbf{x}_{m_n}} \\
 &= \frac{e^{-\int_{\mathbb{R}^2} K_{z_m^*}^! (\mathbf{x}_m, \mathbf{x}_m) \left(1 - \frac{\mathbf{1}_{r_m \leq |\mathbf{x}_m| \leq \mathcal{R}_1}}{1 + \mathfrak{s} P_m \|\mathbf{x}_m\|^{-\alpha}} \right) d\mathbf{x}_m}}{e^{-\int_{b(0, r_m)} K_{z_m^*}^! (\mathbf{x}_m, \mathbf{x}_m) d\mathbf{x}_m}} \\
 &= e^{-\int_{b^c(0, r_m)} K_{z_m^*}^! (\mathbf{x}_m, \mathbf{x}_m) \left(1 - \frac{\mathbf{1}_{r_m \leq |\mathbf{x}_m| \leq \mathcal{R}_1}}{1 + \mathfrak{s} P_m \|\mathbf{x}_m\|^{-\alpha}} \right) d\mathbf{x}_m} e^{-\int_{b^c(0, \mathcal{R}_1)} \frac{K_{z_m^*}^! (\mathbf{x}_m, \mathbf{x}_m)}{1 + \mathfrak{s} P_m \|\mathbf{x}_m\|^{-\alpha}} d\mathbf{x}_m} \tag{C.1}
 \end{aligned}$$

where Laplace transform of interference over DPP $\Phi_m \setminus z_m^*$ in (a) is obtained by applying [Theorem 1, [37]] (b) follows from diagonal approximation [109], and $K_{z_m^*}^!$ is the Gauss DPP Kernel under reduced Palm distribution at z_m^* and is given as, $K_{z_m^*}^! \left(\mathbf{x}_{m_{\bar{i}}}, \mathbf{x}_{m_{\bar{j}}} \right) = \frac{1}{K(z_m^*, z_m^*)} \det \begin{pmatrix} K \left(\mathbf{x}_{m_{\bar{i}}}, \mathbf{x}_{m_{\bar{j}}} \right) & K \left(\mathbf{x}_{m_{\bar{i}}}, z_m^* \right) \\ K \left(z_m^*, \mathbf{x}_{m_{\bar{j}}} \right) & K \left(z_m^*, z_m^* \right) \end{pmatrix}$ [37], and the Gauss DPP kernel $K(\cdot, \cdot)$ is defined after (4.9).

Denote $Q_5 = \int_{b^c(0, r_m)} K_{z_m^*}^! (\mathbf{x}_m, \mathbf{x}_m) \left(1 - \frac{\mathbf{1}_{r_m \leq |\mathbf{x}_m| \leq \mathcal{R}_1}}{1 + \mathfrak{s} P_m \|\mathbf{x}_m\|^{-\alpha}} \right) d\mathbf{x}_m$ and $Q_6 = \int_{b^c(0, \mathcal{R}_1)} \frac{K_{z_m^*}^! (\mathbf{x}_m, \mathbf{x}_m)}{1 + \mathfrak{s} P_m \|\mathbf{x}_m\|^{-\alpha}} d\mathbf{x}_m$ in (C.1). Then Q_5 and Q_6 are simplified as

follows:

$$\begin{aligned}
 Q_5 &\stackrel{(c)}{=} \lambda_m \int_{b^c(0, r_m)} \left(1 - e^{-\frac{2\|\mathbf{x}_m - \mathbf{z}_m^*\|^2}{\kappa^2}}\right) \left(1 - \frac{\mathbf{1}_{r_m \leq \|\mathbf{x}_m\| \leq \mathcal{R}_1}}{1 + \mathfrak{s}P_m \|\mathbf{x}_m\|^{-\alpha}}\right) d\mathbf{x}_m \\
 &\stackrel{(d)}{=} \lambda_m \int_{r_m}^{\infty} \int_0^{2\pi} \left(1 - e^{-\frac{2(r^2 + r_m^2 - 2rr_m \cos \theta)}{\kappa^2}}\right) d\theta \left(1 - \frac{1}{1 + \mathfrak{s}P_m r^{-\alpha}}\right) r dr \\
 &\stackrel{(e)}{=} 2\pi \lambda_m \int_{r_m}^{\infty} \left(1 - \frac{1}{1 + \mathfrak{s}P_m r^{-\alpha}}\right) \left(1 - e^{-\frac{2(r^2 + r_m^2)}{\kappa^2}} I_0\left(\frac{4rr_m}{\kappa^2}\right)\right) r dr \\
 &\stackrel{(f)}{=} \frac{2\pi \lambda_m}{\alpha} \int_0^{r_m^{-\alpha}} \left(1 - \frac{1}{1 + \mathfrak{s}P_m x}\right) \left(1 - e^{-\frac{2(x^{-\delta} + r_m^2)}{\kappa^2}} I_0\left(\frac{4x^{-\delta} r_m}{\kappa^2}\right)\right) x^{-\delta} dx \\
 &\stackrel{(g)}{\approx} 2\pi \lambda_m \sum_{\bar{n}=1}^{\bar{N}} \Psi_{\bar{n}} \left(1 - \frac{1}{1 + \mathfrak{s}P_m r_m^{-\alpha} t_{\bar{n}}}\right), \tag{C.2}
 \end{aligned}$$

where (c) is obtained by using $K_{z_m^*}^!(\mathbf{x}_m, \mathbf{x}_m) = \lambda_m \left(1 - e^{-\frac{2\|\mathbf{x}_m - \mathbf{z}_m^*\|^2}{\kappa^2}}\right)$ for Gauss DPP [37], (d) follows from Cartesian to polar coordinates conversion, (e) results in by integrating over variable θ , (f) is obtained by a change of variable from $r^{-\alpha} \rightarrow x$, and (g) results in by applying Gaussian-Chebyshev quadrature. Following similar steps to (C.2), the integral Q_6 can be simplified as,

$$Q_6 \approx 2\pi \lambda_m \sum_{\bar{l}=1}^{\bar{L}} \frac{\Psi_{\bar{l}}}{1 + \mathfrak{s}P_m \mathcal{R}_1^{-\alpha} t_{\bar{l}}}. \tag{C.3}$$

Based on (C.1), (C.2) and (C.3), $\mathcal{L}_{\mathcal{I}_{nm}^m}$ can be expressed as:

$$\mathcal{L}_{\mathcal{I}_{nm}^m}(\mathfrak{s}) = \mathbb{E}_{R_m} [e^{-Q_5 - Q_6}]. \tag{C.4}$$

Now deconditioning on R_m obtains the result for $\mathcal{L}_{\mathcal{I}_{nm}^m}(\mathfrak{s})$ in (4.15).

Next $\mathcal{L}_{\mathcal{I}_{\text{nm}}^{\text{NDT}}}$ can be derived as follows.

$$\begin{aligned}
 \mathcal{L}_{\mathcal{I}_{\text{nm}}^{\text{NDT}}}(\mathbf{s}) &= \mathbb{E} \left[e^{-\sum_{y_n \in \Phi_{\text{NDR}} \cap b(0, \mathcal{R}_3)} s P_d h_{y_n} \|y_n\|^{-\alpha}} \right] \\
 &= \mathbb{E} \left[\prod_{y_n \in \Phi_{\text{NDR}} \cap b(0, \mathcal{R}_3)} \mathbb{E}_{h_{y_n}} \left(e^{-s P_d h_{y_n} \|y_n\|^{-\alpha}} \right) \right] \\
 &\stackrel{(a)}{=} \mathbb{E}_{\Phi_s} \left\{ \mathbb{E}_{\Phi_1} \left[\prod_{y_n \in (\Phi_1 \cap b(0, \mathcal{R}_3)) \cap E_{\mathcal{R}_2}^c} \frac{1}{1 + s P_d \|y_n\|^{-\alpha}} \right] \right\} \\
 &\stackrel{(b)}{=} \mathbb{E}_{\Phi_s} \left[e^{-pq\lambda_1 \int_{(\mathbb{R}^2 \cap b(0, \mathcal{R}_3)) \cap E_{\mathcal{R}_2}^c} \frac{s P_d \|y_n\|^{-\alpha} dy_n}{1 + s P_d \|y_n\|^{-\alpha}}} \right] \\
 &= \mathbb{E}_{\Phi_s} \left[e^{-\int_{b(0, \mathcal{R}_3)} \frac{pq\lambda_1 dy_n}{1 + \frac{\|y_n\|^{-\alpha}}{s P_d}} + \int_{E_{\mathcal{R}_2}} \frac{pq\lambda_1 dy_n}{1 + \frac{\|y_n\|^{-\alpha}}{s P_d}}} \right] \\
 &\stackrel{(c)}{=} e^{-2\pi pq\lambda_1 s P_d \int_0^{\mathcal{R}_3} \frac{r dr}{s P_d + r^\alpha}} \mathbb{E}_{\Phi_s} \left[e^{\int_{E_{\mathcal{R}_2}} \frac{pq\lambda_1 dy_n}{1 + \frac{\|y_n\|^{-\alpha}}{s P_d}}} \right] \\
 &\stackrel{(d)}{\approx} e^{-2\pi pq\lambda_1 s P_d \sum_{k=1}^K \frac{0.5 \mathcal{R}_3^2 \omega_k \sqrt{1 - \theta_k^2}}{s P_d + (t_k \mathcal{R}_3)^\alpha}} \\
 &\quad \times \mathbb{E}_{\Phi_s} \left[e^{\sum_{x_s \in \Phi_s} \int_{b(x_s, \mathcal{R}_2)} \frac{pq\lambda_1 s P_d dy_n}{s P_d + \|y_n\|^{-\alpha}}} \right] \\
 &\stackrel{(e)}{=} e^{-2\pi pq\lambda_1 s P_d Q_3} \\
 &\quad \times \mathbb{E}_{\Phi_s} \left[\prod_{x_s \in \Phi_s} e^{2pq\lambda_1 s P_d \int_{\|x_s\| - \mathcal{R}_2}^{\|x_s\| + \mathcal{R}_2} \frac{\arccos\left(\frac{r^2 + \|x_s\|^2 - \mathcal{R}_2^2}{2\|x_s\|r}\right)}{s P_d + r^\alpha} r dr} \right] \\
 &\stackrel{(f)}{=} e^{-2\pi pq\lambda_1 s P_d Q_3} e^{-2\pi \lambda_s \int_{\mathcal{R}_2}^\infty (1 - e^{-2pq\lambda_1 s P_d f(v, \mathbf{s})}) v dv}, \tag{C.5}
 \end{aligned}$$

where (a) follows by taking expectation over Rayleigh fading channel gains $h_{y_n} \sim \exp(1)$, (b) is obtained by applying PGFL for PPP Φ_1 given $E_{\mathcal{R}_2}$ and noting the fact that the density of non-clustered DTs is $pq\lambda_1$, (c) results in from Cartesian to Polar coordinates conversion, (d) is derived by the standard machinery, where the integral in first term is approximated by using Gaussian-Chebyshev quadrature. The second term is obtained by ignoring the effect of holes overlap and using the fact that

$\int_{E_{\mathcal{R}_2}} \frac{pq\lambda_1 dy_n}{1 + \frac{\|y_n\|^\alpha}{sP_d}} \approx \sum_{x_s \in \Phi_s} \int_{b(x_s, \mathcal{R}_2)} \frac{pq\lambda_1 sP_d dy_n}{sP_d + \|y_n\|^\alpha}$ [Appendix D, [43]], the second exponential term in (e) is obtained by applying [Lemma 3 and Appendix B, [43]], where interference at typical user from PHP with single hole (conditioned on the location of hole centre) is considered, and (f) results in by first applying PGFL for PPP Φ_s and then converting from Cartesian to Polar coordinates with $\|x_s\| = v$. This obtains the result for $\mathcal{L}_{\mathcal{I}_{nm}^{\text{NDT}}}$ in (4.16).

Next, the Laplace transform of interference $\mathcal{I}_{nm}^{\text{CDT}}$ is expressed as:

$$\begin{aligned}
 \mathcal{L}_{\mathcal{I}_{nm}^{\text{CDT}}} &= \mathbb{E} \left[e^{-\sum_{x_s \in \Phi_s \cap \bar{B}(\mathcal{R}_2, \mathcal{R})} \sum_{y_c \in \mathcal{B}^{x_s} \cap b(0, \mathcal{R}_3)} sP_d h_{y_c} \|x_s + y_c\|^{-\alpha}} \right] \\
 &= \mathbb{E} \left[\prod_{x_s \in \Phi_s \cap \bar{B}(\mathcal{R}_2, \mathcal{R})} \prod_{y_c \in \mathcal{B}^{x_s} \cap b(0, \mathcal{R}_3)} \mathbb{E}_{h_{y_c}} \left(e^{-sP_d h_{y_c} \|x_s + y_c\|^{-\alpha}} \right) \right] \\
 &\stackrel{(a)}{=} \mathbb{E}_{\Phi_s} \left[\prod_{x_s \in \Phi_s \cap \bar{B}(\mathcal{R}_2, \mathcal{R})} \mathbb{E}_{\mathcal{B}^{x_s}} \left(\prod_{y_c \in \mathcal{B}^{x_s} \cap b(0, \mathcal{R}_3)} \frac{1}{1 + sP_d \|x_s + y_c\|^{-\alpha}} \right) \right] \\
 &\stackrel{(b)}{=} \mathbb{E}_{\Phi_s} \left[\prod_{x_s \in \Phi_s \cap \bar{B}(\mathcal{R}_2, \mathcal{R})} e^{-pq\bar{c} \int_{\mathbb{R}^2 \cap b(0, \mathcal{R}_3)} \frac{f_{y_c}(y_c)}{1 + sP_d \|x_s + y_c\|^{-\alpha}} dy_c} \right] \\
 &\stackrel{(c)}{=} \mathbb{E}_{\Phi_s} \left[\prod_{x_s \in \Phi_s \cap \bar{B}(\mathcal{R}_2, \mathcal{R})} \exp \left(-pq\bar{c} \int_0^{\mathcal{R}_3} \int_0^{2\pi} \frac{\bar{r} e^{-\bar{r}^2} d\bar{\theta} d\bar{r}}{1 + sP_d (\bar{r}^2 + \|x_s\|^2 - 2\|x_s\|\bar{r} \cos \bar{\theta})^{-\frac{\alpha}{2}}} \right) \right] \\
 &\stackrel{(d)}{=} e^{-2\pi\lambda_s \int_{\mathcal{R}_2}^{\mathcal{R}} (1 - e^{-pq\bar{c}f(r, s)}) r dr} \tag{C.6}
 \end{aligned}$$

where (a) is obtained by taking the expectation over the channel gains $h_{y_c} \sim \exp(1)$ given \mathcal{B}^{x_s} and PPP Φ_s , (b) follows from the PGFL of a single cluster in TCP [42] and noting the fact that number of DTs per cluster are $pq\bar{c}$, (c) results in by first using the distribution of offspring points (users) by which they are distributed around the parent point (SBSs) in TCP and then applying Cartesian to polar Coordinates conversion, and (d) is obtained by applying PGFL of PPP Φ_s and then converting coordinates from

APPENDIX C. PROOF OF LEMMA 4.3

Cartesian to polar.

Finally, combining (C.4), (C.5) and (C.6) prove the results in Lemma 4.3.

Appendix D

Proof of Lemma 4.4

In order to obtain the results in Lemma 4.4, $\mathcal{L}_{\mathcal{I}_{\text{cm}}^s}$ and $\mathcal{L}_{\mathcal{I}_{\text{cm}}^{\text{CDT}}}$ are required, which are derived as follows:

$$\begin{aligned}
\mathcal{L}_{\mathcal{I}_{\text{cm}}^s}(\mathfrak{s}) &= \mathbb{E}_{\Phi_s} \left[e^{-\mathfrak{s} \sum_{x_s \in \Phi_s b(0, \mathcal{R}_2)} P_s h_{x_s} \|x_s\|^{-\alpha}} \right] \\
&= \mathbb{E}_{\Phi_s} \left[\prod_{x_s \in \Phi_s b(0, \mathcal{R}_2)} \mathbb{E}_{h_{x_s}} \left(e^{-\mathfrak{s} P_s h_{x_s} \|x_s\|^{-\alpha}} \right) \right] \\
&\stackrel{(a)}{=} \mathbb{E}_{\Phi_s} \left[\prod_{x_s \in \Phi_s b(0, \mathcal{R}_2)} \frac{1}{1 + \mathfrak{s} P_s \|x_s\|^{-\alpha}} \right] \\
&\stackrel{(b)}{=} e^{-2\pi\mathfrak{s}\lambda_s P_s \int_0^{\mathcal{R}_2} \frac{r dr}{\mathfrak{s} P_s + r^\alpha}} \\
&\stackrel{(c)}{=} e^{-2\pi\mathfrak{s}\lambda_s P_s Q_3 |_{P_d=P_d, \mathcal{R}_3=\mathcal{R}_2}}, \tag{D.1}
\end{aligned}$$

where (a) follows by taking expectation over channel gains $h_{x_s} \sim \exp(1)$, (b) is obtained by first applying PGFL for PPP Φ_s and then converting coordinates from Cartesian to polar, and (c) is derived by approximating the integral with Gaussian-Chebyshev quadrature (in the same way as step (d) for deriving $\mathcal{L}_{\mathcal{I}_{\text{cm}}^{\text{NDT}}}$ in Appendix C).

Next in order to prove this Lemma, $\mathcal{L}_{\mathcal{I}_{\text{cm}}^{\text{CDT}}}$ is required. Recall that typical user in this

APPENDIX D. PROOF OF LEMMA 4.4

case is a clustered MBS user and the locations of interfering cluster centres are located in $b(0, \mathcal{R})$. Consequently, following similar steps to derive (C.6), the expression for $\mathcal{L}_{\mathcal{I}_{\text{cm}}^{\text{CDT}}}$ in (4.17) can be obtained. This completes the proof of Lemma 4.4.

Appendix E

Proof of Lemma 4.5

In order to prove the results of Lemma 4.5, the expressions for $\mathcal{L}_{\mathcal{I}_s^m}$, $\mathcal{L}_{\mathcal{I}_s^s}$ and $\mathcal{L}_{\mathcal{I}_s^{\text{CDT}}}$ are required. First, start by deriving $\mathcal{L}_{\mathcal{I}_s^m}$, which is expressed as:

$$\begin{aligned}
\mathcal{L}_{\mathcal{I}_s^m}(\mathfrak{s}) &= \mathbb{E} \left[e^{-\mathfrak{s} \sum_{\mathbf{x}_m \in \Phi_m \cap b(0, \mathcal{R}_1)} P_m h_{\mathbf{x}_m} \|\mathbf{x}_m\|^{-\alpha}} \right] \\
&\stackrel{(a)}{=} \mathbb{E}_{\Phi_m} \left[\prod_{\mathbf{x}_m \in \Phi_m \cap b(0, \mathcal{R}_1)} \frac{1}{1 + \mathfrak{s} P_m \|\mathbf{x}_m\|^{-\alpha}} \right] \\
&\stackrel{(b)}{=} \sum_{n=0}^{\infty} \frac{(-1)^n}{n!} \int_{(\mathbb{R}^2 \cap b(0, \mathcal{R}_1))^n} \det \left(K(\mathbf{x}_{m_{\bar{i}}}, \mathbf{x}_{m_{\bar{j}}})_{1 \leq \bar{i}, \bar{j} \leq n} \right) \\
&\quad \times \prod_{\bar{i}=1}^{\bar{n}} \left(1 - \frac{1}{1 + \mathfrak{s} P_m \|\mathbf{x}_{m_{\bar{i}}}\|^{-\alpha}} \right) d\mathbf{x}_{m_1} \dots d\mathbf{x}_{m_n} \\
&\stackrel{(c)}{=} \sum_{n=0}^{\infty} \frac{(-1)^n}{n!} \int_{(b(0, \mathcal{R}_1))^n} \prod_{\bar{i}=1}^{\bar{n}} K(\mathbf{x}_{m_{\bar{i}}}, \mathbf{x}_{m_{\bar{i}}}) \left(1 - \frac{1}{1 + \mathfrak{s} P_m \|\mathbf{x}_{m_{\bar{i}}}\|^{-\alpha}} \right) d\mathbf{x}_{m_1} \dots d\mathbf{x}_{m_n} \\
&= e^{-\mathfrak{s} P_m} \int_{b(0, \mathcal{R}_1)} \frac{K(\mathbf{x}_m, \mathbf{x}_m)}{\mathfrak{s} P_m + \|\mathbf{x}_m\|^{-\alpha}} d\mathbf{x}_m \\
&\stackrel{(d)}{=} e^{-2\pi \lambda_m \mathfrak{s} P_m} \int_0^{\mathcal{R}_1} \frac{dr}{\mathfrak{s} P_m + \|r\|^{-\alpha}} \\
&\stackrel{(e)}{=} e^{-2\pi \lambda_m \mathfrak{s} P_m Q_3 |_{\mathcal{R}_3 = \mathcal{R}_1, P_4 = P_m}}, \tag{E.1}
\end{aligned}$$

where (a) is obtained by taking expectation over channel gains $h_{\mathbf{x}_m} \sim \exp(1)$, (b) results in by applying PGFL of DPP Φ_m [37], (c) follows from diagonal approximation

[109], (d) is obtained by first converting from Cartesian to polar coordinates and then using Gauss DPP kernel $K(x_m, x_m) = \lambda_m$ (similar to step (b) in Appendix B), and (e) is derived by applying Gaussian-Chebyshev quadrature (in the same way as step (d) for deriving $\mathcal{L}_{\mathcal{I}_{nm}^{\text{NDT}}}$ in Appendix C).

Next to prove this Lemma, the expressions for $\mathcal{L}_{\mathcal{I}_s^s}$ and $\mathcal{L}_{\mathcal{I}_s^{\text{CDT}}}$ are required. Conditioned on $R_s = r_s$, the conditional distributions of the interference \mathcal{I}_s^s and $\mathcal{I}_s^{\text{CDT}}$ can be derived as follows:

$$\begin{aligned}
 \mathcal{L}_{\mathcal{I}_s^s | R_s = r_s}(\mathfrak{s}) &= \mathbb{E} \left[e^{-\mathfrak{s} \sum_{x_s \in (\Phi_s \cap \bar{B}(r_s, \mathcal{R}_2)) \setminus z_s^*} P_s h_s \|x_s\|^{-\alpha}} \right] \\
 &\stackrel{(a)}{=} \mathbb{E}_{\Phi_s} \left[\prod_{x_s \in (\Phi_s \cap \bar{B}(r_s, \mathcal{R}_2)) \setminus z_s^*} \frac{1}{1 + \mathfrak{s} P_s \|x_s\|^{-\alpha}} \right] \\
 &\stackrel{(b)}{=} \mathbb{E}_{\Phi_s} \left[\prod_{x_s \in \Phi_s \cap \bar{B}(r_s, \mathcal{R}_2)} \frac{1}{1 + \mathfrak{s} P_s \|x_s\|^{-\alpha}} \right] \\
 &\stackrel{(c)}{=} e^{-2\pi \lambda_s \mathfrak{s} P_s \int_{r_s}^{\mathcal{R}_2} \frac{r dr}{\mathfrak{s} P_s + r^\alpha}} \\
 &\stackrel{(d)}{=} e^{-2\pi \lambda_s \mathfrak{s} P_s \sum_{\tilde{q}=1}^{\tilde{Q}} \frac{0.5(\mathcal{R}_2 - r_s)^2 \omega_{\tilde{q}} \sqrt{1 - \theta_{\tilde{q}}^2} t_{\tilde{q}}}{\mathfrak{s} P_s + t_{\tilde{q}}^\alpha}} \tag{E.2}
 \end{aligned}$$

where (a) is obtained by taking expectations over channel gains $h_{x_s} \sim \exp(1)$, (b) follows from the application of Slivnyak theorem for PPP, (c) results in from the PGFL of PPP and then converting coordinates from Cartesian to polar, and (d) is derived by applying Gaussian-Chebyshev quadrature to approximate the integral in step (c).

Based on (E.2), the Laplace transform of interference \mathcal{I}_s^s can be expressed as,

$$\mathcal{L}_{\mathcal{I}_s^s}(\mathfrak{s}) = \mathbb{E}_{R_s} \left[\mathcal{L}_{\mathcal{I}_s^s | R_s = r_s} \right]. \tag{E.3}$$

Now deconditioning (E.3) on R_s obtains the result for $\mathcal{L}_{\mathcal{I}_s^s}$ in (4.23). Similarly, conditioned on $R_s = r_s$, the conditional Laplace transform for the interference $\mathcal{I}_s^{\text{CDT}}$

can be written as:

$$\begin{aligned} \mathcal{L}_{\mathcal{I}_s^{\text{CDT}}|_{R_s=r_s}}(\mathfrak{s}) = \\ \mathbb{E} \left[e^{-\mathfrak{s} \sum_{x_s \in \Phi_s \cap \bar{B}(R_s, \mathcal{R})} \sum_{y_c \in \mathcal{B}^{x_s} \cap b(0, \mathcal{R}_3)} P_d h_{y_s} \|x_s + y_c\|^{-\alpha}} \right] \end{aligned} \quad (\text{E.4})$$

Recall that in this case, the locations of interfering cluster centres are located in $\bar{B}(r_s, \mathcal{R})$. As a result, following similar steps to derive (C.6), $\mathcal{L}_{\mathcal{I}_s^{\text{CDT}}|_{R_s=r_s}}$ can be expressed as:

$$\mathcal{L}_{\mathcal{I}_s^{\text{CDT}}|_{R_s=r_s}}(\mathfrak{s}) = e^{-2\pi\lambda_s \int_{r_s}^{\mathcal{R}} (1 - e^{-pq\bar{e}f(r, \mathfrak{s})}) r dr}. \quad (\text{E.5})$$

Based on (E.5), the Laplace transform for the interference $\mathcal{I}_s^{\text{CDT}}$ can be written as:

$$\mathcal{L}_{\mathcal{I}_s^{\text{CDT}}}(\mathfrak{s}) = \mathbb{E}_{R_s} \left[\mathcal{L}_{\mathcal{I}_s^{\text{CDT}}|_{R_s=r_s}}(\mathfrak{s}) \right]. \quad (\text{E.6})$$

Now deconditioning on R_s in (E.6) obtains the result for $\mathcal{L}_{\mathcal{I}_s^{\text{CDT}}}(\mathfrak{s})$ in (4.24). This completes the proof for Lemma 4.5.

Appendix F

Proof of Lemma 4.6

Conditioned on the location of serving non-clustered DT at y_n^* , the Laplace transform for the interference $\mathcal{I}_{\text{nd}}^{\text{NDT}}$ is given as:

$$\begin{aligned}
 \mathcal{L}_{\mathcal{I}_{\text{nd}}^{\text{NDT}}}(\mathfrak{s}) &= \mathbb{E} \left[e^{-\mathfrak{s} \sum_{y_n \in (\Phi_{\text{NDT}} \cap b(0, \mathcal{R}_3)) \setminus y_n^*} P_d h_{y_n} \|y_n\|^{-\alpha}} \right] \\
 &\stackrel{(a)}{=} \mathbb{E}_{\Phi_s} \left[\mathbb{E}_{\Phi_1} \left(\prod_{y_n \in ((\Phi_1 \cap b(0, \mathcal{R}_3)) \setminus y_n^*) \cap E_{\mathcal{R}_2}^c} \frac{1}{1 + \mathfrak{s} P_d \|y_n\|^{-\alpha}} \right) \right] \\
 &\stackrel{(b)}{=} \mathbb{E}_{\Phi_s} \left[\mathbb{E}_{\Phi_1} \left(\prod_{y_n \in (\Phi_1 \cap b(0, \mathcal{R}_3)) \cap E_{\mathcal{R}_2}^c} \frac{1}{1 + \mathfrak{s} P_d \|y_n\|^{-\alpha}} \right) \right] \\
 &\stackrel{(c)}{=} \mathcal{L}_{\mathcal{I}_{\text{nm}}^{\text{NDT}}}(\mathfrak{s}), \tag{F.1}
 \end{aligned}$$

where (a) is obtained by taking expectation over channel gains $h_{y_n} \sim \exp(1)$ and using the definition of PHP in (2.11) and noting the fact that $\Phi_{\text{NDT}} \subset \Phi_1$ and the density of non-clustered DTs is $pq\lambda_1$, (b) follows from the application of Slivnyak theorem for PHP [43], and (c) results in by comparing with step (a) in deriving $\mathcal{L}_{\mathcal{I}_{\text{nm}}^{\text{NDT}}}$ in (C.5) (Appendix C).

Appendix G

Proof of Lemma 4.7

The Laplace transform of interference $\mathcal{I}_{\text{cd}}^{\text{CDT}}$, conditioned on the location of serving clustered DT can be written as,

$$\begin{aligned}
\mathcal{L}_{\mathcal{I}_{\text{cd}}^{\text{CDT}}}(\mathfrak{s}) &= \mathbb{E} \left[e^{-\mathfrak{s} \sum_{y_c \in (\Phi_{\text{CDT}} \cap b(0, \mathcal{R})) \setminus y_c^*} P_d h_{y_c} \|x_s + y_c\|^{-\alpha}} \right] \\
&= \mathbb{E} \left[e^{-\sum_{x_s \in \Phi_s \cap b(0, \mathcal{R})} \sum_{y_c \in (\mathcal{B}^{x_s} \cap b(0, \mathcal{R}_3)) \setminus y_c^*} P_d h_{y_c} \|x_s + y_c\|^{-\alpha}} \right] \\
&\stackrel{(a)}{=} \mathbb{E} \left[\prod_{x_s \in \Phi_s \cap b(0, \mathcal{R})} \prod_{y_c \in \mathcal{B}^{x_s} \cap b(0, \mathcal{R}_3)} \frac{1}{1 + \mathfrak{s} P_d \|x_s + y_c\|^{-\alpha}} \right] \\
&\quad \times \int_{\mathbb{R}^2 \cap b(0, \mathcal{R}_2)} e^{-pq(\bar{c}-1) \int_{b(0, \mathcal{R}_3)} \frac{f_{y_c}(y_c) dy_c}{1 + \mathfrak{s} P_d \|x_s + y_c\|^{-\alpha}}} f_{y_c}(x_s) dy_c \\
&\stackrel{(b)}{=} e^{-2\pi\lambda_s \int_0^{\mathcal{R}} (1 - e^{-pq\bar{c}\bar{f}(r, \mathfrak{s})}) r dr} \int_{b(0, \mathcal{R}_2)} e^{-pq(\bar{c}-1)\bar{f}(\|x_s\|, \mathfrak{s})} f_{y_c}(x_s) dy_c \\
&\stackrel{(c)}{=} \mathcal{L}_{\mathcal{I}_{\text{cm}}^{\text{CDT}}}(\mathfrak{s}) \int_0^{\mathcal{R}_2} e^{-[pq(\bar{c}-1)\bar{f}(r, \mathfrak{s}) + r^2]} r dr,
\end{aligned}$$

where (a) is obtained by applying conditional PGFL for TCP [42] and then taking expectation over channel gains $h_{y_c} \sim \exp(1)$, first term in (b) is obtained by following similar steps in deriving (C.6) (Appendix C) and second term follows from Cartesian to polar coordinates conversion (in the same way as done in step (c) to derive $\mathcal{L}_{\mathcal{I}_{\text{nm}}^{\text{CDT}}}$ in Appendix C) and using the function $\bar{f}(r, \mathfrak{s})$ with $r = \|x_s\|$, and in (c), the first term

follows from (4.20) by recognising it as $\mathcal{L}_{\mathcal{I}_{\text{cm}}^{\text{CDT}}}(\mathfrak{s})$. The second term results in by first using the distribution of offspring points (users) by which they are distributed around the parent point (SBSs) in TCP as defined in (2.9) and then applying Cartesian to polar coordinates conversion.

Appendix H

Proof of Theorem 4.1

In order to prove this theorem, the outage probability when m -th MBS user is of type non-clustered/clustered is required i.e., the expressions for P_{ε_5} and P_{ε_6} are needed for SIC and SIE receivers. As such, first start to derive the probability of event ε_5 by using SIC and SIE receivers. Based on (4.4), the outage probability at m -th MBS non-clustered user to decode any of the higher order user \bar{m} , $1 \leq \bar{m} \leq m - 1$ using SIC is given by,

$$\begin{aligned} P_{m \rightarrow \bar{m}} &= \mathbb{P} \left(\frac{\bar{h}_m^m a_{\bar{m}}^m P_m}{\bar{h}_m^m P_m \sum_{i=\bar{m}+1}^M a_i^m + \mathcal{I}_{nm} + \sigma^2} < \tau_{\bar{m}}^m \right) \\ &= \mathbb{P} \left(\bar{h}_m^m < \varphi_{\bar{m}}^m (1 + \rho \mathcal{I}_{nm}) \right), \end{aligned} \quad (\text{H.1})$$

where $\varphi_{\bar{m}}^m = \frac{\tau_{\bar{m}}^m}{\Upsilon_m(a_{\bar{m}}^m - \tau_{\bar{m}}^m \sum_{i=\bar{m}+1}^M a_i^m)}$. Now based on (H.1) and defining $\varphi_m^{\max} = \max \{\varphi_1^m, \dots, \varphi_m^m\}$, the outage overall probability at the clustered m -th MBS user with SIC can be expressed as,

$$\begin{aligned} P_{\varepsilon_5}^{\text{SIC}} &= \mathbb{P} \left(\bar{h}_m^m < \varphi_m^{\max} (1 + \rho \mathcal{I}_{nm}) \right) \\ &= \mathbb{E}_{\mathcal{I}_{nm}} \left[F_{\bar{h}_m^m} \left(\varphi_m^{\max} (1 + \rho x) \right) \right]. \end{aligned} \quad (\text{H.2})$$

In order to obtain $P_{\varepsilon_5}^{\text{SIC}}$, the CDF $F_{\hat{h}_m}$ is required. Denote by $F_{\hat{h}_m}$ as the CDF of unordered channel gain \hat{h}_m . The relationship between CDFs of ordered and unordered channel gains is given as [95]:

$$F_{\hat{h}_m}^-(y) = \mu_m \sum_{\bar{p}=0}^{M-m} \binom{M-m}{\bar{p}} \frac{(-1)^{\bar{p}}}{m+\bar{p}} [F_{\hat{h}_m}(y)]^{m+\bar{p}}. \quad (\text{H.3})$$

The CDF of unordered channel gain $F_{\hat{h}_m}$ is given as [79]:

$$F_{\hat{h}_m}(y) = \int_{\mathcal{D}_1} (1 - e^{z^2 y}) f_{d_m}(z) dz. \quad (\text{H.4})$$

Note that d_m in (H.4) is a distance between an arbitrary and randomly distributed MBS user in a representative macro-cell and its associated MBS. As a result, d_m can be interpreted as a distance between non-clustered cellular user at arbitrary location and its nearest MBS i.e., $d_m = R_m$. Hence, converting coordinates from Cartesian to polar and using $f_{R_m} = f_{d_m}$ from (4.6) in (H.4), $F_{\hat{h}_m}$ can be expressed as:

$$F_{\hat{h}_m}(y) = 2\pi \int_0^{\mathcal{R}_1} (1 - e^{r_m^2 y}) f_{R_m}(r_m) dr_m. \quad (\text{H.5})$$

Based on (H.3) and (H.5), $P_{\varepsilon_5}^{\text{SIC}}$ in (H.2) can be written as:

$$P_{\varepsilon_5}^{\text{SIC}} = \mu_m \sum_{\bar{p}=0}^{M-m} \binom{M-m}{\bar{p}} \frac{(-1)^{\bar{p}}}{m+\bar{p}} \int_0^\infty [F_{\hat{h}_m}(\varphi_m^{\max}(1+\rho x))]^{m+\bar{p}} f_{\mathcal{I}_{nm}}(x) dx \quad (\text{H.6})$$

Now using $\mathcal{L}_{\mathcal{I}_{nm}}$ from (4.14) and applying (4.29) to obtain $f_{\mathcal{I}_{nm}}$, and then approximating the integral in (H.6) by applying Gauss-Laguerre quadrature [103], $P_{\varepsilon_5}^{\text{SIC}}$ can be

expressed as:

$$P_{\varepsilon_5}^{\text{SIC}} = \mu_m \sum_{\bar{p}=0}^{M-m} \binom{M-m}{\bar{p}} \frac{(-1)^{\bar{p}}}{m+\bar{p}} \sum_{\bar{s}=1}^{\bar{S}} \Psi_{\bar{s}} [F_{\hat{h}_m}(\varphi_m^{\max} \varrho_{\bar{s}})]^{m+\bar{p}} \sum_{u=0}^{2U} \Re \left[\mathcal{L}_{\mathcal{I}_{nm}}(c_u) e^{\frac{\iota \pi g \bar{s}}{\Theta}} \right]. \quad (\text{H.7})$$

This proves the result for $P_{\varepsilon_5}^{\text{SIC}}$ in (4.31).

Next, based on (4.4), the outage probability at m -th MBS user of type non-clustered to decode its message signal using SIE is given as,

$$\begin{aligned} P_{\varepsilon_5}^{\text{SIE}} &= \mathbb{P} \left(\frac{\bar{h}_m^m a_m^m P_m}{\mathcal{I}_{nm} + |e|^2 + \sigma^2} < \tau_m^m \right) \\ &= \mathbb{P} \left(\bar{h}_m^m < \phi_m^m (1 + \rho \mathcal{I}_{nm} + \rho |e|^2) \right) \\ &= \mathbb{E}_{|e|^2} \left[\mathbb{E}_{\mathcal{I}_{nm}} \left(F_{\bar{h}_m^m} (1 + \rho x + \rho y) \right) \right]. \end{aligned} \quad (\text{H.8})$$

Now following similar steps to deriving $P_{\varepsilon_5}^{\text{SIC}}$ in (H.7) and replacing φ_m^{\max} with ϕ_m^m , $P_{\varepsilon_5}^{\text{SIE}}$ in (H.8) can be expressed as:

$$P_{\varepsilon_5}^{\text{SIE}} = \int_0^\infty P_{\varepsilon_5}^{\text{SIC}} |_{\varphi_m^{\max}=\phi_m^m, \varrho_{\bar{s}}=\varrho_{\bar{s}}+\rho y} f_{|e|^2}(y) dy. \quad (\text{H.9})$$

This obtains the result for $P_{\varepsilon_5}^{\text{SIE}}$ in (4.31). Combining results in (H.7) and (H.9) proves the first part of the theorem for MBS user of non-clustered type.

Now based on the derivations of (H.7) and (H.9), the results for a case when m -th MBS user is of clustered type can be obtained in a straightforward manner. By replacing $\mathcal{L}_{\mathcal{I}_{cm}}$ from (4.18) with $\mathcal{L}_{\mathcal{I}_{nm}}$ in (H.7), the result for $P_{\varepsilon_6}^{\text{SIC}}$ is obtained. Finally, following similar steps in deriving (H.9), the result for $P_{\varepsilon_6}^{\text{SIE}}$ in (4.32) is obtained in a straightforward manner by replacing $P_{\varepsilon_6}^{\text{SIC}}$ with $P_{\varepsilon_5}^{\text{SIC}}$ in (H.9). This completes the proof for Theorem 4.1.

Appendix I

Proof of Lemma 5.1

In the case of GPP, when desired transmitter is at $x_0 \in \Phi_{GT}$, the $\mathcal{L}_{\mathcal{I}}(s)$ is given by (34) of [81]:

$$\mathcal{L}_{\mathcal{I}}(s) = \Lambda_1 \cdot \Lambda_2, \quad (\text{I.1})$$

where

$$\Lambda_1 = \exp \left\{ 2\pi\lambda_{GT} \int_0^\infty \left[\frac{1-a}{1+sr^{-\alpha}} + \frac{a}{1+sr^{-\alpha}} \cdot \int_0^\infty \int_0^{2\pi} \frac{\tau f_u(\tau) d\psi}{1+s(r^2+\tau^2+2r\tau\cos(\psi))^{-\alpha/2}} d\tau - 1 \right] r dr \right\}, \quad (\text{I.2})$$

and

$$\Lambda_2 = \frac{1-a}{1+a} + \frac{2a}{1+a} \int_0^\infty \int_0^{2\pi} \frac{\tau f_u(\tau) d\psi}{1+s(d^2+\tau^2+2d\tau\cos(\psi))^{-\alpha/2}} d\tau, \quad (\text{I.3})$$

where $1-a$ and a are the probabilities of having one and two transmitters in a group, respectively.

Now let us take X_1 in (I.2) as:

$$\begin{aligned} X_1 &= \int_0^\infty \int_0^{2\pi} \frac{\tau f_u(\tau) d\psi}{1 + s(r^2 + \tau^2 + 2r\tau \cos(\psi))^{-\alpha/2}} d\tau \\ &= \frac{2}{R_D^2} \int_0^{R_D} \tau^2 \underbrace{\int_0^{2\pi} \frac{d\psi}{1 + s(r^2 + \tau^2 + 2r\tau \cos(\psi))^{-\alpha/2}}}_{X_2} d\tau, \end{aligned} \quad (\text{I.4})$$

where $f_u(\tau) = \frac{2\tau}{R_D^2}$ if $0 \leq \tau \leq R_D$.

It is challenging to solve integral X_2 in (I.4). As such, it is approximated by applying the Gaussian–Chebyshev quadrature as [103]:

$$X_2 \approx \sum_{n=1}^N \frac{\varphi_n}{1 + s(r^2 + \tau^2 + 2r\tau \cos(\pi t_n))^{-\alpha/2}}, \quad (\text{I.5})$$

where $\varphi_n = \pi\omega_n\sqrt{1-\theta_n^2}$, $\omega_n = \frac{\pi}{N}$, $\theta_n = \cos\left(\frac{2n-1}{2N}\pi\right)$, $t_n = 1 + \theta_n$ and N is the complexity-accuracy tradeoff parameter.

Based on (I.5), X_1 can now be expressed as:

$$X_1 = \frac{2}{R^2} \int_0^{R_D} \sum_{n=1}^N \frac{\varphi_n \tau^2}{1 + s(r^2 + \tau^2 + 2r\tau \cos(\pi t_n))^{-\alpha/2}} d\tau. \quad (\text{I.6})$$

Note that it is challenging to solve (I.6) analytically. In order to obtain insightful results, (I.6) can be approximated by applying Gaussian–Chebyshev quadrature as:

$$X_1(r) \approx \sum_{v=1}^V \sum_{n=1}^N \frac{2R_D \varphi_n \omega_v \sqrt{1 - \vartheta_v^2 k_v^2}}{1 + s(r^2 + R_D^2 k_v^2 + 2r R_D k_v^2 \cos(\pi t_n))^{-\alpha/2}}, \quad (\text{I.7})$$

where $\omega_v = \frac{\pi}{V}$, $\vartheta_v = \cos\left(\frac{2v-1}{2V}\pi\right)$, $k_v = \frac{1}{2}(\vartheta_v + 1)$ and V is the complexity-accuracy tradeoff parameter.

Based on (I.7), Λ_1 in I.2 is re-written as:

$$\begin{aligned}\Lambda_1 &= \exp \left\{ 2\pi\lambda_{\text{GT}} \int_0^\infty \left[\frac{1-a}{1+sr^{-\alpha}} + \frac{aX_1(r)}{1+sr^{-\alpha}} - 1 \right] r dr \right\} \\ &= \exp \left\{ -2\pi\lambda_{\text{GT}} \int_0^\infty \frac{a(1-X_1(r)) + sr^{-\alpha}}{1+sr^{-\alpha}} \right\}.\end{aligned}\quad (\text{I.8})$$

Next, Gauss–Laguerre quadrature is applied to approximate the integral in (I.8).

Hence, Λ_1 can be expressed after approximation as:

$$\Lambda_1 = e^{-2\pi\lambda_{\text{GT}} \sum_{p=1}^P \Omega_p \frac{a(1-X_1(r_p)) + sr_p^{-\alpha}}{1+sr_p^{-\alpha}}}.\quad (\text{I.9})$$

Following the same approximation procedure for X_1 and applying Gaussian–Chebyshev quadrature twice, Λ_2 in (I.3) is given as:

$$\Lambda_2(d) = \frac{1-a}{1+a} + \frac{2a}{1+a} \sum_{j=1}^S \sum_{i=1}^Q \frac{\varrho_i \xi_j}{1+s(d^2 + R_D^2 z_j^2 + 2dR_D z_j \cos(\pi x_i))^{-\alpha/2}}, \quad (\text{I.10})$$

where $\varrho_i = \pi\omega_i\sqrt{1-\eta_i^2}$, $\omega_i = \frac{\pi}{Q}$, $\eta_i = \cos(\frac{2i-1}{2Q}\pi)$, $x_i = \eta_i+1$, $\xi_j = 2R_D\omega_j\sqrt{1-\Theta_j^2}z_j^2$, $\Theta_j = \cos(\frac{2j-1}{2S}\pi)$, $z_j = \frac{1}{2}(\Theta_j+1)$, $\omega_j = \frac{\pi}{S}$ and Q, S are the complexity-accuracy trade-off parameters.

Finally, the result in Lemma 5.1 is obtained by multiplying (I.9) and (I.10). \square

Appendix J

Proof of Theorem 6.1

$$\begin{aligned}
 P_{\text{out}}^m &= 1 - \text{Pr}(|h_m|^2 > \tau_m^*(\kappa z + 1)) \\
 &= \int_0^\infty \underbrace{\int_0^{\tau_m^*(\kappa z + 1)} f_{|h_m|^2}(x) dx}_{Q_1} f_{\mathcal{I}}(z) dz.
 \end{aligned} \tag{J.1}$$

Since NOMA users are uniformly distributed inside disc A and fading is Rayleigh distributed, the CDF of the unordered channel is given as [79]:

$$\begin{aligned}
 F_{|\tilde{h}|^2}(x) &= \frac{2}{R^2} \int_0^R (1 - e^{-(1+t^\alpha)x}) t dt \\
 &\stackrel{(a)}{=} \frac{2}{\alpha R^2} \int_0^{R^\alpha} (1 - e^{-(1+y)x}) y^{\delta-1} dy \\
 &\stackrel{(b)}{=} 1 - \delta e^{-x} B(1, \delta) \phi(\delta, 1 + \delta; -xR^\alpha) \\
 &= 1 - e^{-x} \phi(\delta, 1 + \delta; -xR^\alpha),
 \end{aligned} \tag{J.2}$$

where (a) is obtained by a change of variable from $t^\alpha \rightarrow y$, (b) results from by applying Eq. 3.383 in [77], $B(\cdot, \cdot)$ is a beta function and $\delta B(1, \delta) = 1$. The PDF $f_{|\tilde{h}|^2}(x)$ is

obtained by taking the derivative of (J.2) as:

$$f_{|\bar{h}|^2}(x) \stackrel{(c)}{=} e^{-x} [\phi(\delta, 1 + \delta; -xR^\alpha) + \varepsilon\phi(1 + \delta, 2 + \delta; -xR^\alpha)] \quad (\text{J.3})$$

where (c) is obtained by applying Eq. 9.213 of [77]. Next, using (6.9), (J.2) and (J.3),

Q_1 in (J.1) can be written as:

$$\begin{aligned} Q_1 &= \mu_m \sum_{q=0}^{M-m} \binom{M-m}{q} (-1)^q \int_0^{\tau_m^*(\kappa z+1)} [1 - e^{-x}\phi(\delta, 1 + \delta; -xR^\alpha)]^{m+q-1} \\ &\quad \times e^{-x} [\phi(\delta, 1 + \delta; -xR^\alpha) + \varepsilon\phi(1 + \delta, 2 + \delta; -xR^\alpha)] dx. \end{aligned} \quad (\text{J.4})$$

It is challenging to solve Q_1 in (J.4). As such, it is approximated by applying the Gaussian-Chebyshev quadrature as:

$$\begin{aligned} Q_1(z) &= \mu_m \sum_{q=0}^{M-m} \binom{M-m}{q} (-1)^q \left\{ \sum_{n=1}^N \psi_n [1 - e^{-x}\phi(\delta, 1 + \delta; -a_n(\kappa z + 1))]^{m+q-1} \right. \\ &\quad \left. [\phi(\delta, 1 + \delta; -a_n(\kappa z + 1)) + \varepsilon\phi(1 + \delta, 2 + \delta; -a_n(\kappa z + 1))] \right\} \end{aligned} \quad (\text{J.5})$$

In order to obtain P_{out}^m , the PDF $f_{\mathcal{I}}(z)$ of interference is required, which is written by using (4.29) as follows:

$$f_{\mathcal{I}}(z) = \frac{e^{vz}}{\Theta} \sum_{k=0}^{2K} \Re [\mathcal{L}_{\mathcal{I}}(s = c_k) e^{\frac{v\pi z}{\Theta}}], \quad (\text{J.6})$$

where $\mathcal{L}_{\mathcal{I}}$ is the Laplace transform of the interference \mathcal{I} and is given as [94]:

$$\mathcal{L}_{\mathcal{I}}(s) = e^{-\lambda\pi} \left[\left(e^{-s d_0^{-\alpha}} - 1 \right) d_0^2 + s^\delta \Upsilon(1 - \delta, s d_0^{-\alpha}) \right], \quad (\text{J.7})$$

where $\Upsilon(a, x) = \int_0^x e^{-t} t^{a-1} dt$ is the lower incomplete gamma function, which is

approximated by using Gaussian-Chebyshev quadrature as:

$$\Upsilon(1 - \delta, sd_0^{-\alpha}) = s^{1-\delta} \sum_{t=1}^T \eta_t e^{-u_t sd_0^{-\alpha}}. \quad (\text{J.8})$$

Now based on (J.5) and (J.6), P_{out}^m in (J.1) can be expressed as:

$$P_{\text{out}}^m = \frac{1}{\Theta} \sum_{k=0}^{2K} \int_0^\infty \Re[\mathcal{L}_{\mathcal{I}}(s = c_k) e^{\frac{t\pi z}{\Theta}}] e^{vz} Q_1(z) dz. \quad (\text{J.9})$$

Finally, using $Q_1(z)$, $\mathcal{L}_{\mathcal{I}}$ and $\Upsilon(1 - \delta, sd_0^{-\alpha})$ from (J.5), (J.7), and (J.8), respectively in (J.9) and applying Gauss-Laguerre quadrature with parameters defined after (6.10) proves the result in Theorem 6.1.

Appendix K

Proof of Theorem 8.1

According to the NOMA scheme, the minimum and maximum transmission powers at the BS are proportional to $\frac{1}{\max|h_m|^2}$ and P_B . Therefore, ρ_t is lower and upper bounded by $\frac{c}{\max|h_m|^2}$, and ρ_B , respectively, where $c > 0$ is a constant. Hence, the CDF of ρ_t is given as:

$$\begin{aligned} F_{\rho_t}(u) &= 1 - \Pr\left(|\hat{h}_m|^2 \leq \frac{cd_m^\alpha}{u}\right) U(\rho_B - u) \\ &\stackrel{(a)}{=} 1 - \left[F_{|\hat{h}_m|^2}\left(\frac{cd_m^\alpha}{u}\right)\right]^M U(\rho_B - u) \end{aligned} \quad (\text{K.1})$$

where (a) is obtained by applying order statistics. Since users are randomly distributed inside disc \mathcal{D} , their spatial distribution can be modeled by applying a thinning function $g(w) = 1(d_w \leq \mathcal{R}_{\mathcal{D}})$ to a homogenous PPP, Φ_h , with intensity λ , where 1 is an indicator function and d_w is the distance between location w and BS. Denote Φ_{th} as a thinned

version of Φ with intensity $\lambda g(w)$ [34], (K.1) can be rewritten as:

$$\begin{aligned}
 F_{\rho_t}(u) &= 1 - \mathbb{E}_{\Phi_{\text{th}}} \left[\prod_{m \in \Phi_{\text{th}}} F_{|\hat{h}_m|^2} \left(\frac{cd_m^\alpha}{u} \right) \right] U(\rho_B - u) \\
 &\stackrel{(b)}{=} 1 - \exp \left(\lambda \int_{\mathbb{R}^2} \left(1 - F_{|\hat{h}_m|^2} \left(\frac{cd_m^\alpha}{u} \right) \right) g(w) \, dw \right) U(\rho_B - u) \\
 &\stackrel{(c)}{=} 1 - \exp \left(\frac{\pi \delta \lambda \Upsilon \left(\delta, \frac{c \mathcal{R}_D^\alpha}{u} \right) u^\delta}{c^\delta} \right), \tag{K.2}
 \end{aligned}$$

where $\Upsilon(\cdot, \cdot)$ is a lower incomplete gamma function [110], (b) is obtained by employing a PGFL for PPP, (c) results by converting in polar coordinates and then applying Eq. 3.381 in [77]. The PDF of ρ_t is obtained by taking derivative of (K.2), which completes the proof.

References

- [1] J. G. Andrews, S. Buzzi, W. Choi, S. V. Hanly, A. Lozano, A. C. K. Soong, and J. C. Zhang, “What will 5G be?” *IEEE Journal on Selected Areas in Communications*, vol. 32, no. 6, pp. 1065–1082, June 2014.
- [2] I. F. Akyildiz, S. Nie, S.-C. Lin, and M. Chandrasekaran, “5G roadmap: 10 key enabling technologies,” *Computer Networks*, vol. 106, pp. 17 – 48, 2016. [Online]. Available: <http://www.sciencedirect.com/science/article/pii/S1389128616301918>
- [3] X. Dai, S. Chen, S. Sun, S. Kang, Y. Wang, Z. Shen, and J. Xu, “Successive interference cancelation amenable multiple access (SAMA) for future wireless communications,” in *Proc. IEEE International Conference on Communication Systems*, Macau, China, Nov 2014.
- [4] Z. Ma, Z. Zhang, Z. Ding, P. Fan, and H. Li, “Key techniques for 5G wireless communications: network architecture, physical layer, and mac layer perspectives,” *Science China Information Sciences*, vol. 58, no. 4, pp. 1–20, Apr 2015. [Online]. Available: <https://doi.org/10.1007/s11432-015-5293-y>
- [5] S. Timotheou and I. Krikidis, “Fairness for non-orthogonal multiple access in 5G systems,” *IEEE Signal Processing Letters*, vol. 22, no. 10, pp. 1647–1651, Oct 2015.
- [6] Y. Saito, A. Benjebbour, Y. Kishiyama, and T. Nakamura, “System-level performance evaluation of downlink non-orthogonal multiple access (NOMA),” in *Proc. IEEE 24th Annual International Symposium on Personal, Indoor, and Mobile Radio Communications (PIMRC)*, London, UK, Sept 2013.
- [7] Z. Ding, Y. Liu, J. Choi, Q. Sun, M. Elkashlan, C. L. I, and H. V. Poor, “Application of non-orthogonal multiple access in lte and 5G networks,” *IEEE Communications Magazine*, vol. 55, no. 2, pp. 185–191, February 2017.
- [8] G. Fodor, E. Dahlman, G. Mildh, S. Parkvall, N. Reider, G. Miklós, and Z. Turányi, “Design aspects of network assisted device-to-device communications,” *IEEE Communications Magazine*, vol. 50, no. 3, pp. 170–177, March 2012.

REFERENCES

- [9] K. Doppler, M. Rinne, C. Wijting, C. B. Ribeiro, and K. Hugl, "Device-to-device communication as an underlay to LTE-advanced networks," *IEEE Communications Magazine*, vol. 47, no. 12, pp. 42–49, Dec 2009.
- [10] X. Lin, J. G. Andrews, and A. Ghosh, "Spectrum sharing for device-to-device communication in cellular networks," *IEEE Transactions on Wireless Communications*, vol. 13, no. 12, pp. 6727–6740, Dec 2014.
- [11] X. Lin, J. G. Andrews, A. Ghosh, and R. Ratasuk, "An overview of 3gpp device-to-device proximity services," *IEEE Communications Magazine*, vol. 52, no. 4, pp. 40–48, April 2014.
- [12] M. Shirvanimoghaddam, M. Dohler, and S. J. Johnson, "Massive non-orthogonal multiple access for cellular IoT: Potentials and limitations," *IEEE Communications Magazine*, vol. 55, no. 9, pp. 55–61, 2017.
- [13] Z. Ding, Z. Yang, P. Fan, and H. V. Poor, "On the performance of non-orthogonal multiple access in 5G systems with randomly deployed users," *IEEE Signal Processing Letters*, vol. 21, no. 12, pp. 1501–1505, Dec 2014.
- [14] R. M. Buehrer, "Code division multiple access (cdma)," *Synthesis Lectures on Communications*, vol. 1, no. 1, pp. 1–192, 2006.
- [15] A. Goldsmith, *Wireless Communications*. Cambridge university press, 2005.
- [16] D. P. Agrawal and Q.-A. Zeng, *Introduction to Wireless and Mobile Systems*. Cengage learning, 2015.
- [17] M. D. Yacoub, *Foundations of Mobile Radio Engineering*. CRC press, 1993.
- [18] T. S. Rappaport *et al.*, *Wireless Communications: Principles and Practice*. prentice hall PTR New Jersey, 1996, vol. 2.
- [19] A. J. Viterbi and A. J. Viterbi, *CDMA: Principles of Spread Spectrum Communication*. Addison-Wesley Reading, MA, 1995, vol. 122.
- [20] A. R. Bahai, B. R. Saltzberg, and M. Ergen, *Multi-Carrier Digital Communications: Theory and Applications of OFDM*. Springer Science & Business Media, 2004.
- [21] Y. S. Cho, J. Kim, W. Y. Yang, and C. G. Kang, *MIMO-OFDM Wireless Communications with MATLAB*. John Wiley & Sons, 2010.
- [22] N. DoCoMo, "Requirements, candidate solutions and technology roadmap for lte rel-12 onward." in *3GPP Workshop on Release 12 Onward RWS-120010*, Ljubljana, Slovenia, June 2012.

REFERENCES

- [23] S. Tomida and K. Higuchi, "Non-orthogonal access with SIC in cellular downlink for user fairness enhancement," in *Proc. International Symposium on Intelligent Signal Processing and Communications Systems (ISPACS)*, Chiang Mai, Thailand, Thailand, Dec 2011.
- [24] T. Takeda and K. Higuchi, "Enhanced user fairness using non-orthogonal access with SIC in cellular uplink," in *Proc. IEEE Vehicular Technology Conference (VTC Fall)*, San Francisco, CA, USA, Sept 2011.
- [25] A. Benjebbour, Y. Saito, Y. Kishiyama, A. Li, A. Harada, and T. Nakamura, "Concept and practical considerations of non-orthogonal multiple access (NOMA) for future radio access," in *Proc. International Symposium on Intelligent Signal Processing and Communication Systems*, Naha, Japan, Nov 2013.
- [26] X. Chen, A. Benjebbour, Y. Lan, A. Li, and H. Jiang, "Impact of rank optimization on downlink non-orthogonal multiple access (NOMA) with SU-MIMO," in *Proc IEEE International Conference on Communication Systems*, Macau, China, Nov 2014.
- [27] A. Asadi, Q. Wang, and V. Mancuso, "A survey on device-to-device communication in cellular networks," *IEEE Communications Surveys Tutorials*, vol. 16, no. 4, pp. 1801–1819, Fourthquarter 2014.
- [28] K. Doppler, M. P. Rinne, P. Janis, C. Ribeiro, and K. Hugl, "Device-to-device communications; functional prospects for LTE-advanced networks," in *Proc. IEEE International Conference on Communications Workshops*, Dresden, Germany, June 2009.
- [29] N. Golrezaei, P. Mansourifard, A. F. Molisch, and A. G. Dimakis, "Base-station assisted device-to-device communications for high-throughput wireless video networks," *IEEE Transactions on Wireless Communications*, vol. 13, no. 7, pp. 3665–3676, July 2014.
- [30] N. Golrezaei, A. G. Dimakis, and A. F. Molisch, "Device-to-device collaboration through distributed storage," in *Proc. IEEE Global Communications Conference (GLOBECOM)*, Anaheim, CA, USA, Dec 2012.
- [31] Q. Wang and B. Rengarajan, "Recouping opportunistic gain in dense base station layouts through energy-aware user cooperation," in *Proc. IEEE 14th International Symposium on "A World of Wireless, Mobile and Multimedia Networks" (WoWMoM)*, Madrid, Spain, June 2013.
- [32] S. Mukherjee, *Analytical Modeling of Heterogeneous Cellular Networks*. Cambridge University Press, 2014.
- [33] H. ElSawy, E. Hossain, and M. Haenggi, "Stochastic geometry for modeling, analysis, and design of multi-tier and cognitive cellular wireless networks: A

REFERENCES

- survey,” *IEEE Communications Surveys Tutorials*, vol. 15, no. 3, pp. 996–1019, Third 2013.
- [34] M. Haenggi, *Stochastic Geometry for Wireless Networks*. Cambridge University Press, 2012.
- [35] D. J. Daley and D. Vere-Jones, *An Introduction to the Theory of Point Processes: Volume II: General Theory and Structure*. Springer Science & Business Media, 2007.
- [36] J. F. C. Kingman, *Poisson Processes*. Clarendon Press, 1992, vol. 3.
- [37] Y. Li, F. Baccelli, H. S. Dhillon, and J. G. Andrews, “Statistical modeling and probabilistic analysis of cellular networks with determinantal point processes,” *IEEE Transactions on Communications*, vol. 63, no. 9, pp. 3405–3422, Sept 2015.
- [38] T. Shirai and N. Miyoshi, “A cellular network model with ginibre configured base stations,” *Advances in Applied Probability*, 2013.
- [39] J. B. Hough, M. Krishnapur, Y. Peres *et al.*, *Zeros of Gaussian Analytic Functions and Determinantal Point Processes*. American Mathematical Soc., 2009, vol. 51.
- [40] F. Lavancier, J. Møller, E. Rubak *et al.*, “Statistical aspects of determinantal point processes,” Department of Mathematical Sciences, Aalborg University, Tech. Rep., 2012.
- [41] T. Shirai and Y. Takahashi, “Random point fields associated with certain fredholm determinants i: fermion, poisson and boson point processes,” *Journal of Functional Analysis*, vol. 205, no. 2, pp. 414–463, 2003.
- [42] R. K. Ganti and M. Haenggi, “Interference and outage in clustered wireless ad hoc networks,” *IEEE Transactions on Information Theory*, vol. 55, no. 9, pp. 4067–4086, Sept 2009.
- [43] Z. Yazdanshenasan, H. S. Dhillon, M. Afshang, and P. H. J. Chong, “Poisson hole process: Theory and applications to wireless networks,” *IEEE Transactions on Wireless Communications*, vol. 15, no. 11, pp. 7531–7546, Nov 2016.
- [44] F. Baccelli and B. Błaszczyszyn, “Stochastic geometry and wireless networks: Volume I theory,” *Foundations and Trends® in Networking*, vol. 3, no. 3–4, pp. 249–449, 2010. [Online]. Available: <http://dx.doi.org/10.1561/1300000006>
- [45] A. Benjebbour, A. Li, Y. Kishiyama, H. Jiang, and T. Nakamura, “System-level performance of downlink NOMA combined with SU-MIMO for future LTE enhancements,” in *Proc. IEEE Globecom Workshops (GC Wkshps)*, Austin, TX, USA, Dec 2014.

REFERENCES

- [46] R. M. Buehrer, N. S. Correal-Mendoza, and B. D. Woerner, "A simulation comparison of multiuser receivers for cellular cdma," *IEEE Transactions on Vehicular Technology*, vol. 49, no. 4, pp. 1065–1085, Jul 2000.
- [47] Z. Ding, P. Fan, and H. V. Poor, "Impact of user pairing on 5g nonorthogonal multiple-access downlink transmissions," *IEEE Transactions on Vehicular Technology*, vol. 65, no. 8, pp. 6010–6023, Aug 2016.
- [48] Z. Rui, S. Zhongwei, H. Zhiqiang, N. Kai, and T. Baoyu, "A joint detection based on the DS evidence theory for multi-user superposition modulation," in *Proc. 4th IEEE International Conference on Network Infrastructure and Digital Content*, Beijing, China, Sept 2014.
- [49] M. S. Ali, H. Tabassum, and E. Hossain, "Dynamic user clustering and power allocation for uplink and downlink non-orthogonal multiple access (noma) systems," *IEEE Access*, vol. 4, pp. 6325–6343, 2016.
- [50] Z. Yang, Z. Ding, P. Fan, and G. K. Karagiannidis, "On the performance of non-orthogonal multiple access systems with partial channel information," *IEEE Transactions on Communications*, vol. 64, no. 2, pp. 654–667, Feb 2016.
- [51] J. Men, J. Ge, and C. Zhang, "Performance analysis of nonorthogonal multiple access for relaying networks over nakagami- m fading channels," *IEEE Transactions on Vehicular Technology*, vol. 66, no. 2, pp. 1200–1208, Feb 2017.
- [52] J. Zhao, Y. Liu, K. K. Chai, A. Nallanathan, Y. Chen, and Z. Han, "Resource allocation for non-orthogonal multiple access in heterogeneous networks," in *Proc. IEEE International Conference on Communications (ICC)*, Paris, France, May 2017.
- [53] H. Tabassum, E. Hossain, and J. Hossain, "Modeling and analysis of uplink non-orthogonal multiple access in large-scale cellular networks using poisson cluster processes," *IEEE Transactions on Communications*, vol. 65, no. 8, pp. 3555–3570, Aug 2017.
- [54] P. Parida and S. S. Das, "Power allocation in OFDM based NOMA systems: A DC programming approach," in *Proc. IEEE Globecom Workshops (GC Wkshps)*, Austin, TX, USA, Dec 2014.
- [55] Z. Zhang, H. Sun, R. Q. Hu, and Y. Qian, "Stochastic geometry based performance study on 5G non-orthogonal multiple access scheme," in *Proc. IEEE Global Communications Conference (GLOBECOM)*, Washington, DC, USA, Dec 2016.
- [56] Y. Liu, Z. Qin, M. ElKashlan, Y. Gao, and A. Nallanathan, "Non-orthogonal multiple access in massive MIMO aided heterogeneous networks," in *Proc. IEEE Global Communications Conference (GLOBECOM)*, Washington, DC, USA, Dec 2016.

REFERENCES

- [57] Z. Zhang, Z. Ma, M. Xiao, G. Liu, and P. Fan, "Modeling and analysis of non-orthogonal MBMS transmission in heterogeneous networks," *IEEE Journal on Selected Areas in Communications*, vol. 35, no. 10, pp. 2221–2237, Oct 2017.
- [58] Y. Liu, Z. Qin, M. ElKashlan, A. Nallanathan, and J. A. McCann, "Non-orthogonal multiple access in large-scale heterogeneous networks," *IEEE Journal on Selected Areas in Communications*, vol. 35, no. 12, pp. 2667–2680, Dec 2017.
- [59] Z. Zhang, Z. Ma, M. Xiao, Z. Ding, and P. Fan, "Full-duplex device-to-device-aided cooperative nonorthogonal multiple access," *IEEE Transactions on Vehicular Technology*, vol. 66, no. 5, pp. 4467–4471, May 2017.
- [60] K. S. Ali, H. ElSawy, and M. S. Alouini, "Modeling cellular networks with full-duplex d2d communication: A stochastic geometry approach," *IEEE Transactions on Communications*, vol. 64, no. 10, pp. 4409–4424, Oct 2016.
- [61] M. Afshang and H. S. Dhillon, "Spatial modeling of device-to-device networks: Poisson cluster process meets poisson hole process," in *Proc. 49th Asilomar Conference on Signals, Systems and Computers*, Pacific Grove, CA, USA, Nov 2015.
- [62] H. Sun, Y. Xu, and R. Q. Hu, "A NOMA and MU-MIMO supported cellular network with underlaid D2D communications," in *Proc. IEEE 83rd Vehicular Technology Conference (VTC Spring)*, Nanjing, China, May 2016.
- [63] L. Pei, Z. Yang, C. Pan, W. Huang, M. Chen, M. ElKashlan, and A. Nallanathan, "Energy-efficient d2d communications underlaying noma-based networks with energy harvesting," *IEEE Communications Letters*, 2018.
- [64] Y. Pan, C. Pan, Z. Yang, and M. Chen, "Resource allocation for d2d communications underlaying a noma-based cellular network," *IEEE Wireless Communications Letters*, vol. 7, no. 1, pp. 130–133, Feb 2018.
- [65] Y. B. Song, H. S. Kang, and D. K. Kim, "5G cellular systems with D2D assisted NOMA relay," in *Proc URSI Asia-Pacific Radio Science Conference (URSI AP-RASC)*, Seoul, South Korea, Aug 2016.
- [66] J. Zhao, Y. Liu, K. K. Chai, Y. Chen, M. ElKashlan, and J. Alonso-Zarate, "Noma-based d2d communications: Towards 5g," in *Proc. IEEE Global Communications Conference (GLOBECOM)*, Washington, DC, USA, Dec 2016.
- [67] J. Zhao, Y. Liu, K. K. Chai, Y. Chen, and M. ElKashlan, "Joint subchannel and power allocation for noma enhanced d2d communications," *IEEE Transactions on Communications*, vol. 65, no. 11, pp. 5081–5094, Nov 2017.
- [68] Z. Shi, S. Ma, H. E. Sawy, G. Yang, and M. S. Alouini, "Cooperative harq assisted noma scheme in large-scale d2d networks," *IEEE Transactions on Communications*, pp. 1–1, 2018.

REFERENCES

- [69] Z. Yang, Z. Ding, P. Fan, and Z. Ma, "Outage performance for dynamic power allocation in hybrid non-orthogonal multiple access systems," *IEEE Communications Letters*, vol. 20, no. 8, pp. 1695–1698, Aug 2016.
- [70] H. Jin, K. Peng, and J. Song, "A spectrum efficient multi-user transmission scheme for 5g systems with low complexity," *IEEE Communications Letters*, vol. 19, no. 4, pp. 613–616, April 2015.
- [71] N. I. Kim and D. H. Cho, "Hybrid multiple access system based on non orthogonality and sparse code," in *Proc IEEE Wireless Communications and Networking Conference (WCNC)*, San Francisco, CA, USA, March 2017.
- [72] S. L. Shieh, C. H. Lin, Y. C. Huang, and C. L. Wang, "On gray labeling for downlink non-orthogonal multiple access without sic," *IEEE Communications Letters*, vol. 20, no. 9, pp. 1721–1724, Sept 2016.
- [73] M. Xu, F. Ji, M. Wen, and W. Duan, "Novel receiver design for the cooperative relaying system with non-orthogonal multiple access," *IEEE Communications Letters*, vol. 20, no. 8, pp. 1679–1682, Aug 2016.
- [74] J. G. Andrews, A. K. Gupta, and H. S. Dhillon, "A primer on cellular network analysis using stochastic geometry," *arXiv preprint arXiv:1604.03183*, 2016.
- [75] M. Afshang, H. S. Dhillon, and P. H. J. Chong, "Modeling and performance analysis of clustered device-to-device networks," *IEEE Transactions on Wireless Communications*, vol. 15, no. 7, pp. 4957–4972, July 2016.
- [76] M. Haenggi, "On distances in uniformly random networks," *IEEE Transactions on Information Theory*, vol. 51, no. 10, pp. 3584–3586, Oct 2005.
- [77] I. S. Gradshteyn and I. M. Ryzhik, *Table of Integrals, Series, and Products*. Academic press, 2014.
- [78] K. L. Kuhlman, "Review of inverse laplace transform algorithms for laplace-space numerical approaches," *Numerical Algorithms*, vol. 63, no. 2, pp. 339–355, 2013.
- [79] Z. Ding and H. V. Poor, "Cooperative energy harvesting networks with spatially random users," *IEEE Signal Processing Letters*, vol. 20, no. 12, pp. 1211–1214, Dec 2013.
- [80] P. H. J. Nardelli, M. Kountouris, P. Cardieri, and M. Latva-aho, "Throughput optimization in wireless networks under stability and packet loss constraints," *IEEE Transactions on Mobile Computing*, vol. 13, no. 8, pp. 1883–1895, Aug 2014.

REFERENCES

- [81] A. Guo, Y. Zhong, W. Zhang, and M. Haenggi, "The Gauss-Poisson process for wireless networks and the benefits of cooperation," *IEEE Transactions on Communications*, vol. 64, no. 5, pp. 1916–1929, May 2016.
- [82] Z. Yang, Z. Ding, Y. Wu, and P. Fan, "Novel relay selection strategies for cooperative noma," *IEEE Transactions on Vehicular Technology*, vol. 66, no. 11, pp. 10 114–10 123, Nov 2017.
- [83] Z. Ding, H. Dai, and H. V. Poor, "Relay selection for cooperative noma," *IEEE Wireless Communications Letters*, vol. 5, no. 4, pp. 416–419, Aug 2016.
- [84] Z. Ding, L. Dai, and H. V. Poor, "Mimo-noma design for small packet transmission in the internet of things," *IEEE Access*, vol. 4, pp. 1393–1405, 2016.
- [85] Y. Sun, D. W. K. Ng, J. Zhu, and R. Schober, "Multi-objective optimization for robust power efficient and secure full-duplex wireless communication systems," *IEEE Transactions on Wireless Communications*, vol. 15, no. 8, pp. 5511–5526, Aug 2016.
- [86] F. Zabini, A. Bazzi, B. M. Masini, and R. Verdone, "Optimal performance versus fairness tradeoff for resource allocation in wireless systems," *IEEE Transactions on Wireless Communications*, vol. 16, no. 4, pp. 2587–2600, April 2017.
- [87] Y. Liu, Z. Ding, M. ElKashlan, and J. Yuan, "Nonorthogonal multiple access in large-scale underlay cognitive radio networks," *IEEE Transactions on Vehicular Technology*, vol. 65, no. 12, pp. 10 152–10 157, Dec 2016.
- [88] C. Prommak and S. Modhirun, "Minimizing energy consumption in wireless sensor networks using multi-hop relay stations," in *Proceedings of the 11th WSEAS international conference on Applied computer science*, Penang, Malaysia, October 2011.
- [89] A. Gurijala and P. Das, "Broadcast server architecture for wireless sensor networks," in *Proc. International Conference on Wireless Networks (ICWN)*, Las Vegas, NV, USA, June 2006.
- [90] Y. Liu, B.-C. Seet, and A. Al-Anbuky, "Ambient intelligence context-based cross-layer design in wireless sensor networks," *Sensors*, vol. 14, no. 10, pp. 19 057–19 085, 2014.
- [91] N. Imran, B.-C. Seet, and A. C. Fong, "A comparative analysis of video codecs for multihop wireless video sensor networks," *Multimedia systems*, vol. 18, no. 5, pp. 373–389, 2012.
- [92] B. Nazir, H. Hasbullah, and S. A. Madani, "Sleep/wake scheduling scheme for minimizing end-to-end delay in multi-hop wireless sensor networks," *EURASIP Journal on Wireless Communications and Networking*, vol. 2011, no. 1, p. 92, 2011.

REFERENCES

- [93] P. Yang, Y. Yan, X. Y. Li, Y. Zhang, Y. Tao, and L. You, "Taming cross-technology interference for wi-fi and zigbee coexistence networks," *IEEE Transactions on Mobile Computing*, vol. 15, no. 4, pp. 1009–1021, April 2016.
- [94] J. Venkataraman, M. Haenggi, and O. Collins, "Shot noise models for outage and throughput analyses in wireless ad hoc networks," in *Proc. IEEE Military Communications conference (MILCOM)*, Washington, DC, USA, Oct 2006.
- [95] H. A. David and H. N. Nagaraja, *Order Statistics*. Wiley Online Library, 1970.
- [96] S. Cui, A. J. Goldsmith, and A. Bahai, "Energy-efficiency of mimo and cooperative mimo techniques in sensor networks," *IEEE Journal on Selected Areas in Communications*, vol. 22, no. 6, pp. 1089–1098, Aug 2004.
- [97] R. Min, T. Furrer, and A. Chandrakasan, "Dynamic voltage scaling techniques for distributed microsensor networks," in *Proc. IEEE Computer Society Workshop on VLSI*, Orlando, FL, USA, August 2000.
- [98] J.-J. Chen and T.-W. Kuo, "Procrastination determination for periodic real-time tasks in leakage-aware dynamic voltage scaling systems." in *Proc. IEEE/ACM International Conference on Computer-Aided Design*, San Jose, CA, USA, Nov 2007.
- [99] Z. He, Y. Liang, L. Chen, I. Ahmad, and D. Wu, "Power-rate-distortion analysis for wireless video communication under energy constraints," *IEEE Transactions on Circuits and Systems for Video Technology*, vol. 15, no. 5, pp. 645–658, May 2005.
- [100] S. M. Martin, K. Flautner, T. Mudge, and D. Blaauw, "Combined dynamic voltage scaling and adaptive body biasing for lower power microprocessors under dynamic workloads," in *Proc. IEEE/ACM international conference on Computer-aided design (ICCAD)*. San Jose, CA, USA: ACM, Nov 2002.
- [101] J. Ivkovic and J. L. Ivkovic, "Analysis of the performance of the new generation of 32-bit microcontrollers for iot and big data application," in *Proc. International Conference on Information Society and Technology (ICIST)*, Kopaonik, Serbia, Mar 2017.
- [102] R. C. Gonzalez and R. E. Woods, *Digital Image Processing*. Upper Saddle River, NJ: Prentice Hall, 2012.
- [103] F. B. Hildebrand, *Introduction to Numerical Analysis*. Courier Corporation, 1987.
- [104] F. Büsching, S. Schildt, and L. Wolf, "Droidcluster: Towards smartphone cluster computing – the streets are paved with potential computer clusters," in *Proc. 32nd International Conference on Distributed Computing Systems Workshops (IDCSW)*, Macau, China, June 2012.

REFERENCES

- [105] Qualcomm, “Qualcomm snapdragon benchmark report,” Tech. Rep., Sep 2013. [Online]. Available: <https://www.qualcomm.com/documents/qualcomm-snapdragon-benchmark-report>
- [106] *Samsung Galaxy S4 Exynos 5 Octa Benchmarks*, Apr 2013. [Online]. Available: <http://www.fonearena.com/blog/67821/samsung-galaxy-s4-exynos-5-octa-benchmarks.html>
- [107] E. Baştuğ, M. Bennis, M. Kountouris, and M. Debbah, “Edge caching for coverage and capacity-aided heterogeneous networks,” in *Proc. IEEE International Symposium on Information Theory (ISIT)*, Barcelona, Spain, July 2016.
- [108] M. Afshang and H. S. Dhillon, “Optimal geographic caching in finite wireless networks,” in *Proc. IEEE 17th International Workshop on Signal Processing Advances in Wireless Communications (SPAWC)*, Edinburgh, UK, July 2016.
- [109] I. C. Ipsen and D. J. Lee, “Determinant approximations,” *arXiv preprint arXiv:1105.0437*, 2011.
- [110] Y. A. Brychkov, *Handbook of Special Functions: Derivatives, Integrals, Series and other Formulas*. CRC press, 2008.